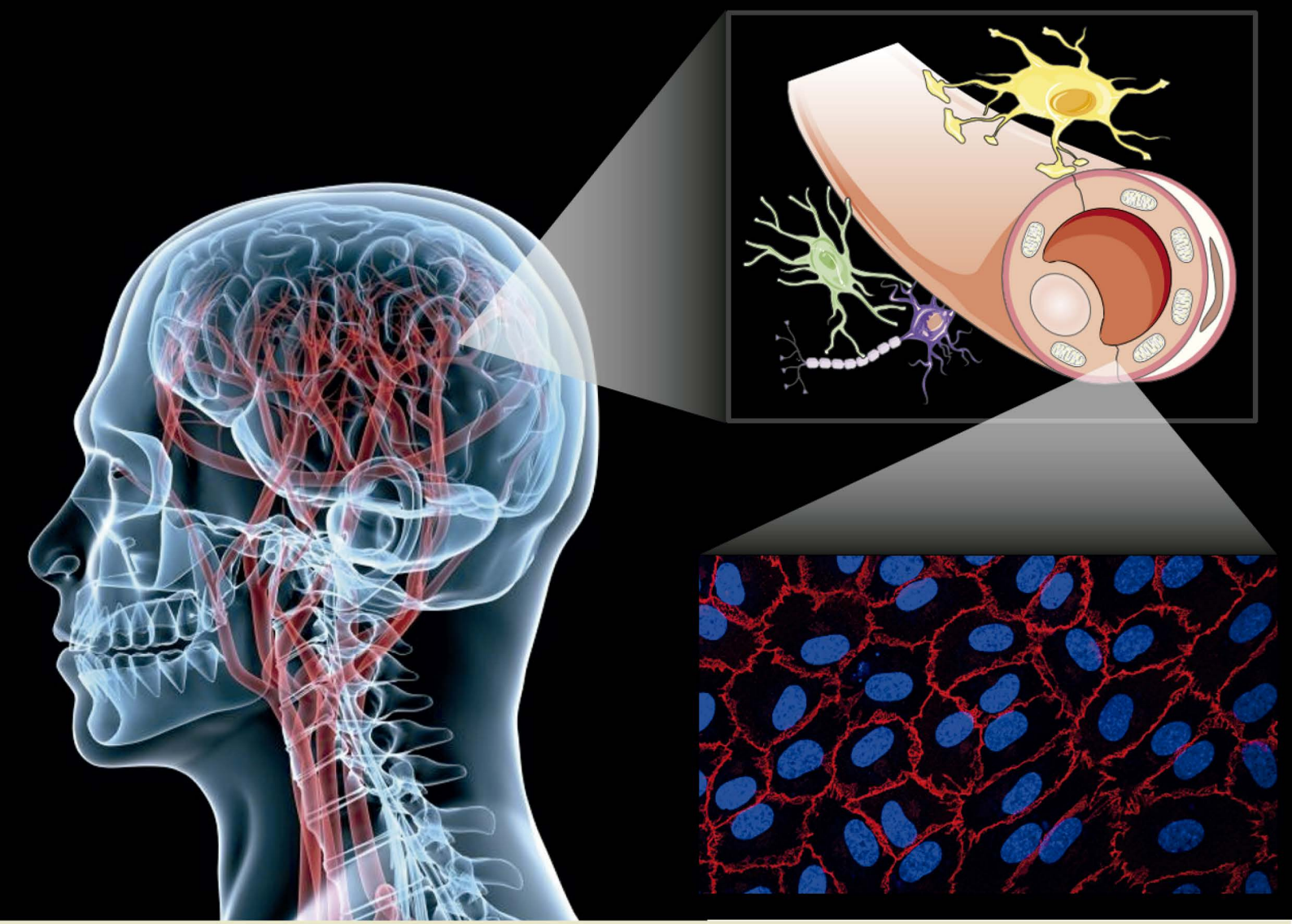

Catarina Oliveira Praça de Almeida

BRAIN-LIKE ENDOTHELIAL CELLS DERIVED FROM STEM CELLS TO STUDY BBB DEVELOPMENT AND TARGETING

Tese de Doutoramento em Biologia Experimental e Biomedicina, ramo de Biotecnologia e Saúde,
orientada pelo Doutor Lino Ferreira e pela Doutora Marie-Pierre Dehouck,
apresentada ao Instituto de Investigação Interdisciplinar da Universidade de Coimbra.

Setembro 2016

· U C ·

Universidade de Coimbra

Catarina Oliveira Praça de Almeida

BRAIN-LIKE ENDOTHELIAL CELLS DERIVED FROM STEM CELLS TO STUDY BBB DEVELOPMENT AND TARGETING

September 2016

Thesis submitted to the Institute for Interdisciplinary Research of the University of Coimbra to apply for the degree of Doctor in Philosophy in the area of Experimental Biology and Biomedicine, specialization in Biotechnology and Health

UNIVERSIDADE DE COIMBRA

“One day, when *you look back*, *you*'ll *see* that the *most beautiful days* were *those* in which *you fought*.”

Sigmund Freud

To my parents and grandparents

To Renato

AGRADECIMENTOS

No fim desta etapa, nada faz mais sentido do que agradecer às pessoas que me acompanharam e me apoiaram, e que de uma forma ou de outra modelaram aquilo que sou hoje.

Ao meu orientador, **Dr Lino Ferreira**, agradeço por me ter aceite no seu grupo de investigação e por me ter proporcionado todas as condições de trabalho que permitiram o desenvolvimento deste projecto, bem como pela imensa contribuição na idealização, realização e discusão de todos os resultados presentes nesta tese. Gostaria também de agradecer por toda a paciência e apoio ao longo destes anos e por me lembrar sempre que sou uma Mulher do Norte.

To my co-supervisor **Dra Marie-Pierre Dehouck** I would like to thank for accepting to be part of this cotuttele project and for all the help during my briefs stays in Lens. I would like to thank for being always available to help me with my doubts along these years, and for all the scientific contributions. To **Dr Roméo Cecchelli** I would like to thank for receiving me in Lens, providing me all the necessary means to perform the experimental work and for all the scientific contributions.

Ao Professor **João Ramalho** e ao respectivo comité de avaliação um muito obrigada por me terem escolhido para fazer parte da X Edição do PDBEB.

À **Susana Rosa** agradeço por toda a ajuda, paciência e orientação que foram cruciais para o desenvolvimento deste trabalho. Obrigada por todos os conhecimentos transmitidos e discussão constante dos resultados. Acima de tudo Su, agradeço-te pela amizade que construímos nestes 5 anos!

To **Akhilesh Rai**, I would like to thank for all the help in the laboratory, for all the suggestions and discussions of the work.

Aos meus amigos da X Edição do PDBEB, **André**, **António**, **Dominique**, **Joana**, **João**, **Marcelo**, **Maríline**, **Patrícia**, **Sara**, **Sofia** e **Tânia** muito obrigada por serem quem são. O nosso primeiro ano foi sem dúvida memorável! Um agradecimento especial ao **André**, à **Joaninha** e à **Sarocas** por estarem sempre presente.

Aos meus colegas do laboratório por tornarem todos os dias de trabalho mais alegres. Apesar de muitos, somos sem dúvida um grupo Fantástico!

To **Emmanuel Sevin** and **Lucie Dehouck** I would like to thank for being always available to help me and to answer to all of my doubts. I will never forget your help during my visits to Lens.

À **Liliana Bernardino** e **Tiago Santos** pela colaboração nas experiênias *in vivo* e por estarem sempre disponíveis para as discussões científicas.

As amizades que se construíram ao longo deste percurso. À **Paty**, à **Xica** (já és mais antiguinha tu!!), à **Su**, à **Helena**, à **Sandra**, à **Susana**, ao **Migas**, ao **Bitó,** ao **Quartins** e ao **Luís** obrigada pelo apoio, pelas belas gargalhadas e por toda a ajuda em momentos de desespero.

Às amizades de sempre, **Mi**, **Raquelita**, **Luisito** e **Miguelito**, que apesar dos km que nos separam estão sempre perto. Obrigada pela amizade, pelo carinho e pela paciência das minhas ausências. Obrigada pelos bons momentos que partilhamos e pelas memórias que criámos. Apesar da distância, é bom sentir que quando estamos juntos é como se não tivesse passado sequer um dia!

Às minhas meninas **Carlinha**, **Anocas**, **Maroca** e **Ritxinha** obrigada pela amizade e por toda a preocupação. Apesar da distância, vocês estão sempre perto.

À minha família, aos meus **avós**, aos meus **tios** e aos meus **primos** obrigada pelo amor e pela preocupação. Não há nada melhor que ir a casa para ter um bom jantar de Família! À minha família do Luso, **Dona Ana Maria**, **Sr Zé**, **Sofia**, **Alexandre** e os piqueninos **Francisca** e **Henrique** obrigada por me fazerem sentir como parte da família. Obrigada por todo o carinho e amor!

Gostaria de dedicar esta tese aos meus pais, **Lucinda** e **Fernando** porque aquilo que sou hoje é sem dúvida graças a vocês. Muito obrigada por tudo, por me terem acompanhado sempre nesta jornada, por terem sempre acredito em mim mesmo nos momentos em que eu mais duvidava. Foi o vosso amor, carinho e incentivo que sempre me fez lutar pelos meus sonhos.

O meu ultimo e mais especial agradecimento vai para o **Renato**. Obrigada por todo o amor, paciência e compreensão! É bom saber que posso contar contigo Sempre… Não há palavras para descrever a importânica que tens na minha vida, mas espero que as minhas acções mostrem todos os dias o quanto és Importante! Tenho a certeza que o nosso futuro será recheado de momentos especiais…

SUPPORT AND FINANCIAL ACKNOWLEDGMENTS

This work was conducted at the Center for Neuroscience and Cell Biology (CNC) of Coimbra University, under the scientific supervision of Doctor Lino da Silva Ferreira and Professor Marie-Pierre Dehouck from Artois Univsersity. Part of this work was also performed in the Laboratoire de la Barrière Hémato-Encéphalique (LBHE) at Artois University.

Catarina Praça de Almeida was a student of the Doctoral Programme in Experimental Biology and Biomedicine coordinated by the Center for Neuroscience and Cell Biology (CNC) of Coimbra University and a recipient of the fellowship SFRH/BD/51667/2011 from the Portuguese Foundation for Science and Technology (FCT). The execution of this work was supported by FCT and FEDER/COMPETE (StrokeTherapy project and UID/NEU/04539/2013), the European Research Council (Nanotrigger: 307384), COMPETE2020 and *Conselho de Reitores das Universidades Portuguesas* (CRUP).

PUBLICATIONS AND COMMUNICATIONS

Publications

Saraiva C.*, Praça C. *, Ferreira R., Santos T., Ferreira L. and Bernardino L., *Nanoparticle-mediated brain drug deliver: Overcoming blood-brain barrier to treat neurodegenerative disease*, Journal of Controlled Release (2016), pp 34-47.

Pitrez P. R., Rosa S.C., Praça C., Ferreira L., *Vascular disease modeling using induced pluripotent stem cells: Focus in Hutchinson-Gilford Progeria Syndrome*, Biochem Biophysl Res Commun (2015) pp 1-9.

Cecchelli R., Aday S., Sevin E., Almeida C., Culot M., Dehouck L., Coisne C., Engelhardt B., Dehouck MP., Ferreira L., *A Stable and Reproducible Human Blood-Brain Barrier Model Derived from Hematopoietic Stem Cells*, Plos One 9 (2014), pp 1-13.

Praça C., Rosa S.C., Cecchelli R., Dehouck MP. and Ferreira L., *Derivation of brain-like endothelial cells from iPSC-derived endothelial progenitor cells.* (Manuscript in preparation).

Praça C., Rai A., Santos T., Cecchelli R., Dehouck MP., Bernardino L. and Ferreira L. *Targeting the brain: Enhanced brain accumulation of nanoparticles by fine-tuning surface chemistry.* (Manuscript in preparation).

Communications

German-Portuguese Student Workshop within the DAAD-Programme “Dialogue with Institutions of Higher Education in Southern Europe” Translation in Biomaterials and Stem Cell Research - Cantanhede, Portugal, 7-8 July 2016. Invited speaker*: Targeting the brain: Enhanced brain accumulation of nanoparticles by fine-tuning surface chemistry.*

PhD in Experimental Biology and Biomedicine. Advanced Therapies Module. Cantanhede, Portugal, 13-17 June 2016. Invited speaker: *BBB models for Drug Delivery and Disease Modeling.*

5th International Iberian Biophysics Congress – Oporto, Portugal, 15-17 June 2016. Oral presentation: Praça C., Rai A., Santos T., Cecchelli R., Dehouck MP., Bernardino L. and Ferreira L. *Targeting the brain: Enhanced brain accumulation of nanoparticles by fine-tuning surface chemistry.*

10th World Biomaterials Congress – Montreal, Canadá, 17-22 May 2016. Poster: Praça C., Rosa S.C., Cecchelli R., Dehouck MP. and Ferreira L. *Derivation of a human in vitro BBB model from hiPSCs.*

XIII Annual Meeting Center for Neuroscience and Cell Biology and Annual Meeting of the PhD Programme in Experimental Biology and Biomedicine – Coimbra, Portugal, 17-18 December 2015. Poster: Praça C., Rosa S.C., Cecchelli R., Dehouck MP. and Ferreira L. *Derivation of a human in vitro BBB model from hiPSCs.*

9th International Meeting of the Portuguese Society for Stem Cells – Oeiras, Portugal, 15-16 October 2015. Poster: Praça C., Rosa S.C., Cecchelli R., Dehouck MP. and Ferreira L. *Derivation of a human in vitro BBB model from hiPSCs*.

Workshop Hovione-MIT – Lisbon, Portugal, 30 June 2014. Poster: Cecchelli R., Aday S., Sevin E., Almeida C., Culot M., Dehouck L., Coisne C., Engelhardt B., Dehouck MP., Ferreira L., *A Stable and Reproducible Human Blood-Brain Barrier Model Derived from Hematopoietic Stem Cells.*

Patents

Praça C., Rai A. and Ferreira L. Preparation of NPs and functionalization with transferrin. PAT20161000039889.

TABLE OF CONTENTS

LIST OF FIGURES

LIST OF TABLES

ABSTRACT

The blood-brain barrier (BBB) is a dynamic and complex structure that physically separates the bloodstream from the brain being responsible for its homeostasis and protection. *In vitro* BBB models are important to understand the crucial steps that occur during BBB development and maintenance. Moreover, they allow to disclosure important features related to the transport mechanisms of neuropharmaceuticals and nanoformulations from the blood to the brain.

During the development of this PhD thesis, two major projects were fostered in order to understand the role of soluble and non-soluble cues in the process of BBB differentiation/development, and how different parameters can affect the nanoformulations targeting to the brain neurogenic niches. In the first work, we have generated brain-like endothelial cells derived from induced pluripotent stem cells (iPSCs), using a novel methodology of a two-step differentiation protocol. The iPSCs cells were initially differentiated into endothelial progenitor cells followed by the induction of BBB properties with a combination of soluble factors and extracellular matrices. Our results show that soluble factors, namely vascular endothelial growth factor, Wnt3a and retinoic acid are crucial for the induction of the BBB phenotype as observed by a better maintenance of the endothelial markers and BBB functionality. In the second work, we have combined three major elements in the nanoformulations, *i)* nanoparticles morphology, *ii)* transferrin (Tf) peptide density on the surface of the nanoparticles and *iii)* responsiveness to light stimuli, to fine-tune the BBB penetration, and more importantly to promote the accumulation of the nanoformulations in the neurogenic niches. Results obtained in a human *in vitro* BBB model, derived from hematopoetic stem cells, showed that spherical (Au NPs) and rod shape (Au NRs) nanoparticles conjugated with a number of Tf peptides between 169 and 230 crossed more efficiently the barrier than formulations with higher or lower peptide density per nanoformulation. Using mice animal model, we further showed that intravenously administered of Au NRs-Tf_{169} activated by a near infrared light had the highest accumulation in the neurogenic niches. Moreover, we have proved with this work, that our human BBB *in vitro* model, derived from hematopoietic stem cells, is able to predict in a reliable manner the *in vivo* outcome.

With these two works we were able to give a step forward into a deep understanding of the crucial factors involved in the BBB development and the mechanisms underlying the BBB crossing and particularly the targeting to the neurogenic niches.

RESUMO

A barreira hemato-encefálca (BHE) é uma estrutura complexa e dinâmica que separa fisicamente a corrente sanguínea do cérebro, sendo a principal responsável pela proteção e homeostasia deste. Os modelos *in vitro* de BHE têm sido importantes não só na compreensão das diferentes fases de desenvolvimento e manutenção desta barreira, mas também no estudo detalhado dos mecanismos de transporte de neuro-fármacos e nanoformulações da corrente sanguínea para o cérebro.

Durante esta tese de doutoramento, foram desenvolvidos dois projetos distintos que no essencial ambicionam compreender o papel de fatores solúveis e não solúveis no processo de diferenciação/desenvolvimento da BHE e avaliar o impacto de diferentes parâmetros físico-químicos na permeação da BHE e acumulação nas diferentes regiões neurogénicas. Num primeiro trabalho, células endoteliais com fenótipo semelhante às de cérebro foram derivadas a partir de células estaminais com pluripotência induzida (iPSCs), usando um protocolo inovador de diferenciação. O protocolo desenvolvido consiste em duas fases distintas, em que inicialmente as iPSCs foram diferenciadas em células endoteliais progenitoras, seguido pela indução de propriedades de BHE através da combinação de fatores solúveis e matriz extracelular. Os resultados obtidos demonstram que os fatores solúveis, nomeadamente o factor de crescimento vascular endotelial, Wnt3a e o ácido retinóico, mantêm de forma consistente os marcadores endoteliais e a funcionalidade da BHE nestas células, apresentando-se como fatores cruciais para a indução do fenótipo de BHE. No segundo trabalho, combinámos três elementos fundamentais em diferentes nanoformulações *i)* morfologia da nanopartícula, *ii)* densidade de peptídeo de transferrina (Tf) na superfície da nanopartícula e *iii)* capacidade de resposta a um estímulo de luz, que nos permitem modelar a permeação da BHE e essencialmente, promover a acumulação das nanoformulações nos nichos neurogénicos. Observou-se usando um modelo *in vitro* da BHE, derivado de células estaminais hematopoiéticas, que as nanopartículas esféricas (Au NPs) e em forma de bastão (Au NRs), quando conjugadas com um número de peptídeos de Tf entre 169 e 230, atravessam de forma mais eficiente a BHE. Adicionalmente, em murganhos, demonstrou-se que a administração na veia da cauda de Au NRs-Tf_{169} apresentam uma maior acumulação nas regiões neurogénicas, quando ativados por luz próxima do infra vermelho. Com este estudo, fomos também capazes de confirmar que o nosso modelo *in vitro* de BHE, obtido a partir de células estaminais hematopoiéticas, é capaz de prever os resultados obtidos *in vivo*.

Com estes dois trabalhos, desenvolvidos ao longo desta tese de doutoramento, fomos capazes de avançar na compreensão dos fatores cruciais envolvidos no desenvolvimento da BHE e dos mecanismos subjacentes à capacidade de permeação da BHE pelas nanoformulações, e em particular o direcionamento para os nichos neurogénicos.

RÉSUMÉ

La barrière hémato-encéphalique (BHE) est une structure dynamique assurant l'homéostasie du tissu cérébral. Localisée au niveau des cellules endothéliales des capillaires cérébraux, elle constitue un filtre sélectif entre le compartiment sanguin et le compartiment cérébral. L'utilisation de modèles *in vitro* permet l'étude du développement et du maintien du phénotype de la BHE. Elle permet également de comprendre la fonctionnalité de la BHE notamment les mécanismes de transport qui interviennent lors des échanges spécifiques entre les compartiments sanguin et cérébral.

Dans un premier temps, de façon à étudier, *in vitro*, le rôle de différents facteurs dans le développement de la BHE, la différenciation de cellules endothéliales cérébrales a été réalisée à partir de cellules pluripotentes induites. Les résultats montrent que les facteurs solubles en particulier le VEGF, Wnt3a et l'acide rétinoïque sont cruciaux pour l'induction du phénotype de BHE dans les progéniteurs vasculaires.

Dans un deuxième temps, le ciblage de niches neurogènes a été exploré *in vivo* en fonction de la formulation de nanovecteurs. En combinant 3 éléments majeurs de la formulation (morphologie, densité de la transferrine en surface et réponse à la lumière), l'accumulation des nanoparticules a été favorisée au niveau des niches neurogènes montrant ainsi que la pénétration cérébrale a été améliorée. L'utilisation en parallèle d'un modèle cellulaire de BHE réalisée à partir de cellules souches hématopoïétiques, a montré que les résultats obtenus *in vitro* prédisent de façon fiable, l'augmentation du passage à travers la BHE observée *in vivo.*

LIST OF ABBREVIATIONS

γ-GT	γ-glutamyl transpeptidase
ABC	ATP-binding cassette transporters
AJ	Adherent junction
Ang	Angiopoietin
Au	Gold
BBB	Blood-brain barrier
bBCECs	Bovine brain capillary endothelial cells
BCRP	Breast cancer resistance protein
bFGF	Basic fibroblast growth factor
BLECs	Brain like-endothelial cells
BM	Basal media
BM	Basement membrane
BMVECs	Brain microvascular endothelial cells
BMP	Bone morphogenic protein
BSA	Bovine serum albumin
$CD31^+$	Endothelial progenitor cells
CDM	Chemically defined medium
CNS	Central nervous system
CSF	Cerebrospinal fluid
DAPI	4', 6' –diamidino-2-phenylindole
DG	Dentate gyrus
DMEM	Dulbecco's modified eagle medium
DNA	Deoxyribonucleic acid
EBs	Embryonic bodies
ECs	Endothelial cells
ECM	Extracellular matrix
EDTA	Ethylenediamine tetraacetic acid
EGM	Endothelial growth medium
ESCs	Embryonic stem cells
eNOS	Endothelial nitric oxide synthase
FBS	Fetal bovine serum
FGF	Fibroblast growth factor

Glut-1	Glucose transporter 1
GNDF	Glial-derived neurotrophic factor
GUK	Guanylate kinase homologs
HUVECs	Human umbilical vein endothelial cells
ICAM	Intracellular adhesion molecule
ICP-MS	Inductively coupled plasma mass spectrometry
iNOS	Inducible nitric oxide synthase
IMDM	Iscove's modified dulbecco's medium
iPSCs	Induced pluripotent stem cells
JAM	Junctional adhesion molecules
LDL	Low-density lipoprotein
LY	Lucifer Yellow
MACS	Magnetic activated cell sorting
MAGUK	Membrane-associated guanylate kinase homologs
MAO	Monoamine oxidase
MMP	Metalloproteinase
MNCs	Mononuclear cells
MRI	Magnetic resonance imaging
MRP	Multidrug resistance protein
MW	Molecular weight
NPs	Nanoparticles
NPC	Neural progenitor cell
NSC	Neural stem cell
NRs	Nanorods
NVU	Neurovascular unit
RA	Retinoic acid
ROS	Reactive oxygen species
RT	Room temperature
PAPP	Apparent permeability
PAMAM	Poly(alkylcyanoacrylates),poly(amidoamine)
PASA	Poly(lysine), poly(aspartic acid)
PBS	Phosphate- buffered saline
PCL	Poly(ε-caprolactone)
PDGF	Platelet-derived growth factor
PDGFR	Platelet-derived growth factor receptor
PEG	Poly(ethylene glycol)

PEI	Poly(ethylenimine)
Pen-strep	Penicillin- streptomycin
PET	Positron emission tomography
PFA	Paraformaldehyde
Pgp	P-Glycoprotein
PLA	Polyesters (poly(lactic acid)
PLGA	Poly(lactic-co-glycolic acid)
PSCs	Pluripotent stem cells
RNA	Ribonucleic acid
TEER	Transendothelial electrical resistance
TEM	Transmission electron microscopy
Tf	Transferrin
TGF	Transforming growth factor
TJ	Tight junctions
TEM	Transmission electron microscopy
TNF	Tumor necrosis factor
S1P	Sphingosine-1-phosphate
SEM	Scanning electron microscopy
SGZ	Subgranular Zone
SLC	Solute carrier
Shh	Sonic hedgehog
SPR	Surface plasmon resonance
SVZ	Subventricular zone
UV	Ultra-violet
VCAM	Vascular cell adhesion molecule
VE-cadherin	Vascular endotlehial cadherin
VEGF	Vascular endothelial growth factor
Vis	Visible
vWF	von Willebrand Factor
ZO	Zonnula Occludens

Chapter 1

RESEARCH AIMS AND THESIS OUTLINE

RESEARCH AIMS AND THESIS OUTLINE

The present thesis explores the generation of iPSCs-derived brain like-endothelial cells, using a well define population of vascular progenitor cells and the development of nanoformulations that are able to cross the blood-brain barrier targeting specifically the neurogenic niches.

The thesis is divided in 6 chapters:

The present section (**Chapter 1**) introduces the main goals that drove the following thesis.

Chapter 2 overviews the fundamental concepts of the blood-brain barrier, the use of pluripotent stem cells to derive endothelial cells and human *in vitro* BBB models. Also revise the main factors that can influence the brain targeting by nanoparticles, specially the target to the neurogenic niches.

Chapter 3 presents experimental data regarding the generation of human brain like-endothelial cells from iPSCs. It describes the role of soluble (inductive factors) and insoluble cues (extracellular matrix) in this differentiation and maturation process.

Chapter 4 presents experimental data related to the development of nanoformulations able to cross the blood-brain barrier *in vitro* and *in vivo* and target to the neurogenic niches.

Chapter 5 discusses the overall experimental results, summarizing the relevant findings described in the preceding chapters.

Chapter 6 gathers the future studies that emerged from the questions still open in the present thesis.

Chapter 2

STATE OF THE ART

2.1. BLOOD BRAIN BARRIER

2.1.1.GENERAL OVERVIEW: WHY GOOD BBB MODELS ARE NEEDED?

The central nervous system (CNS) is a fragile structure that needs to be protected in order to maintain the neuronal microenvironment homeostasis for its properly function. The barriers of the brain are responsible for protecting the brain from the entry of toxic molecules and pathogenic organisms, while supplying the brain with metabolites, nutrients and hormones [1]. There are four principal barriers between the brain and the blood responsible for this regulation [2-5].

1. Blood - cerebrospinal fluid (CSF) barrier: formed by the epithelial cells of the choroid plexus, which lies in the four ventricles of the brain. This structure is formed by fenestrated capillary endothelial cells (ECs) and tight junctions (TJs) linking the epithelial cells;
2. CSF – brain barrier: this barrier is only present in the embryo and results from the separation of the ventricular system from the extracellular fluid of the brain;
3. Arachnoid barrier: is a multilayer formed by closely adhering cells with TJs in the inner layer that lies under the dura mater involving the brain
4. Blood-brain barrier (BBB) (**Figure 2.1A**): this barrier is formed by the brain ECs that line the walls of the capillaries, creating a large interface for blood-brain exchanges. Together with the pericytes, astrocytes, microglia, neurons and basement membrane they form the neurovascular unit (NVU) (**Figure 2.1**). The BBB is present in all brain regions with the exception of the regions controlling the autonomic nervous system and the endocrine glands of the body.

Among the barriers of the brain, the BBB (**Figure 2.1A**) is the most studied and the most well documented. The first concept of the BBB appeared in the Nineteenth century by Claude Bernard, a French physiologist that said *"La fixité du milieu intérieur est la condition d'une vie libre et indépendante"*. The clear demonstration of an existing BBB between the brain and the bloodstream came later on by Paul Ehrlich [6, 7] followed by complementary studies by his student Edwin Goldman [8]. The BBB should be perceived as a physical and dynamic barrier, responsible for the restriction of noxious substances

entry into the brain and for facilitating the entry of essential nutrients for brain cells normal metabolism [1, 9]. Also, the presence of a set of intracellular and extracellular enzymes, confers to the BBB the notion of a metabolic barrier capable of inactivating several neuroactive and toxic compounds [2, 9]. Under pathological conditions such as stroke, infectious diseases, brain trauma, and neurodegenerative disorders (e.g. Alzheimer's and Parkinson's disease and multiple sclerosis) the integrity of the BBB is affected and thus its permeability (**Figure 2.1B**) [9-11].

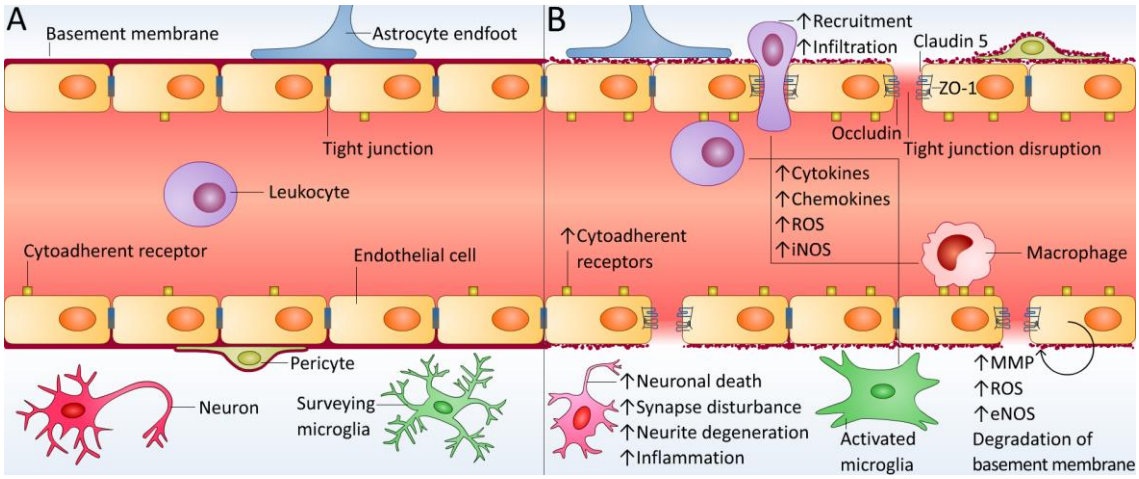

Figure 2.1 - BBB composition in a health and disease state. A| The BBB is mainly composed of vascular ECs, highly connected by adherent (AJs) and tight (TJs) junctions, and a sparse layer of pericytes. A basement membrane and a layer of astrocyte end-foot processes surround the endothelium. Neurons and surveying microglia are also important mediators of BBB integrity in physiological conditions. **B|** In pathological conditions several BBB alterations occur culminating in increased permeability. Increased matrix metalloproteinase (MMP) activity, higher reactive oxygen species (ROS) and nitric oxide levels (derived from endothelial cells — via endothelial nitric oxide synthase (eNOS) or from microglia/macrophage cells — via inducible NOS (iNOS)) along with release of cytokines and chemokines by activated microglia/macrophages lead to basement membrane degradation, TJ disruption (namely in occludin, zonula occludens (ZO) -1 and claudin-5 integrity) and an inflammatory response. Altogether these events culminate in neuroinflammation, leukocyte recruitment and brain parenchyma invasion, neuronal dysfunction and neurodegeneration.

Nowadays the researchers are focused in the development of more reliable *in vitro* BBB models that will allow the comprehension of the mechanisms involved in the cerebrovascular response to a number of physiological and pathological stimuli, investigating the signaling pathways involved in BBB development, homeostasis and disease. Furthermore, this will provide new strategies to accelerate the development of

new drug therapies for the treatment of neurodegenerative diseases and to identify potential toxicological effects of new drugs while reducing the use of animals [12]. In the drug discovery and development area, compounds identified by high-throughput screening need adequate characterization in terms of BBB permeability, metabolism and toxicity. The cost of advancing a compound to phase I trials can reach up to US$100 million and getting the drug to the market around US$1 billion [13]. The purpose of *in vitro* tests is to eliminate weak candidates. How the candidate drug penetrates the BBB is determinant for its efficacy and toxicity profile in clinical trials. Candidate drugs for CNS that have *in vitro* efficacy but are unable to penetrate BBB are unlikely to have *in vivo* efficacy in patients. In recent years, only 3-5% of CNS drugs have reach the market, and the principal reason for the low success is related to the failure in demonstrating efficacy in phase II studies [13]. By properly modulating the BBB [14], it is possible to make predictions whether the interaction of a compound with the BBB will compromise its functionality and therefore also cause unwanted, indirect effects on the brain *in vivo* [15], or whether a compound will reach the CNS compartment in significant amounts to have a direct effect on brain cells [16].

For the generation of a reliable *in vitro* BBB model is of must importance to understand the components of the functional NVU. This structure allows the brain protection and homeostasis, nevertheless some BBB plasticity for adaptation to changing conditions is needed. These different properties are due to many of the structural and functional aspects of the BBB components [17].

2.1.2.STRUCTURE

2.1.2.1. Brain Capillary Endothelial Cells

Brain ECs are located in the interface between the brain and the blood, being the main responsible for performing essential functions such as barrier, transport of nutrients, receptor-mediated signaling, leukocyte trafficking and osmoregulation [10]. These cells present special structure features, which allows them to perform these functions, namely the presence of TJs, adherent junctions (AJs) and junctional adhesion molecules (JAM) (**Figure 2.2**); a polarized surface between the apical and basal membranes and a negative surface charge generated by the presence of glycocalix [18] which repulse negatively charged compounds [1, 10, 14]. These ECs are linked to the

basal lamina by transmembrane proteins (selectins, immunoglobulin superfamily and integrins) that contribute also for intercellular adhesion [1]. Additionally, brain ECs perform a metabolic activity due to the presence of intracellular and extracellular enzymes such as monoamine oxidase (MAO), γ-glutamyl transpeptidase (γ-GT), alkaline phosphatase, several specific peptidases, nucleotidases and cytochrome P450 enzymes [14] (**Figure 2.2**).

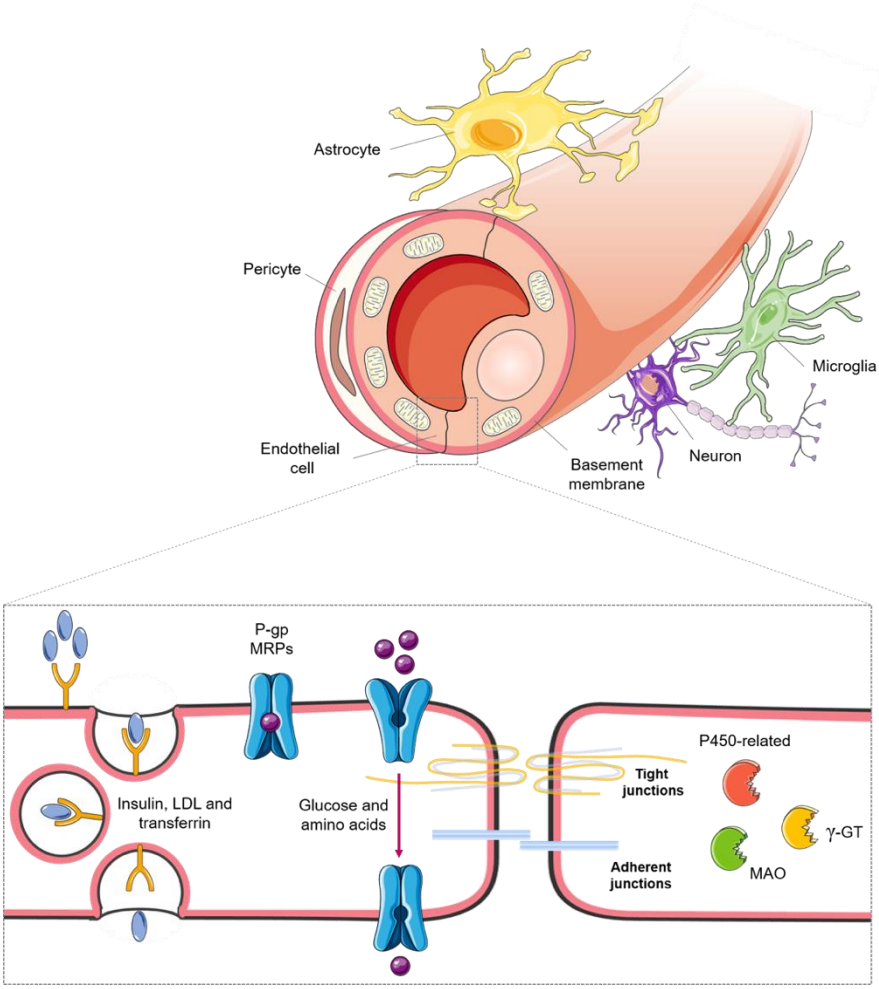

Figure 2.2 - NVU: Molecules and proteins expressed by the brain ECs. The cerebral ECs present a complex of TJ proteins that seal the paracellular permeability and AJ proteins which stabilize cell-cell interactions. The large presence of transporters and enzymes allow these cells, and consequently the BBB to perform their function. Large molecules can be transferred to the brain by adsorptive-mediated transcytosis or by receptor-mediated transcytosis, which includes receptors for insulin, low-density lipoprotein (LDL), iron transferrin (Tf) and leptin. Influx or efflux transporters are also present to do the uptake or extrusion of molecules into or out to the brain (Pgp, MRPs, glucose transporter and amino-acid transporters). Pgp, P-glycoprotein; MRP, multidrug resistance-associated protein.

Brain capillary ECs differ from the peripheral ECs due to their tightness which is 50-100 times higher than in peripheral ECs, causing a major restriction in the paracellular pathway of hydrophilic solutes [19]. Additionally, brain ECs present a thin cytoplasm (1.5 to 2 µm maximum [20]), without fenestrations and with very low pinocytic activity [21]. A high number and volume of mitochondria is also present, demonstrating the high energetic demand of these cells for the break down of molecules and also for the transport systems of nutrients and other molecules from into and out of the brain [10].

Tight Junctions

The TJs (**Figure 2.3**) are one of the major characteristic of the brain ECs, being the main responsible for BBB barrier properties [1]. They are also responsible for the ECs polarity, demonstrated by the asymmetric distribution of proteins (e.g. transporters) between the two cellular membranes (**Figure 2.2**) [17, 22]. These proteins seal the paracellular permeability between apical and basolateral plasma membrane to ions and polar solutes [3, 10, 17], and this blockage in the ion movement results in high electrical resistance potential [3, 17]. Another important function that as been proposed to the TJs is related with cell signaling. The TJs can either receive a stimulus from the cell interior to regulate their assembly and function, or can conduct information to the cell interior to regulate gene expression and subsequent cell responses, in a bi-directional cell signaling way. So, it has been proposed that these junctions are involved in control of gene expression, cell proliferation and differentiation [1]. These TJ proteins are a well organized and dynamic complex of proteins behind the tight regulation of the brain microenvironment, which are composed of a parallel, interconnected, transmembrane and cytoplasmatic proteins arranged as a succession of multiple barriers [21]. The proteins can be grouped according the number of times they crossed the membrane, either in single pass-membrane protein such as the JAM or in four-pass transmembrane protein such as the claudins and occludin. Cytoplasmic TJ accessory proteins, which combine the zonula occludens (ZO), cingulin, 7H6 and AF-6, are responsible for linking the TJ transmembrane proteins to the actin cytoskeleton (**Figure 2.3**) [1, 3, 5, 17].

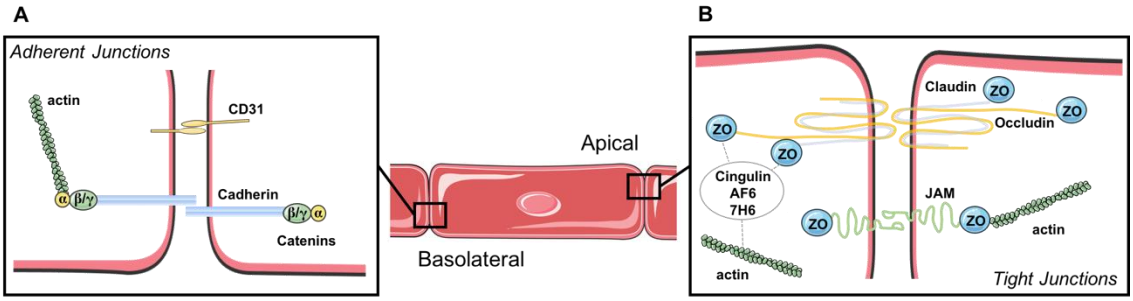

Figure 2.3 - Brain ECs present a complex of tight and adherent junctions localized in different regions of cell membrane. A| The AJs are located below the TJs and are composed by transmembrane glycoproteins linked to the cytoskeleton by cytoplasmatic proteins giving the tissue structural support. **B|** The TJs are localized in the apical part of the ECs forming a well organized and dynamic complex of transmembrane and cytoplasmatic proteins that seal the paracellular permeability.

Claudins

Until now, 24 members of this protein family have been described in mice and humans [1, 23]. The claudins, (**Figure 2.3**) with approximately 20-27 kDa, are phosphoproteins consisting of four transmembrane domains, being expressed in a tissue specific manner with most of the cell types expressing more than 2 isoforms [1]. Claudin-1, -3 and -5 are the mainly expressed in the brain microvascular endothelial cells (BMVECs) [10, 21, 22], and the loss of claudin-3 [24] or -5 [25] seems to compromised the BBB function *in vivo*. The claudin from one EC binds to the claudin of the adjacent EC and the COOH-cytoplasmatic terminal domain is responsible for the bind to the PDZ motifs of ZO proteins, important for the stabilization and assembly of the junctions [5, 17, 23]. It is believed that these proteins form the first seal of the TJ, controlling the passive diffusion to charged molecules [5, 22, 23], and for the recruitment of the occludin for the TJs [26].

Occludin

Occludin (**Figure 2.3**) is a transmembrane protein of approximately 60-65 kDa, with regulatory functions increasing electrical resistance and decreasing permeability across the barrier [27]. The 2 extracellular loops of claudin and occludin bind to form the paracellular component of the TJs, and, as described for claudins, its cytoplasmatic domain connects with ZO proteins, allowing the connection to the cytoskeleton [5, 10, 17]. This protein is highly expressed and shows a continuous stain in brain endothelium, contrarily to what is observed in the non-brain ECs [5, 21, 22]. It seems that occludin

expression is not essential for TJ formation, contrary to claudins, but it is crucial to enhance the TJ tightness, with its decrease is associated with disrupted BBB function in several disease states [28-30]. Recently, it has been demonstrated that occludin might be also important for epithelial cell differentiation [11] and regulation of several signaling pathways important for signal transduction [23].

Together, the presence and proper localization of claudins and occludin seems to be crucial for the correct function of the TJs and, consequently, for the proper role of the BBB.

Cytoplasmic accessory proteins

The cytoplasmatic proteins associated with the TJs are the ZO proteins, cingulin and 7H6, among others (**Figure 2.3**) [5]. The submembranous TJ-associated proteins ZO-1, -2 and -3 are members of the MAGUK (membrane-associated guanylate kinase homologs) family, which are characterized by the presence of PDZ domain, SH3 domain and guanylate kinase (GUK) homologs domain, responsible for the bind to TJs and AJs in addition to actin cytoskeleton [1, 23]. It has been reported that claudin proteins bind directly through their COOH-terminal to the PDZ domain of the ZO proteins and, on the other hand, the occludin interacts with the GUK domain of the ZO-1 protein. Importantly, actin recognize and binds to the COOH-terminal of the ZO-1 and -2 , providing the structural support needed to the ECs [5]. Indeed, the ZO proteins act as recognition proteins for TJ replacement and as structural support for signaling transduction proteins [31]. It was demonstrated that ZO-1 protein (220 kDa) is mostly expressed in the endothelial and epithelial cells that typically form the TJ assembly, binding the transmembrane TJ proteins to actin cytoskeleton [10]. Although, ZO-1 can also be expressed in cells that do not form TJs, there is no TJ without ZO-1 protein [1]. The loss or disarrangement of this protein from the TJ complex is associated with increase in barrier permeability [32]. ZO-2 protein (160 kDa) has shown a significant homology with ZO-1, binding to transmembrane proteins and transcription factors and, it is localized in the nucleus during stress and proliferation [1, 10]. On the other hand, ZO-3 is mainly concentrated in TJs of epithelial cells [10].

Taking all together, the cytoplasmatic ZO-1 and ZO-2 proteins binds the transmembrane proteins claudin and occludin to the actin cytoskeleton, creating a cross-link of elements that are crucial for the maintenance of the proper structure and function of the brain ECs.

Adherent Junctions

Below the TJs, in the basal region of the lateral plasma membrane, are localized the AJs (**Figure 2.3**) which are responsible for the adhesion of one cell to another providing structural support, besides the role in the phenomena of contact inhibition (natural process of cell growth arrest) during vascular growth and remodeling, initiation of cell polarity and regulation, at least in part, of paracellular permeability [1, 3, 22]. These proteins are another example of tightening structures between ECs, which are formed by a large family of single-pass transmembrane proteins, the cadherins, which in turn are, bond intracellularly to the catenins [1, 5]. The main component of the AJ, is the vascular endothelial (VE)-cadherin, a Ca^{2+}-dependent cell-cell adhesion protein that binds to extracellular domains of the proteins expressed in adjacent cells. On the other hand, the cytoplasmatic domain binds to beta or gamma catenin which in turns links to actin cytoskeleton via alpha catenin, holding the AJ complex [5, 22, 23]. Components of the TJ and AJ are known to interact with each other, in particularly the ZO-1 and catenins, which influences the TJ assembly [33]. The AJs are crucial for the formation of the TJs, and alterations and disruptions in these junctions leads to barrier disruption [3], namely increase in permeability [34].

Endothelial Transport Systems

Although there is a strong cohesive system keeping ECs tightly connected, the BBB sanctions the selective passage of cells and small molecules to the brain. Small molecules with correct lipophilicity, molecular weight (MW) and charge can diffuse from blood into the CNS. Nevertheless, the majority (98%) of small molecules (MW>500 Da) and almost all the large molecules (MW>100 kDa) do not cross the BBB [35, 36]. The mechanism of passage between ECs is named paracellular, and is utilized for ions and solutes that depend on a gradient of concentration. The passage occurring through ECs is termed transcellular, and the balance between paracellular-transcellular transport is decisive to define permeability in the healthy BBB (**Figure 2.4**) [21].

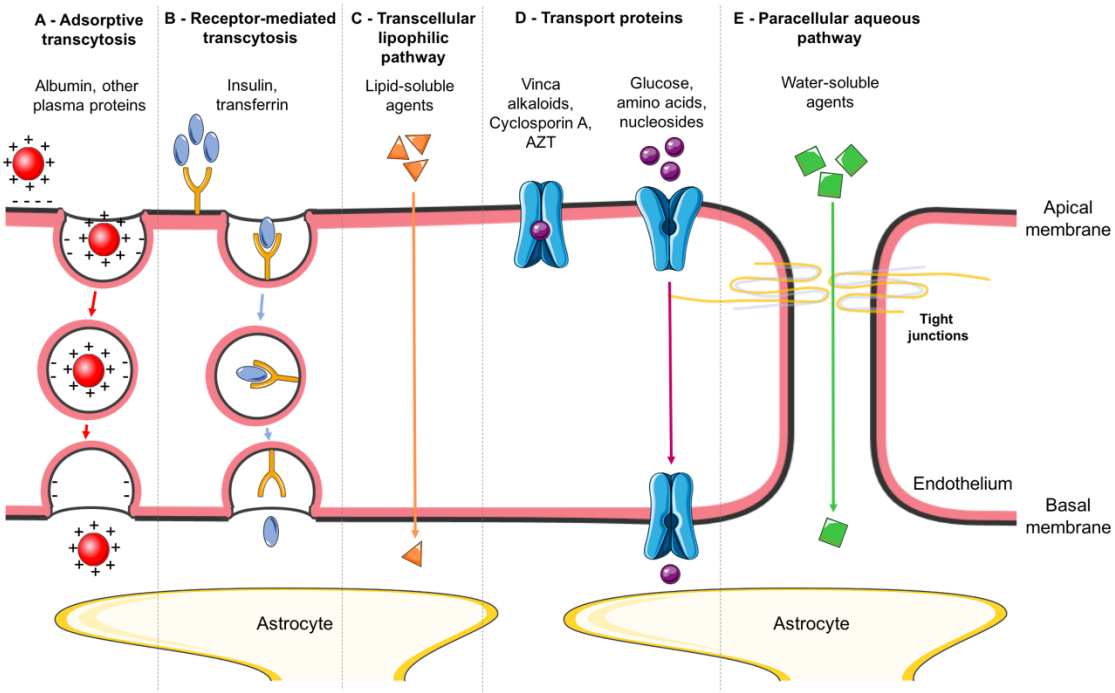

Figure 2.4 - The main transport systems across the BBB for molecular traffic. The BBB is highly selective, presenting specific mechanisms that allows a controlled crossing of molecules/cells into the brain parenchyma. **A|** Cationization of native molecules can increase their uptake by adsorptive-mediated endocytosis and transcytosis. **B|** Larger proteins, such as Tf and insulin are transported by receptor-mediated endocytosis and transcytosis. **C|** The large surface of the lipid membranes presents as effective route for passive diffusion of lipid-soluble molecules. **D|** The brain ECs present carriers for transport of several nutrients (e.g. glucose and amino acids); Some of these transporters are ATP-dependent and act as efflux pumps (e.g Pgp). **E|** TJs restrict the paracellular permeability of water-soluble compounds, including polar drugs. (Adapted from [2]).

The paracellular pathway (**Figure 2.4E**) is limited by the TJs, forcing most of the molecules to take another route [2]. In turn, the transcellular pathway allows the passive diffusion of lipophilic molecules, such as CO_2 and O2, and also of drugs like barbiturates and ethanol (**Figure 2.4C**) [3]. The solute carriers (SLC), which facilitates the transport of nutrients, include 300 members organized in 48 subfamilies [9], which are present in the cell membranes and it's expression and insertions can be polarized, resulting in a preferential flux from blood to brain or the other way around. One important member of this family is the glucose transporter-1 (Glut-1) responsible for glucose uptake which is highly expressed by the brain ECs (**Figure 2.4D**) [3, 9, 23]. Proteins and peptides, which are hydrophilic molecules, depend on specific types of transport to enter the brain. Molecules with an excess of positive charge can cross the endothelial layer by

adsorptive-mediated transcytosis (**Figure 2.4A**) (protamine, histones). On the other hand specific receptors expressed in the luminal side of the membrane involved in the transport of insulin or transferrin (Tf), among others, are responsible for the transcytosis receptor-mediated of these molecules (**Figure 2.4B**). In both cases, there is a formation of vesicles and a need to escape the lysosomal compartment to achieve a effective transcytosis [2, 3, 10]. This form of transport occurs via the formation of cellular invaginations known as caveolae [23]. This structure forms around the molecule to be transported to the brain or from the brain to the blood. Caveolin-1, a surface protein that is involved in this type of transport, is also known to regulate the expression of junction-associated proteins and metalloproteinase (MMP) activity [37, 38]. An important aspect, and one of the main reason why most of the molecules do not reach effectively the brain parenchyma by passive diffusion, is the presence of ATP-binding cassette (ABC) transporters containing 48 members grouped in 7 sub-families [3, 10, 14]. The most important BBB ABC transporters are the active efflux pumps, such us the P-Glycoprotein (Pgp), Multidrug Resistance-associated Proteins (MRPs) and Breast Cancer Resistance Protein (BRCP) that are predominantly expressed in the luminal side of the membrane, transporting neurotoxic lipid-soluble molecules or other pharmaceutics drugs from the brain capillary endothelium and CNS into the blood circulation (**Figure 2.4D**) [3, 10, 39].

2.1.2.2. Pericytes

Pericytes are an important cellular component of the BBB communicating actively with other cells of the NVU, namely with the ECs in abluminal face and astrocytes in the luminal face (**Figure 2.2**) [40]. They are flat, undifferentiated and contractile connective tissue cells that develop around the capillary walls, being embedded within the basal lamina of microvessels, sharing the same basement membrane (BM) with the ECs [1, 10]. The degree of vascular coverage by the pericytes depends on the tissue type and seems to correlate with the tightness of the interendothelial junctions. It is known that the CNS microvessels are highly coverage by the pericytes, however the real extension is not entirely consensual [41]. Due to their localization, vascular pericytes synthesizes several components of the BM, including several proteoglycans and laminal proteins [42, 43]. Direct connections between the pericytes and ECs are through gap junctions, TJs, adhesion plaques and soluble factors such as transforming growth factor (TGF)-β, angiopoietin 1 (Ang 1), platelet-derived growth factor (PDGF)-β, sphingosine-1-phosphate (S1P) and Wnt [44-47]. *In vitro*, pericytes are able to increase BBB properties,

such as increase transendothelial electrical resistance (TEER), decrease permeability to Lucifer yellow and increase the expression of TJ proteins and transporters in the brain ECs [47-50]. Interestingly, Daneman *et al*. [51] showed in mice with null and hypomorphic alleles of *pdgfrb*, that pericytes are needed during BBB development, by inducing an important inhibition of molecules that increase vascular permeability and immune cell filtration, but contrarily to the expected, do not induce BBB-specific gene expression. Similar, Armulik *et al.* [52], have shown that BBB markers are unaffected by pericytes deficiency at mRNA levels, but there is an increase in permeability by endothelial transcytosis. Moreover, pericytes seems to induce polarization of the astrocytes end-feet surrounding the CNS blood vessels.

2.1.2.3. Glial Cells

The close anatomical association of astrocytes and ECs (**Figure 2.2**), allows them to influence each other structure, being critical for the BBB development and/or maintenance [10, 22]. Astrocytes end-feet form a rosette-like structure closely opposed to the outer surface of the vessel endothelium, and these vessels can be covered with multiple end-feet originated from different astrocytes [1, 19, 53]. Astrocytes present a molecular and structural heterogeneity which is responsible for the astrocytes polarization. Vascular abluminal face present several specialized proteins, such as Glut-1, Pgp, purinergic and adrenergic receptors [53], and on the other hand, a high density of water channel aquaporin 4 and Kir4.1 potassium channel that are important for ion and volume regulation are present in the end-feet of the astrocytes [2, 53]. These glial cells promote extracellular matrix (ECM) proteins production, like proteoglycan, fibronectin and laminin [1, 42] and induce BBB functions by secreting several chemical agents, such us TGF-β, basic fibroblast growth factor (bFGF), Ang-1 and glial-derived neurotrophic factor (GNDF) [2, 9, 54]. Several *in vitro* studies showed that brain ECs coculture with astrocytes or astrocytes-conditioned medium leads to an improvement in the BBB properties by up-regulating TJ proteins (e.g. ZO-1 and occludin), efflux transporters (e.g. Pgp), reducing permeability and increasing TEER [49, 53, 55, 56], suggesting that the importance of the astrocytes in the BBB is mainly due to the secretion of the soluble factors. Recently, Alvarez *et al.* [57] and Mizee *et al.* [58], have shown that astrocytes promote BBB formation and integrity along the embryonic development and adulthood by secreting sonic hedgehog (Shh) and retinoic acid (RA), respectively. The activation of both signaling pathways improves the BBB properties by increasing the TJ

proteins levels, decreasing permeability and increasing TEER; and *in vivo* the blockage of these pathways increase the extravasation of fluorescent tracers [57, 58] and perivascular blood-derived leucocytes [57].

2.1.2.4. Microglia and Neurons

The role of neurons and microglia in the BBB development and function is still unknown, however due to the close proximity of neurons and microglia in the perivascular space (**Figure 2.1**) is plausible to assume that their interaction with the brain ECs may contribute for BBB properties [1]. Indeed, 3 works by Eric Shusta's group [59-61] has shown that neural progenitor cells (NPCs) may modulate the BBB properties *in vitro* (this topic will be further explore in the next section). Different types of neurons, such as noradrenergic, serotonergic, cholinergic and GABAergic, can innervate the brain ECs and/or be associated with astrocytic processes [10, 22], and a mature endothelium is responsible for keeping the brain microenvironment stable that leads to a proper neuronal activity [1]. Microglial cells are important due to their immunological role, however their contribution for BBB properties is not well understood [1, 9].

2.1.2.5. Basement Membrane – The Extracellular Matrix

In addition to all the cellular components of the NVU, the ECM of the BM is also an essential part of the BBB (**Figure 2.2**). It surrounds and interacts with the brain ECs, engulfs the pericytes and serves as anchor for the cells to be kept in the right place establishing the link with the neighboring brain resident cells [1]. Both ECs, pericytes and astrocytes contribute to generate and maintain the BM, which is formed by three opposed laminas composed by different ECM proteins [10, 42]. The BM is composed by structural elements (e.g. type IV collagen and elastin), specialized proteins (e.g. laminins, vitronectin and fibronectin) and proteoglycans (e.g. heparin sulfate proteoglycans, perlecan and agrin); and also by matrix adhesion receptors and signaling proteins [1, 42]. The two main types of receptors/adhesion proteins present in the BBB and involved in the cell-cell and cell-matrix interactions, are the integrins and dystroglycan, which are expressed by the ECs, astrocytes and pericytes. These receptors are responsible for regulating signaling pathways which allows cell adaptations to changes in the

microenvironment, and to form a physical link between the ECM and the cytoskeleton keeping the cells in place and regulating their motility [22, 42]. Matrix proteins have been shown to influence the expression of TJ proteins [62, 63], and the disruption of the ECM has been strongly associated with a increased BBB permeability in several CNS pathologies [11, 42]. Moreover, ECM produced by cells forming the NVU (astrocytes and pericytes) improve the BBB function of porcine BMVECs assessed by an increase in cell impedance *in vitro* [64], which was consistent with the increase expression of TJ proteins [65].

All the constituents of the BBB, either cellular or not, are fundamental contributors of the barrier integrity. If one of these elements fails, a breakdown of the BBB occurs leading to dramatic consequences, such us neuroinflammation and neurodegeneration. Taking in account this well orchestrated NVU, it is important to understand the mechanisms and signaling pathways involved in the development and maintenance of the BBB.

2.1.3.BBB DEVELOPMENT AND MAINTENANCE

The development of the BBB is a multistep process that comprises three distinct phases: (1) angiogenesis; (2) differentiation/maturation and (3) maintenance **(Figure 2.5**) [66, 67]. The initial phase of the BBB development, starts with the ECs proliferation, sprouting and migration from pre-existing vessels into the embryonic neuroectoderm, giving rise to new vessels. These early sprouts already present some BBB properties, such us expression of TJ proteins and nutrient transporters. The angiogenesis event occurs due to the secretion of several factors by the NPCs, including vascular endothelial growth factor (VEGF), which is the major player in the sprouting of ECs [66, 67]. Other factors, like Ang-1 and -2 are also expressed by neurons in the vicinity of the neuroectoderm invading vessels, suggesting a role in the angiogenic phase [66, 68-70]. Despite the importance of these factors in the angiogenic process, these mechanisms also occur in a similar way outside the brain, suggesting that these factors are not the main responsible for the specification of the ECs into a BBB phenotype [71]. Several studies have suggested that Wnt-β-catenin pathway is crucial for the CNS angiogenesis, but not for the non-neural tissues. Stenman *et al.* [72] showed that large areas of the neuroepithelium of the developing CNS express Wnt7a and Wnt7b, promoting the vascular formation and the initiation of the BBB development. The absence of the Wnts

causes abnormal vascular sprouting, severe vascular leakage and absence of Glut-1 expression. Similar, Daneman *et al.* [73] has reported that the Wnt-β-catenin pathway is activated in the CNS ECs during embryogenesis, event not observed in the non-neural tissues. The blockage of this pathway *in vivo*, leads to vessel number reduction, capillary bed loss and hemorrhagic vascular malformations in CNS. Their work identified also Wnt7a and Wnt7b as required for normal angiogenesis in ventral regions of the CNS, regulating the expression of several transporters, including the Glut-1 transporter, but not of TJ proteins. Moreover, Liebner and co-authors [74] reported that Wnt3a, but not Wnt5a, is required for the initiation of BBB formation in mice ECs, enhancing claudin-3 expression at gene and protein levels. In a transgenic mouse model, the expression of plasmalemmal vesicle-associated protein-1 and claudin-3 correlates with the gain or loss of β-catenin activity while claudin-5 expression was only affected by the loss of β-catenin activity. These results indicate that claudin-3 is a downstream player of the Wnt-β-catenin pathway, whereas claudin-5 is more ubiquitous and more stably expressed. These results further suggest that claudin-3 has a major role in the BBB phenotype and together with claudin-5 maintains the low permeability of the barrier.

The second stage of the BBB development starts with the recruitment of pericytes and lately of astrocytes to cover the ECs, which is responsible for the differentiation and maturation of the BBB [66, 67]. The brain ECs of the new vessels secret PDGF-β recruiting the pericytes that express PDGFR-β to the endothelial surface. The cross-talk between the ECs and the pericytes occurs in a bi-direccional way through the TGFβ pathway. This leads to an up-regulation of endothelial-cadherin-2 in the ECs, responsible for the firm adhesion between the two cells, and the secretion of ECM proteins by the pericytes contributing for the BM formation. Also, when pericytes are proper located they limit the permeability of ECs by producing Ang-1 [67]. The suitable coverage of the ECs by the pericytes leads to ECs TJ formation, decrease in transcytosis and leukocyte adhesion molecules expression in the developing BBB [46, 51]. Pericytes may guide astrocytic foot process into the endothelial tube, initiating a proper end-foot polarization [52]. Although some components of the BBB and the NVU develop before astrocytes differentiation and localization in the ECs vicinity, astrocytes are required for the stabilization of the BBB [75]. The crosstalk between ECs and astrocytes is through the Shh [57], Ang-1 [69] and RA [58] signaling pathways, among others, that are released by the astrocytes back signaling to the ECs respective receptor, leading to more advanced TJs, loss of leukocyte adhesion molecules and inhibition of transcytosis. The communications between the NVU cells and the BM are crucial for the activation of signaling pathways that control cell growth, differentiation, migration and survival during

BBB development and maintenance [67]. The interaction between the integrin receptor and laminin is important for EC differentiation and vessel stabilization [76], and also influences claudin-5 expression, controlling BBB permeability [77].

The third and final stage of the BBB development is related with the BBB maintenance [66, 67]. In order to keep the BBB phenotype, the crosstalk between the ECs with the other components (cellular and non-cellular) of NVU is crucial. The communication mainly responsible for the maintenance occurs through the same signaling pathways important during the differentiation phase, such as the Wnt, TGFβ, Ang-1, Shh, among others [67, 78]. Nevertheless, despite the significant advances in the field, the mechanisms behind the BBB maintenance are still not fully understood [66].

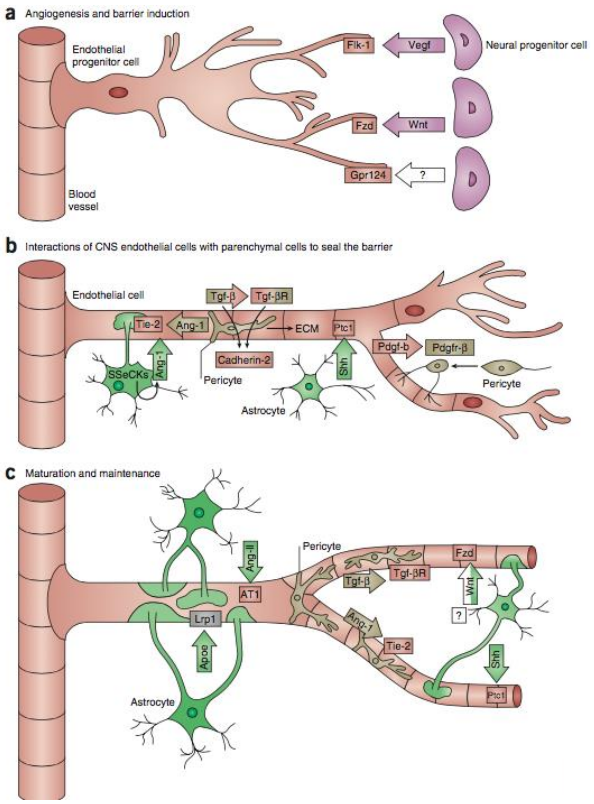

Figure 2.5 - Major signaling pathways in BBB development. A| The BBB development starts with angiogenesis when endothelial progenitor cells invade the embryonic neuroctedorm in response to VEGF. The release of Wnt by the NPCs starts the induction of the barrier phenotype. **B|** The second stage of BBB development is characterized by the recruitment of pericytes and astrocytes to the vicinity of ECs. The crosstalk between pericytes-ECs is bidirectional through TGF-β-TGF-βR and when pericytes are set in place they limit the BBB permeability by producing Ang-1. Astrocytes show their importance in the maturation of the developed BBB phenotype, through the release of Shh and Ang-1. **C|** The stabilization and maintenance of the BBB phenotype is not fully understood, however it is clear that the close contact and interaction between all the components of the NVU is crucial (from [67]).

2.2. HUMAN IN VITRO BBB MODELS

Several *in vitro* BBB models have been developed from different species, however the most common and widely used are from mouse, rat, pig and bovine origin [79]. Nevertheless, species differences in terms of expression of transporters, receptors and TJ proteins may lead to wrong extrapolations to humans [80]. For pharmaceutical purposes, the development of a functional and well-characterized human BBB model is of utmost importance. Human BBB models based on primary cells obtained from fresh human tissue have been reported for more than 10 years [81]; however limitations in obtaining human tissue and loss of human brain EC phenotype during cell culture, limits their general use. During the last years, efforts were made to immortalize human brain ECs [82, 83]. From all the cell lines reported, the hCMEC/D3 cell line [82] is the most used in the scientific field, being cited in more than 150 publications (see review [84]) after their generation and initial characterization. Despite its widespread use, this cell line presents low TEER and lack important TJ proteins (e.g. claudin-5). Recently, brain ECs derived from human stem cells, including pluripotent stem cells (induced pluripotent and embryonic stem cells) [61, 85] and multipotent stem cells (e.g. hematopoietic progenitor or circulating endothelial progenitors) [47, 86] have been reported. These stem cells are promising sources of human BBB models since, they have the capacity to differentiate into brain ECs that can proliferate *in vitro* and be used for disease BBB modeling.

2.2.1.STEM CELL BASED MODELS

2.2.1.1. Human *In Vitro* Models Derived from Multipotent Stem/Progenitor Cells

In the literature, 2 studies have reported the derivation of brain ECs from cord-blood stem cells, specifically from human endothelial progenitor cells and from human hematopoietic stem/progenitor cells. In the first study [86], mononuclear cells (MNCs) isolated from human cord blood were cultured in type I rat tail collagen until endothelial colony-forming cells appeared, normally between day 8 and 12. The cells were seeded in collagen/fibronectin coated polyester filters and co-cultured with rat astrocytes for

approximately 14 days, when the lowest permeability to Lucifer yellow (MW: 457 Da) was observed (1.23 $x10^{-3}$ cm/min). Moreover, an increase in mRNA levels with the co-culture was reported for occludin and Glut-1, and also an increase in protein levels of active efflux transporter Pgp. Importantly, the activity of the Pgp transport was improved by the co-culture with rat astrocytes. By immunofluorescence staining a continuous expression of VE-cadherin, ZO-1, occludin, claudin-3 and -5 was observed after 14 days of co-culture. This BBB model presented still some limitation, since the paracellular permeability was only optimal for 4 days, after that the ECs present morphological changes and some detach from the filters; the TEER values detected were low, even in the co-culture system (below 60 Ωxcm^2) and finally no correlation between *in vitro* and *in vivo* data for different drugs was given. The second study [47], developed in our group, reported the development of a stable and reproducible human *in vitro* BBB model derived from cord-blood hematopoietic stem/progenitor cells ($CD34^+$ cells). These cells were isolated from the MNCs by magnetic activated cell sorting (MACS) and cultivated during 15-20 days in gelatin-coated wells until the appearance of the ECs. These cells were further expanded for 4 passages and platted on matrigel-coated polycarbonate filters for 6 days in co-culture with bovine pericytes. With the induction of the BBB phenotype by the bovine pericytes, these BECs present low values of permeability to Lucifer yellow (0.61 $x10^{-3}$ cm/min) and high values of TEER (160 Ωxcm^2). Moreover, cells cultured for 6 days present higher transcripts of ZO-1, claudin-1, influx transporters (SLC and Glut-1), receptors (Tf receptor and large molecules receptors) and influx receptors (Pgp, BCRP and MRP). Continuous expression of ZO-1, occludin, claudin-1 and -5 in the cell-cell borders was also observed. This BBB is very reproducible between different donors and different laboratories (paracellular permeability data were similar between cells derived from 3 different donors and in 3 different laboratories) and also very stable, since the permeability to Lucifer yellow was the same for at least 20 days. Importantly, this work was the first to show a good correlation for several drugs between the human *in vitro* data with the pharmacokinetic results obtained by positron emission tomography (PET) in humans.

Adult (multipotent) or stem progenitor cells may be also used to obtain cells from the NVU. Human NPCs have been used to induce BBB properties in a co-culture system with rat BMVECs [60]. The NPCs were initially differentiated for 12 days into a mixed population of astrocytes and neurons (3:1) with specific culture media. After this differentiation, the rat BMVECs were co-cultured with the mix population in a Transwell system for 4 days and improvements in the BBB phenotype, such as an high TEER

(~250 Ωxcm^2), low passive permeability and TJ proteins continuous in the cell membrane was observed.

2.2.1.2. Human *In Vitro* Models Derived from Pluripotent Stem Cells

Endothelial Cell Derivation

In 2006 the first induced pluripotent stem cells (iPSCs) were created by Takahashi and colleagues [87], using a cocktail of transcription factors, Kruppel-like factor 4 (Klf4), Sox2, octamer binding protein (Oct4/POUF5F1) and c-Myc. They converted mouse fibroblasts cells to pluripotent stem cells resembling embryonic stem cells (ESCs). These cells have a similar morphology and growth properties of ESC, express similar markers, were able to form embryoid bodies *in vitro* and teratomas *in vivo* and when injected into mouse blastocysts contributed to the formation of diverse tissues in chimeric embryos. The first human iPSCs were generated in 2007 [88] from adult human dermal fibroblasts using the same combination of transcription factors. From 2007 until the present several laboratories have generated human iPSCs from a variety of cell types. Dermal fibroblasts due to their accessibility and higher reprogramming efficiency are the preferential source of somatic cells to generate iPSCs; however peripheral blood cells [89, 90] and cord blood cells [91] are also an attractive source of cells since they can be isolated by non-invasive methods.

Differentiation of iPSCs into vascular lineages is a multistep process that involves mesoderm formation, differentiation and specification of progenitors of the vascular lineage and its functional maturation (**Figure 2.6**). The main strategies for deriving ECs from iPSCs includes a (i) differentiation step through embryoid bodies (EBs) in serum-supplemented medium [92] or (ii) a differentiation step through a monolayer. Both of these methods can be combined with the sequential addition of factors important for ECs derivation and through co-culture with stromal feeder cells (OP9, S17 or M210B4) [93]. Serum-free and chemically defined media for generating ECs [94, 95] have been published recently. TGF-β, RA and Wnt/β-catenin signaling pathways have been shown to be important for the differentiation of ECs from iPSCs [93]. FGFβ and bone morphogenic protein (BMP) 4 are two key signaling pathways important not only for mesoderm formation [96] but also for the differentiation of the mesoderm progenitor cells into ECs. Another key regulator of vasculogenesis and EC differentiation is VEGF. The

presence of this factor increases the percentage of derived ECs from iPSCs, probably though the regulation of ECs survival and propagation [93]. The small molecule SB431542, a TGFβ inhibitor, has been shown to increase the yield of ECs form ESCs [97].

The majority of EC differentiation protocols yield low percentage of ECs and thus a need for additional purification steps, which can be done by cell sorting or MACS based on specific EC markers. ECs express CD31/PECAM1, CD34, VEFGR1/Flt1, VEGFR2/Flt2, CD144/VE-cadherin, CD106/Vascular Cell Adhesion Protein (VCAM)-1, endothelial nitric oxide synthase (eNOS) and von Willebrand Factor (vWF). At functional level, ECs are able to uptake acetylated LDL and generate tube-like structures on top of matrigel [93].

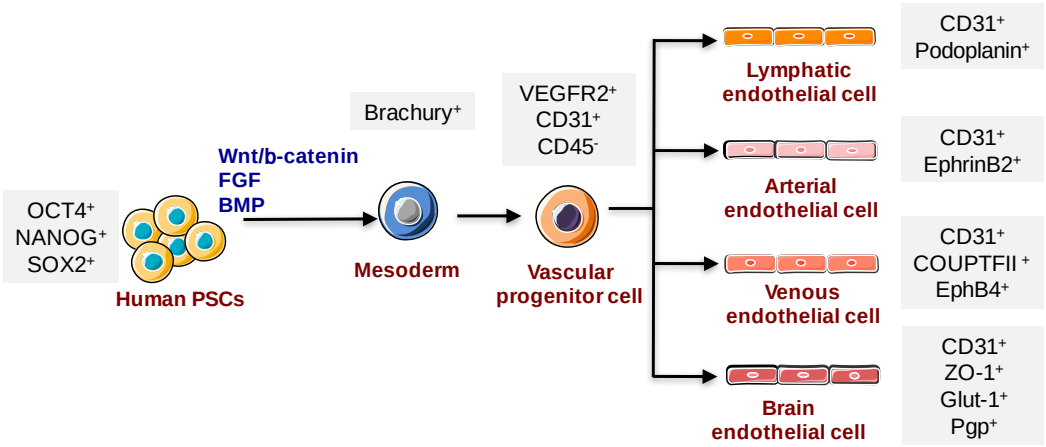

Figure 2.6 - Signaling pathways involved in the differentiation of ECs from iPSCs. The differentiation of the vascular lineage is a complex process involving several steps from mesoderm induction to derivation of vascular progenitor cells and finally to the specification into several endothelial phenotypes (adapted from [98]).

By modulating the differentiation of iPSCs by soluble cues, ECM, intercellular interactions and mechanotransduction it is possible to obtain cells at different stages of maturation (progenitors or fully maturated cells), somewhat very difficult to obtain from human tissue [99]. Another important aspect related the iPSCs is the possibility to study the phenotype of several genetic diseases. Isolating patient-specific cells (e.g. fibroblasts) it is possible to generate iPSCs that can be differentiated into specific cell type(s) affected by the disease which then can be used for drug screening and the study of the disease at a tissue/cell level [99-101]. Several disorders including multiple sclerosis, Alzheimer's and Parkinson's disease are associated with brain EC dysfunction

[102]. Although it has been already established patient-derived iPSCs from these diseases [103-107], no study has reported so far the derivation of ECs from these iPSCs. Therefore, the coming years will be very exciting from a disease modeling perspective.

iPSCs represent a very promising cell source for the generation of *in vitro* BBB models and human brain disease modeling [108]. These cells can be used for the derivation of brain ECs, presenting several advantages relatively to multipotent stem/progentior cells: (i) allow the generation of a high number of ECs due to the self-renew capacity of the iPSCs, in an undifferentiated state, (ii) give the opportunity to study the specification of ECs into brain ECs from an embryological point of view and (iii) allow the derivation of pathological brain ECs from iPSCs generated from neurological disease patients.

Brain Endothelial Cell Derivation

The derivation of human brain-like ECs (BLECs) from iPSCs was first described by Shusta's lab in 2012 [61]. In this work, BLECs were obtained from ECs co-differentiated with neural cells. The crosstalk between the two types of cells involving Wnt/β-catenin signaling pathway was crucial for the development of the BBB phenotype in ECs. Almost all the neural progenitors, immature neurons and neurons present in the co-culture were positive for Wnt7a and Wnt7b while ECs were positive for nuclear β-catenin localization and Glut-1 expression. BLECs were then purified by sub-culturing in collagen-fibronectin ECM. Cells expressed claudin-5, occludin and ZO-1, presented a TEER of 222±51 Ωxcm^2 or 1450±140 Ωxcm^2, in monoculture or in co-culture with rat astrocytes, respectively, showed low sucrose paracellular permeability (0.34×10^{-6} cm/min), and they were functional and polarized for efflux transporters (Pgp, BCRP and MRP) [61].

The initial differentiation protocol developed by Shusta's Lab was optimized by supplementing the basal media (BM) with differentiation factors (e.g. RA [109]), defining the best iPSC seeding density [110] and Matrigel source [111]. The supplementation with RA promoted an early onset in the expression of VE-cadherin and occludin in BLECs and increased the TEER (2940±800 Ωxcm^2). A sequential tri-culture of purified BLECs with pericytes followed by differentiated NPCs yielded TEER values above 5000 Ωxcm^2. Nevertheless, the TEER values decreased overtime, reaching values below 3000 Ωxcm^2 after three days. Searson's lab validated the protocol of Shusta's lab in another human iPSC line (BC1; also GFP-labeled BC1). The authors showed many of the characteristics

reported in terms of expression of TJ proteins, efflux pumps and transporters, polarized Pgp efflux pumps, high TEER and low permeability [112].

Recently, the derivation of BLECs has been reported by differentiating the iPSCs into endothelial progenitor cells followed by their specification into BLECs by co-culture with C6 rat glioma cells [85]. The differentiation of iPSCs into endothelial progenitor cells was mediated by an EB differentiation step in the presence of BMP4, VEGF, SB431542 and FGFβ, at variable times, during 9 days. Endothelial progenitor cells were isolated by cell sorting against CD34 marker. Cells were then platted in fibronectin-coated dishes or Transwell inserts. By co-culturing these cells with C6 rat glioma cells, it was observed an increase in TEER from 22-28 Ωxcm^2 to 55 Ωxcm^2, an increase in gene expression of TJ proteins (claudin-5, occludin and ZO-1) and in influx and efflux transporters (MDR1, MDR-1, BCRP and Glut-1). Also a decrease in dextran transport was observed when using the co-culture system. Similar data were observed when using conditioned medium from rat C6 glioma cells, suggesting that the derived-soluble factors can be sufficient to promote the BBB specification in the iPSCs-derived ECs.

2.2.2. EVALUATION OF BBB STRUCTURE AND FUNCTION *IN VITRO*

Several parameters can be used to evaluate the BBB properties *in vitro* including cell morphology, inter-cellular organization, TEER and paracellular permeability.

2.2.2.1. Morphology

The morphology of ECs is an important parameter to take into account in BBB structure/function analyses. Both phase-contrast and electron microscopes may be used for this purpose [1]. Phase-contrast microscopy allows the monitoring in a daily basis of cell-culture progression, i.e. typical EC cobblestone morphology, cell confluence, presence of contaminants and the right moment to perform the experiments [1]. Fluorescence microscopy is crucial for the observation of BBB-related proteins. We can evaluate the proper localization of TJ proteins (ZO-1, claudin-5, occludin, among other) and the polarization of specific transporters in the cell membrane (e.g. RAGE and

OCTN2 localized in opposite membranes). Moreover, we can evaluate BBB disruption upon an insult and also to evaluate activation of signaling cascades [1]. Electron microscopy allows the study of relevant features at subcellular level. This type of microscopy can be used to evaluate the TJs and AJs between the brain ECs, the organization of the NVU components, the events of cell transcytosis, among others [47, 102, 113].

2.2.2.2. Properties

Transendothelial electric resistance (TEER)

TEER is an indicator of the BBB permeability to small ions and reflects the complexity (and quality) of the TJs. Values above 1000 Ωxcm^2 indicate high resistance [1]. This measurement has been considered one of the most accurate and sensitive measurements of BBB integrity; however, the values are affected by the cell culture well and the TEER equipment used [114]. For example, a bovine BBB model may present a TEER value of 661 Ωxcm^2 (measured with the ERS-Milicell apparatus [115]) or 358 Ωxcm^2 (measured with EVOM^{TM} from World Precision Instruments [116]), depending in the equipment used.

Permeability

Brain ECs show low paracellular permeability, which is an indication of the presence of TJ proteins [1]. Low endothelial permeability is an indicator of a diffusion barrier, and in combination with TEER, is one of the most important aspects of a good BBB *in vitro* model. Hydrophilic molecules (e.g. radiolabelled sucrose or inulin, or fluorescent compounds such us Lucifer yellow and fluorescein), are know to cross poorly the BBB, and because of that are used to assess the endothelial monolayer permeability. It is important to correlate the *in vitro* values with the *in vivo* permeability values. For example, the permeability values for sucrose *in vivo* and *in vitro* are of the order of 10^{-7} cm/s and 10^{-6} cm/s, respectively [117].

2.3. NANOPARTICLES FOR DRUG DELIVERY INTO THE BRAIN

2.3.1.TYPES OF NPs FOR BRAIN DRUG DELIVERY AND THEIR PATHWAYS TO CROSS THE BBB

The development of new strategies to treat brain diseases is one of the most challenging and expensive market niches for pharmaceutical companies. During the process of development and discovery of new compounds for the CNS, the costs for reaching phase I clinical trials can go up to US$100 million and around US$1 billion before reaching the consumer [13]. Taking into consideration these numbers it is of utmost importance to be effective in the development phase. However, in recent years, only a minor number of brain-directed pharmaceuticals have reached the market (3-5%) since most of them were incapable of crossing the BBB *in vivo* [118]. Currently, advances in the field of nanomedicine have generated several platforms that improve drug transport across the BBB, namely nanoparticles (NPs) [119-122].

NPs are colloidal carriers (**Figure 2.7**) that can have a natural or synthetic origin and can vary from 1 to 1000 nm in size [119, 123, 124]. Synthetic NPs may be prepared from polymeric materials such as poly(ethylenimine) (PEI), poly(alkylcyanoacrylates), poly(amidoamine) dendrimers (PAMAM), poly(ε-caprolactone) (PCL), poly(lactic-co-glycolic acid) (PLGA), polyesters (poly(lactic acid) (PLA), or from inorganic materials such as gold (Au), silicon dioxide (silica), among others (**Figure 2.7**). These carriers can transport drugs by adsorbing, entrapping or bounding covalently to them [123-125]. Inorganic NPs offer advantages over polymeric NPs in terms of control over size and shape and simplicity of preparation and functionalization. Most importantly, inorganic NPs are easier to track by microscopy techniques [e.g. magnetic resonance imaging (MRI) and transmission electron microscopy (TEM)] or analytic techniques (e.g. inductively coupled plasma mass spectrometry; ICP-MS). However, inorganic NPs also have disadvantages because they might not be degraded (or eliminated through the kidneys) or present undesired toxicity (e.g. carbon nanotubes and fullerenes may lead to lipid peroxidation and oxygen radical formation). On the other hand, natural NPs are produced from natural polymers, such as polysaccharides (chitosan, alginate), amino acids (poly(lysine), poly(aspartic acid) (PASA)), or proteins (gelatin, albumin) [126, 127].

Natural NPs (**Figure 2.7**) have the advantage of providing biological signals to interact with specific receptors/transporters expressed by ECs but they have the disadvantage of batch-to-batch variability, limited ability for controlled modification and poor tracking capacity by imaging platforms.

The physico-chemical properties of NPs determine which is the passage mechanism across the BBB. The following transport mechanisms have been described (**Figure 2.4**): (i) NPs open TJs between ECs or induce local toxic effects which leads to a localized permeabilization of the BBB allowing the penetration of the drug in a free form or conjugated with the NPs [128, 129]; (ii) NPs pass through ECs by transcytosis [130]; (iii) NPs are transported through ECs by endocytosis, their content is released into the cell cytoplasm and then exocytosed in the endothelium abluminal side [131]; or (iv) a combination of several of the mechanisms described previously. According to some studies, mechanisms ii, iii and iv are the main transport mechanisms of NPs. In case of mechanism ii, several receptors have been targeted by NP including Tf [132] and LDL receptors [133, 134]. The targeting has been achieved by peptides [133, 135], proteins [134] or antibodies [132] physically or chemically immobilized on top of the NPs.

NPs are exciting systems for brain drug delivery due to the possibility to modulate them in terms of shape, size, hydrophobicity, coating, chemistry and surface charge (**Figure 2.7**). Control over these features can enhance the ability of NPs to improve the therapeutic agent stability in circulation, to control the cargo release into the desired target site, to enhance BBB penetration efficiency and to escape the reticuloendothelial system [119, 123, 124].

2.3.2.FACTORS THAT INFLUENCE NPs TRANSPORT ACROSS THE BBB

There are several parameters that affect the efficiency of NPs systemic circulation, BBB passage and cellular delivery. These features (size, shape, NP chemistry, ligand density, NP charge and antifouling properties) are summarized in **Figure 2.7**.

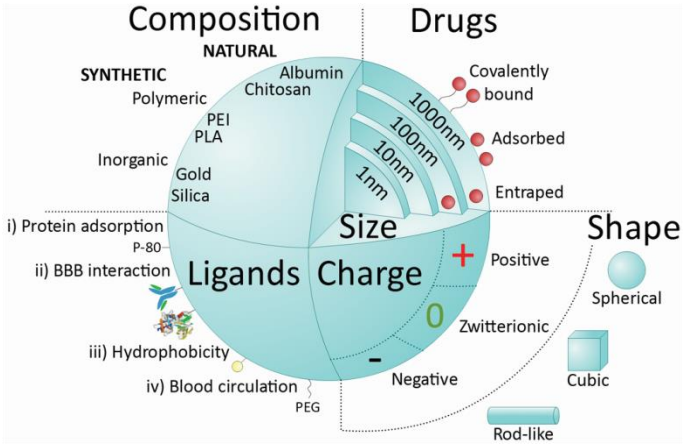

Figure 2.7 - Main NP features influencing systemic delivery and BBB passage. NPs can be classified into natural, when molecules such as proteins (albumin), polysaccharides, chitosan, among others are used, or synthetic. Synthetic NPs can be made of very common polymers such as PLGA, PEI, PLA, or from inorganic agents like gold, silica or alumina. NPs can vary in their size (1-1000 nm) and are able to deliver drugs into cells by entrapping, adsorbing or covalently bounding them. NPs can assume different shapes (spherical, cubic, rod-like) and charges (negative, zwitterionic, positive); negatively charged spheres are widely used in intravenous applications. Another important feature of NPs is the possibility of functionalization with different types of ligands. Ligands are distributed into four major categories: i) capable of mediating protein adsorption (e.g. poly(sorbate) 80 (P-80)); ii) able to interact directly with the BBB (e.g. Tf protein, antibody or peptide); iii) capable of increasing hydrophobicity (e.g. amphiphilic peptides); and iv) able to improve blood circulation (e.g. poly(ethylene glycol) (PEG)).

Several studies have been shown a clear inverse correlation among NP size and BBB penetration [136-138] (**Figure 2.7**). In particular, most of the studies performed so far have used NPs with diameters between 50 nm to 100 nm. The shape of NPs also influences body distribution and cellular uptake [139], and it can vary from spherical, cubic, rod-like, among other forms (**Figure 2.7**). Most of the studies have been performed with spherical NPs since they are relatively easy to prepare. Although, *in vitro* studies

have also demonstrated that nanorods (NRs) coated with specific antibodies have higher adhesion propensity than their spherical counterparts. Specifically, polysterene NPs with a rod shape (501 ± 43.6 × 123.6 ± 13.3 nm) coated with an antibody against the Tf receptor showed *in vivo* a 7-fold increase in brain accumulation when compared to their spherical NP counterpart (200 ± 0.01 nm) [140]. Zeta potential is another important parameter that affects the passage of NPs through the BBB. It has been shown that NPs with high zeta potential (high positive charge) cause immediate toxicity to the BBB [141]. Therefore, most of the NP formulations described in the literature for brain delivery have moderate (between -1 to -15 mV) [129, 130, 142, 143] or high (between -15 to -45 mV) [139, 144] negative zeta potentials. Yet, some NP formulations with moderate (up to 15 mV) or high positive zeta potential (above 15 mV) have been able to cross the BBB and in some cases are efficient brain delivery systems (**Figure 2.7**) [128, 145].

A number of ligands have been conjugated to NP to facilitate BBB penetration. Such molecules can be grouped into four different types (**Figure 2.7**): (i) ligands that mediate the adsorption of proteins from the bloodstream that interact directly with BBB receptors or transporters [146]; (ii) ligands that have direct interaction *per se* with BBB receptors or transporters [130, 147, 148], (iii) ligands that increase charge and hydrophobicity [149] and (iv) ligands that improve blood circulation time (e.g. PEG) [129]. In the first case, we can include poly(sorbate 80) (also known as Tween 80) that can adsorb apolipoprotein E and/or A-I. The surfactant allows the anchoring of apolipoproteins whose interaction with lipoprotein receptors expressed in the brain endothelium enables the crossing of the BBB. In the second case, we can include several targeting ligands such as the ones for Tf receptor (Tf peptide, Tf protein or antibody against Tf receptor) [130, 150, 151], insulin receptor [147, 152], Glut-1 transporter [148], among others (**Figure 2.4**). In the third case, NP have been coated with amphiphilic peptides to facilitate the uptake by BBB ECs. In addition, the number of ligands as well as their receptor affinity has an important impact in the transport of NPs across the BBB (avidity). Ligand density depends of both the NP surface area and the ligand size. Typically, the ligand affinity to its receptor is reduced when conjugated to NPs. NPs avidity and selectivity increases when multiple targeting ligands are conjugated [129, 153]. However, NPs avidity must be modulated for effective BBB transcytosis. High avidity will impede NPs bound to the receptor to be released into the brain parenchyma. It has been shown that Au NPs conjugated with high concentrations of Tf (100-200 molecules of Tf *per* NP) stay bound to brain ECs. In contrast, Au NPs conjugated with low amounts of Tf (20-30 molecules of Tf *per* NP) can interact effectively with the receptor, undergo transcytosis and be released into brain parenchyma [130].

When NPs enter a physiological environment there is a rapid adsorption of proteins from the bloodstream to the NPs surface forming a protein coating – the “protein corona” [154, 155]. Over 70 different serum proteins have been reported to adsorb to the surface of Au NPs [154]. The protein corona may alter the surface chemistry of the NPs along with its aggregation state. Very often it also accelerates blood clearance of the NPs through the reticuloendothelial system localized mostly in the spleen and liver [119, 156], what may decrease the NPs dose available for accumulation in the brain as well as induce inflammation. The most common way to overcome this issue is to use molecules with the capacity to minimize surface fouling in order to maintain performance and safety of materials. In this sense, antifouling properties can be enhanced by using PEG-coated NPs. PEGylated NPs present minimal surface charge leading to lower NPs opsonization and lower reticuloendothelial system uptake [157]. Grafting NPs with PEG (5 kDa; between 0.16 to 0.64 PEG molecules *per* nm^2) decreases protein adsorption and slows down the clearance of the nanomaterials [154, 158]. Moreover, due to its improved blood circulation time, PEGylated NPs accumulate more efficiently in the brain [153, 159]. For instance, polystyrene NPs (below 200 nm) coated with PEG (5 kDa; 9 PEG molecules *per* 100 nm^2) are able to cross the BBB. Additionally, PLGA NPs (ca. 78 nm) coated with PEG are also able to rapidly penetrate rat brain tissue *ex vivo*, in contrast with uncoated NP [159].

In summary, several parameters influence the transport of NPs through the BBB at different extents. The characterization of the NPs is highly variable and some aspects such as ligand density and its impact in NPs transport through the BBB are not well studied. So far, the NPs with the best performance presented sizes between 10 and 20 nm, rod and spherical shape, were conjugated with ligands for interaction with BBB receptors but at a relatively low density to show low avidity. Yet, it is important to note that the best formulations administered intravenously deliver up to 5% of the initial dose effectively across the brain. NPs brain deliver improvement might require systems that target and cross more efficiently the BBB but also systems that are slowly clear from the bloodstream. Regarding this last issue, the charge and the morphology of the NP have a very important effect in the clearance. Neutral and zwitterionic NP have a longer circulation time after intravenous administration, in contrast to negatively and positively charged NPs [160]. In addition, short-rod NP are preferentially retained in the liver and present a rapid clearance rate, while long-rod NP are caught in the spleen and have a lower clearance rate. If the surface is modified with PEG, retention increases in lung for both formulations [143].

2.3.3.MODELS TO STUDY NPs TRANSPORT THROUGH THE BBB

The study of NPs transport through the BBB requires animal models, generally, rodents since they are relatively cheaper than large animals and have also been used for many years as an initial study model. TEM [130, 161], fluorescence microscopy [162], ICP-MS or neutron activation [149], radiolabeling, or capillary depletion techniques [163] enable the monitoring of NPs transport in the brain. To screen NPs formulations capacity to cross the brain, several studies have used Au NPs since they are easy to synthesis, easily modified through reactions with thiol groups, easily quantified by ICP-MS and easily imaged by TEM [138, 139, 147, 149]. In most cases, healthy animals have been used. No systematic study has been performed with animals at different development stages and, in particular, with aged animals. Also very few studies have characterized the transport of NP in disease animal models.

The study of NPs transport through the BBB requires a specific concentration of NP able to be quantified by analytical techniques (fluorescence, radioligands, ICP-MS) or imaging (TEM). Both mice (e.g. BALB/c mice [130, 147]) and rat animal models (e.g. Sprague Dawley [139, 149]) have been used to study NPs transport though the BBB. The doses of NPs injected per animal can vary from 1.86 mg of Au/Kg [149] to 240 mg of Au/Kg [130, 147].

NPs are very rapid to deliver biomolecules into the brain, 30 min after intravenous injection they are already observed in the brain capillary ECs of mice and rats [161, 162]. This is in line with *in vitro* studies showing that the endocytic process of ECs is relatively rapid and, after 30 min NPs are observed in the endolysosomal compartment of the cells [142, 164]. Sixty minutes after administration NPs are observed across the brain tissue [162]. According to several studies using different NPs formulations in mice models, the transport of NPs through the brain peaks during the first few hours (typically below 5 h) [126, 128, 139, 147, 149] and then decreases. The kinetics of transport is affected by the size and surface chemistry of the NP.

Because in most formulations only up to 5% of the initial dose can effectively cross the BBB, it is important to evaluate the bio-distribution of NPs. NP administered intravenously accumulate preferentially in the liver, spleen, kidney and lung [160, 165]. Au NPs (15 nm), administrated intravenously, accumulate predominantly in liver followed by lung, kidney, brain and spleen. On the other hand, Au NPs (200 nm) accumulate in liver followed by spleen, lung and kidney [137]. A distinct profile was observed for PLGA NPs (163 nm) administered intravenously where most of the NPs accumulated in spleen,

followed by liver and lung, and finally kidney [166]. These results demonstrate that NPs bio-distribution is, in part, size- and chemistry-dependent. Three other variables affect the bio-distribution of the NPs: surface charge, shape and route of administration. Neutral and zwitterionic Au NP have a longer circulation time after intravenous administration, in contrast to negative and positive charged NPs [160]. In addition, silica NPs with different shapes have different accumulation and clearance rate profiles. Short-rod NPs are preferentially retained in the liver and present a rapid clearance rate, while long-rod NPs are caught in the spleen and have a lower clearance rate. If the surface is modified with PEG, retention increases in lung for both formulations [143]. Finally, the route of administration can affect NPs bio-distribution. For example, Au NP administered by oral and intraperitoneal routes induce more toxicity than the ones injected intravenously [167].

Although *in vivo* studies are important to study NPs transport, *in vitro* BBB models offer interesting opportunities to study the mechanism of transport and cytotoxicity of NPs. Non-human [128, 138, 139] or human [142, 148, 164] *in vitro* BBB models have been used to study the uptake and permeability of NP. Inter-species differences in the concentration of transporters and TJs may affect the final readouts of the assay [168]. Recently, we have developed a stable human *in vitro* BBB model (for more than 20 days) using cord blood-derived hematopoietic stem cells [47]. The model is very reproducible since it can be generated from stem cells isolated from different donors, and can be used to predict CNS distribution of compounds in human. This model represents a promising tool to study the *in vitro* BBB crossing by the NPs.

2.3.4.TARGETING THE NEUROGENIC NICHES

The subventricular zone (SVZ) and the hippocampal subgranular zone (SGZ) comprise two main germinal niches in the adult mammalian brain. Within these regions there are self-renewing and multipotent neural stem cells (NSCs) which can ultimately give rise to new neurons, astrocytes and oligodendrocytes [169]. Adult neurogenesis is a dynamic process that is modulated by several physiological, pathological and pharmacological stimuli [170], and can be divided into four phases: precursor cell phase, an early survival phase, a postmitotic maturation phase, and a late survival phase. It is estimated that the entire process can take approximately seven weeks [171]. Several molecular features, like DNA methylation, transcription factors, non-coding RNAs and soluble factors such us, Shh, VEGF, bFGF, neuropeptide Y, brain derived neurotrofic

factor, among others are involved in NSC differentiation [172]. In case of injury, surrounding activated microglia and astrocytes send signals to promote neurogenesis [173]. Moreover, immune cells can secrete inflammatory mediators, like tumor necrosis factor (TNF)-α and nitric oxide that can promote post-injury neurogenesis [174-176]. Importantly, pre-clinical and clinical studies have shown that is possible to stimulate neurogenesis after an ischemic episode [177-182]. This occurs in clusters nearby vessels, suggesting a close relationship between angiogenesis and neurogenesis [183-185]. These results indicate that is possible to regenerate, at least in part, the damaged area in the post-ischemic brain. Nevertheless, despite the present knowledge in the field, there are still big challenges regarding the induction of enough proliferation, mobilization and differentiation of these cells to repair the damaged area in a controlled way, making connections with pre-existing cells in the neural circuitry. Indeed, approximately only 50% of the new neurons that are able to migrate and differentiate, survive for longer than 1 month [186]. Moreover, problems related with exogenous stimulation are also present, due to solubility, stability, spatial and temporal control. Biomaterials have emerged as feasible scaffolds to modulate the differentiation and activity of the endogenous NSCs, either by promoting structural support or by delivering neurogenic factors [172]. In this sense, NPs are promising carriers to delivery to the brain neuroprotective drugs that can modulate NSC activity, which in their free form cannot pass the BBB or pass in very low amount being cleared rapidly by the reticuloendothelial system [172]. Only recently it was demonstrated, that small molecules transported by NPs systems can promote activity/differentiation of native NSCs [187-189]. These NPs may be delivered by intracerebroventricular/intracerebral infusion, BBB disruption (e.g. ultrasound, light, among others), intranasal, intravenous or intraperitoneal administration. The intravenous administration will be the ideal route since is less invasive than the other ones. However, this requires the development of NPs able to reach the brain, cross the BBB, target preferentially the NSCs and deliver their cargo at the cell cytoplasm at different dosages and times points. Some ligands have been reported to target NSCs [190] and the modulation of NSCs by NPs has been also demonstrated [187, 189, 191-197].

In the context of neurological disorders, such as stroke, Alzheimer's and Parkinson's disease, NPs can be a good strategy to promote cell proliferation, recruitment and differentiation of the NSCs to repopulate the injured areas. Some studies in literature have already shown that NPs containing bioactive molecules are able to promote neurogenesis and, at some extent, induce the recovery of the damaged area. For example the intravenous administration of chitosan NPs loaded with caspase-3 inhibitor (Z-DEVD-FMK) and bFGF [132] or NPs of adenosine conjugated with squalene

[198], were able to decrease the infarct volume and to improve the motor function deficit scores in the animals. On the other hand, in Alzheimer's disease, which is the most prevalent type of dementia, PLGA NPs containing curcumin are capable to cross the BBB and accumulate in hippocampus inducing neurogenesis and rescuing the learning and memory deficits in a rat model [195].

The targeting of neurogenic niches by NPs might be facilitated by the permissive vasculature of the BBB at those sites. Indeed, the SVZ region located on the walls of the lateral ventricles, relies a more permissive vasculature [199]. The SVZ is in close contact with blood vessels that feed this region with spatial cues and small regulatory molecules. For this process to occur, the SVZ vasculature has defined characteristics, namely areas that do not have contacting astrocyte endfeet or pericytes, rendering it thinner and more permeable [184]. Interestingly, there are studies that claim that new neurons can also arise in the circumventricular organs which lies the walls of the third and fourth ventricles [200, 201]. All of these brain areas share a common trait, a leaky BBB, which endows them with a greater ability to perceive damage and to engage in brain repair. Strong evidences suggest that these brain regions, which rely on a leaky BBB, may provide an alternative route for NPs entrance into the brain and, importantly, modulate the regenerative ability of neural stem/progenitor cells [188]. It should be noted that these brain regions may account for other forms of obstruction to therapeutic drugs, by having increased enzymatic activity (i.e. enzymatic barrier) in circumventricular organs. Recent studies have shown that intravenous injection of NPs, independently of their cargo and mechanism of transport across the BBB, accumulate at high levels in these leaky regions [166, 195, 202]. Nevertheless, it would be important to identify specific targets of the neurogenic niches in order to increase specificity and efficiency and decrease the side effects of the NPs and with this, a major step towards the development of new therapies for brain repair can emerge.

Chapter 3

DERIVATION OF BRAIN-LIKE ENDOTHELIAL CELLS FROM iPSCs-DERIVED ENDOTHELIAL PROGENITOR CELLS

3.1. ABSTRACT

The human BBB is a selective barrier formed by brain ECs, which is important to ensure adequate neuronal function and protect the CNS from disease. The development of human *in vitro* BBB models is thus of utmost importance for drug discovery programs related to CNS diseases. Here, we describe a two-step differentiation protocol to derive brain-like endothelial cells (BLECs) from iPSCs. The cells were initially differentiated into endothelial progenitor cells followed by the induction of BBB properties with a combination of soluble factors and extracellular matrices. Along the maturation process, there is an increase in the co-localization of the CD31 marker with BBB markers (claudin-5, ZO-1 and Pgp), suggesting a specification for the BBB phenotype. Functionally, these cells when cultured in the Transwell systems, present relatively low permeability to Lucifer yellow, high TEER values, are able to generate a continuous monolayer presenting ZO-1 and claudin-5 in the cell membrane and to respond to a inflammatory stimuli.

KEYWORDS: Blood-brain barrier, iPSCs, brain endothelial cells, soluble factors, extracellular matrices

3.2. INTRODUCTION

The BBB is a physical and metabolic barrier formed by a specialized network of BMVECs that together with pericytes, astrocytes, microglia, neurons and ECM form the functional neurovascular unit [1, 3, 14]. The barrier maintains the homeostasis of the CNS [3, 203]. Human *in vitro* BBB models offer a relatively simple tool to study mechanisms involved in the cerebrovascular response to a number of physiological and pathological stimuli, to accelerate the development of new drug therapies for the treatment of neurodegenerative diseases and to identify potential toxicological effects of new drugs while reducing the use of animals [12, 14]. In the last 5 years, we [204] and others [61, 112] have reported human *in vitro* BBB models based on stem cells. Human stem cells such as pluripotent or multipotent (e.g. hematopoietic/progenitor stem cells, neural progenitor cells) stem cells are a promising source of cellular components for the generation of human *in vitro* BBB models because they have the capacity to differentiate into brain ECs (although this capacity is dependent in the origin of the stem cells), they can give rise to a significant number of BBB cells (in contrast to somatic cells, brain EC progenitor cells can be expanded *in vitro*), and they can be used to model BBB pathologies. iPSCs represent a promising source of brain ECs with specific disease phenotypes such as Alzheimer, Parkinson and other neurodegenerative diseases. Lippmann and collaborators [61] were the first to demonstrate that human iPSCs could be differentiated into ECs with BBB properties when co-differentiated with neural cells. However, the derivation of brain ECs from a well-characterized endothelial progenitor cells has not been described. In addition, it is unclear the role of the ECM in the differentiation/specification process of the progenitor ECs into brain ECs.

Here we described a novel methodology to derive BLECs from iPSCs [91] using a two-step protocol comprising an initial differentiation of iPSCs into endothelial progenitor cells ($CD31^+$ cells) followed by a differentiation step into BLECs. Initially, we screened soluble and non-soluble factors (ECM) to induce the BBB properties in endothelial progenitor cells. We monitored the process by following EC and BBB markers expression by flow cytometry, immunocytochemistry and gene expression analyses. The cells were then cultured for 6 days in a Transwell system to reach confluence and TEER and paracellular permeability assays were performed. We further characterized the BLECs ability to respond to pro-inflammatory stimuli. The BLECs reported here opens interesting opportunities for future BBB disease modelling and also for drug screening initiatives.

3.3. RESULTS

BLECs were obtained by a two-step protocol (**Figure 3.1**). To promote mesoderm differentiation, iPSCs were differentiated for 10 days in the presence of BMP-4, bFGF, TB4 and VEGF, added at specific time points. Then, endothelial progenitor cells ($CD31^+$ cells) were isolated by magnetic activated cell sorting (MACS) and further maturated and expanded for 5 passages in different conditions to induce their possible specification into BLECs (**Figure 3.1**)

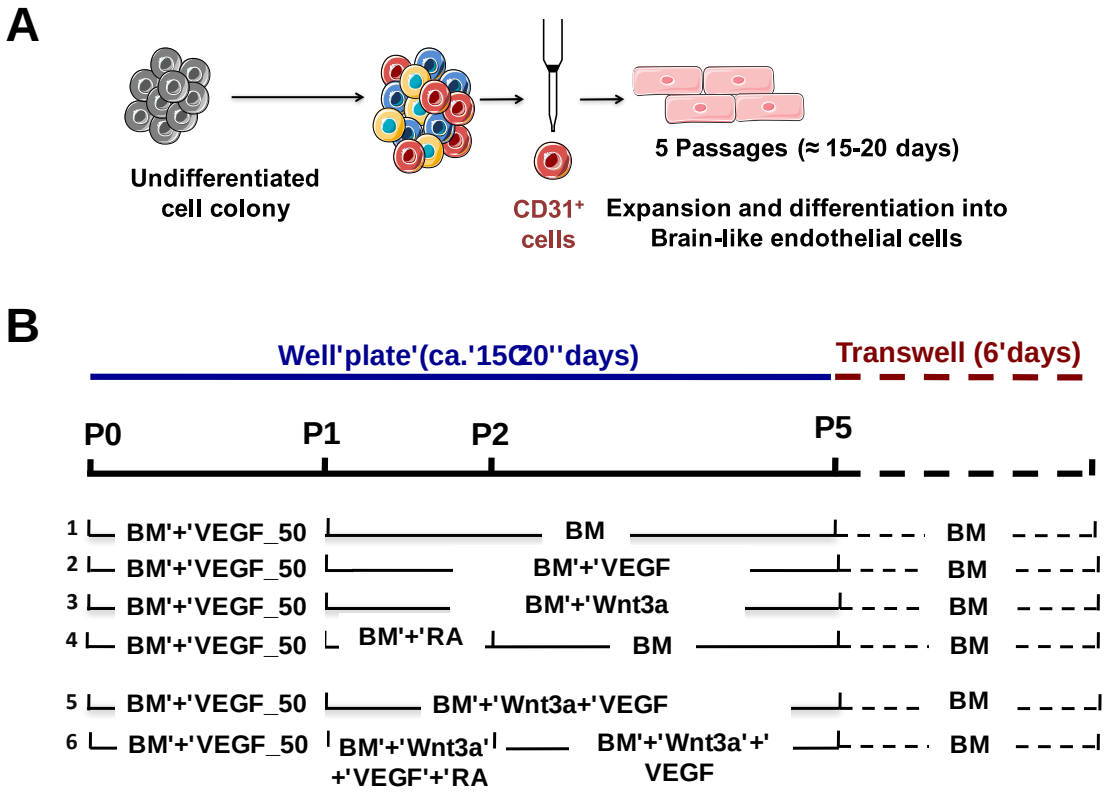

Figure 3.1 - Schematic representation of the methodology used to derive iPSCs into $CD31^+$ cells and further maturation into BLECs. **A|** Scheme of iPSCs differentiation to BLECs. iPSCs were first differentiated during 10 days into $CD31^+$ cells and further maturated and expanded into BLECs for 5 passages. **B|** Schematic representation of the protocols used to maturate the $CD31^+$ to BELCs during 5 passages.

Characterization of endothelial progenitor cells ($CD31^+$ cells). $CD31^+$ cells isolated by MACS at day 10 were characterized for EC and BBB markers by flow

cytometry (**Figure 3.2A**) and immunocytochemistry (**Figure 3.2B**). Approximately 91% of the cells expressed CD31, 97% Glut-1, 57% ZO-1, 41% claudin-5, 25% occludin, and no Pgp (**Figure 3.2A**). Furthermore, our immunocytochemistry results confirm these data and further show that occludin, claudin-5 and ZO-1 are not entirely located at cell junctions and Pgp is weakly detected, demonstrating that $CD31^+$ cells are not yet specified into BLECs (**Figure 3.2B**).

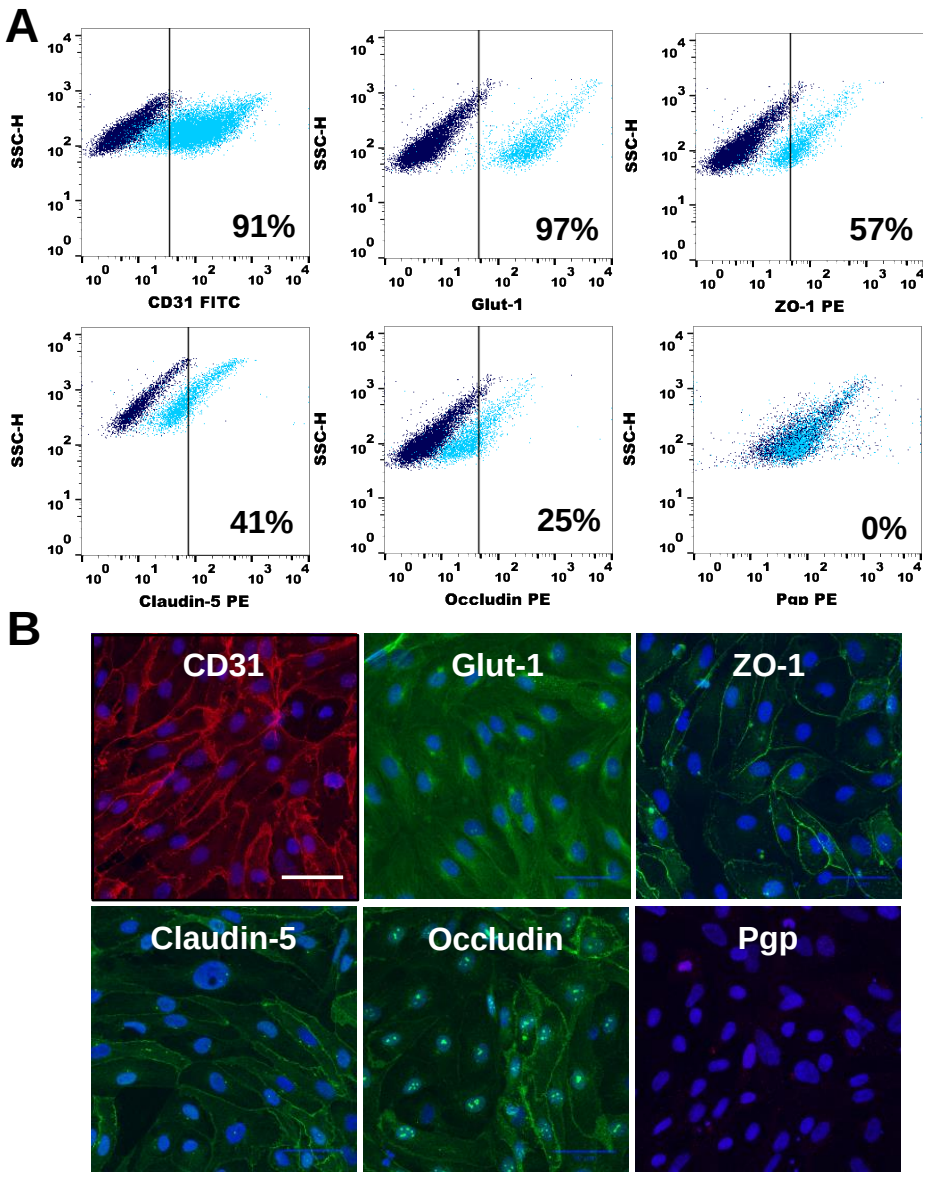

Figure 3.2 - Characterization of the $CD31^+$ cells regarding endothelial and BBB markers. A| Expression of endothelial and BBB markers was assessed by flow cytometry in isolated $CD31^+$ cells (CD31, Glut-1, ZO-1, claudin-5, occludin and Pgp). **B|** The same markers were evaluated. Scale bar corresponds to 50 μm.

Screening of soluble factors for the induction of BBB properties in CD31$^+$ cells. To specify CD31$^+$ cells into BLECs, we attempted several protocols using $VEGF_{165}$ (named as VEGF from now) [205], Wnt3a [73, 74, 204] and RA [58, 109] as inductive agents (**Figure 3.1B**). The concentrations used for each factor were in the range of concentrations published in previous studies [109, 204]. Cells were cultured for 4 passages (approximately 16 days) in fibronectin coated dishes in basal media (BM) supplemented or not with different factors, and EC markers (CD31) as well as BBB markers (ZO-1, occludin, claudin-1, claudin-5, Pgp, and Glut-1) [61, 204] monitored overtime, At passage 5, all cells or cells purified for CD31 marker were grown to confluence on matrigel-coated filters for 6 days after which paracellular permeability to Lucifer yellow and TEER analyses were performed.

Cells cultured in BM (protocol 1; **Figure 3.1B**) loose overtime their EC phenotype. Only 50% of the cells expressed CD31 marker (**Figure 3.3A**). The non-purified monolayer of cells showed discontinuous expression of ZO-1 at cell-cell contacts (**Figure 3.4C**), exhibited high permeability to Lucifer yellow (12.0±0.8 $x10^{-3}$ cm/min) and low TEER (ca. 22.7±1.7 Ωxcm^2) (**Figure 3.4A and B**). The monolayer of cells purified for CD31 marker still showed a high permeability to Lucifer yellow (3±0.6 $x10^{-3}$ cm/min) (**Figure 3.5A**) and low TEER (ca. 22.3±1.5 Ωxcm^2) (**Figure 3.5B)**.

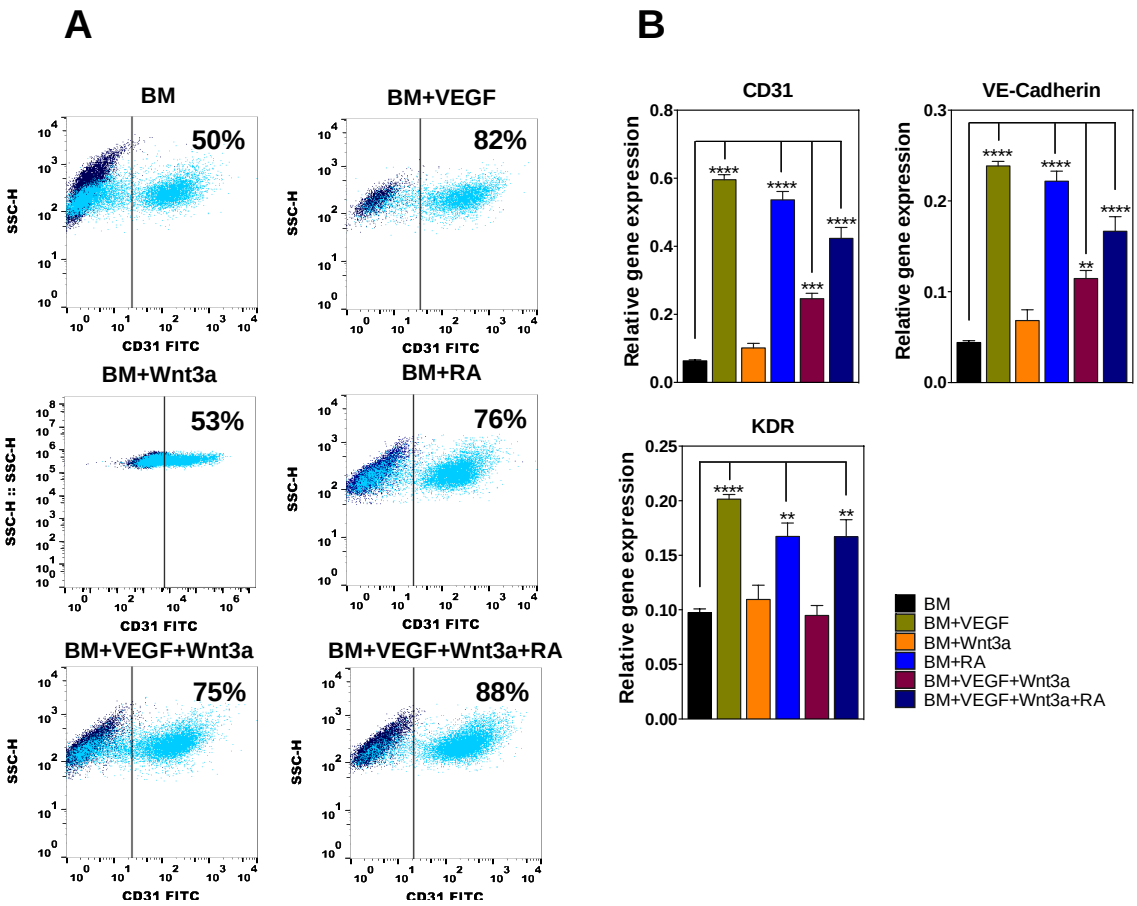

Figure 3.3 - Effect of soluble factors in the maintenance of the endothelial phenotype in the BLECs. A| Expression of CD31 marker in all the conditions used was assessed by flow cytometry at passage 4. **B|** Gene expression of endothelial markers (CD31, VE-cadherin and KDR) in all the conditions at passage 4 (without purification) was determined by Fludigm. Genes are normalized against the control gene β-actin. Values are Mean ± SEM (n=3). ***P<0.01, ***P<0.001, ****P<0.0001*.

VEGF [66, 206], Wnt [47, 207-209] and RA [58, 109] signaling have been reported to be an important player in early phases of BBB development. Cells cultured in media supplemented with each factor (protocols 2, 3 and 4; **Figure 3.1B**)had higher expression of CD31 marker than cells cultured in BM (53-88% vs. 50%) (**Figure 3.3A**). At passage 5, all cells or cells purified for CD31 marker were grown to confluence on filters for 6 days after which paracellular permeability to Lucifer yellow and TEER analyses were performed. Non-purified monolayer of cells showed discontinuous expression of ZO-1 at cell-cell contacts (**Figure 3.4C**), had relatively high paracellular permeability to Lucifer yellow (above 2 $x10^{-3}$ cm/min) and low TEER values (below 50 Ωxcm^2) (**Figure 3.4A and B**). The purified monolayer of cells showed high (VEGF: 50±1.2 Ωxcm^2) or modest

TEER values (Wnt3a: 31±2.2 Ωxcm^2; RA: 32.3±2.4 Ωxcm^2) (**Figure 3.5A**) and high permeability values to Lucifer yellow (VEGF: 1.8±0.3 x10^{-3} cm/min; Wnt3a: 1.6±0.1 x10^{-3} cm/min; RA: 2.4±0.3 x10^{-3} cm/min) (**Figure 3.5B**) as the ones reported previously by us for human BLECs in co-culture with bovine pericytes [204].

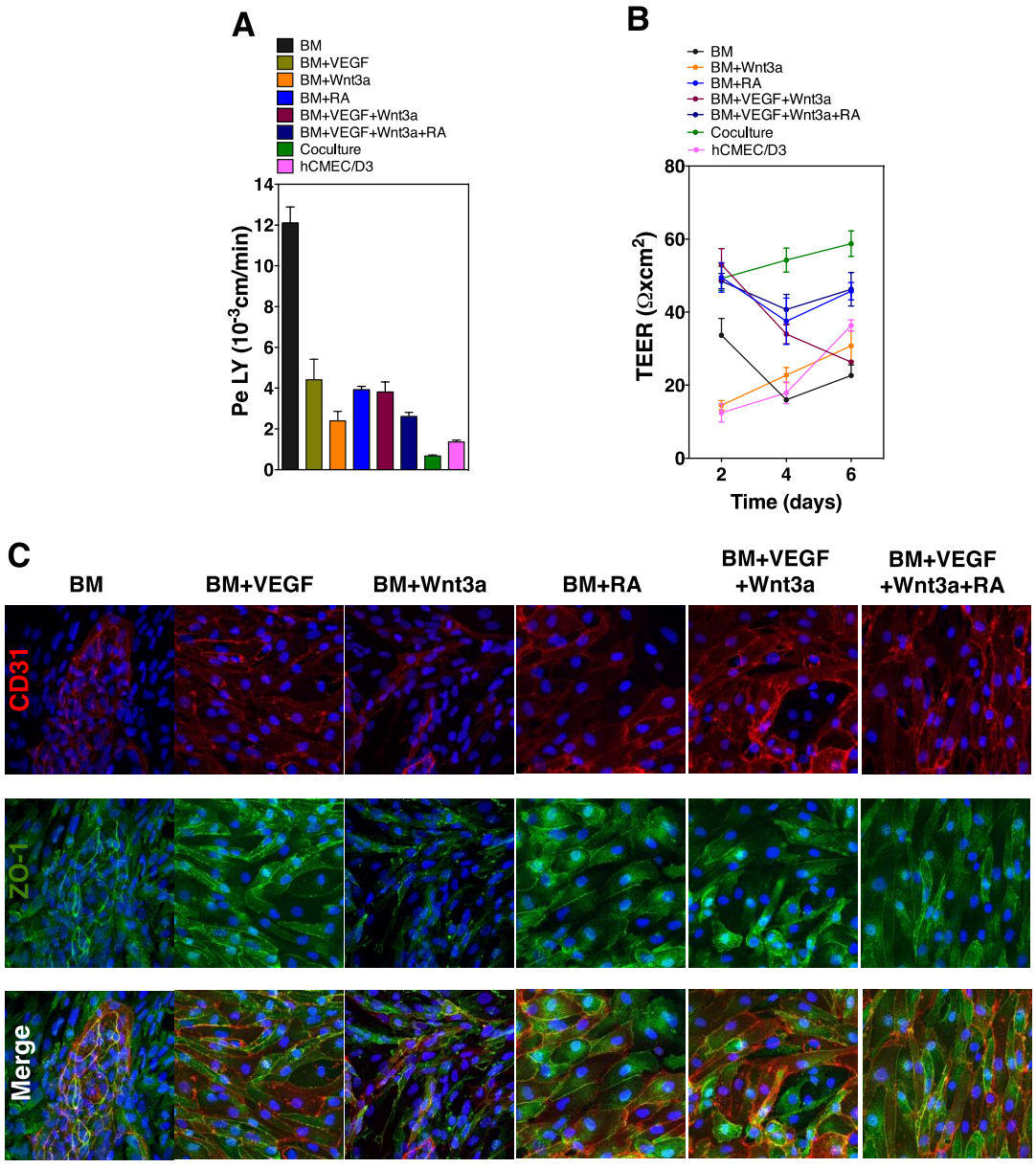

Figure 3.4 - Functional characterization of non-purified ECs after 6 days of culture in a Transwell system. A| Paracellular permeability of cells to Lucifer yellow (LY) after 6 days of culture in a Transwell system. **B|** TEER at different time points (day 2, day 4 and day 6) for all the conditions tested in matrigel-coated filters. **C|** Co-localization of CD31 and ZO-1 markers in the cells after 6 days of culture in the Transwell system. Values are Mean ± SEM. Scale bar corresponds to 50 µm.

We further evaluated the combination of both VEGF and Wnt3a, with or without RA. $CD31^+$ cells were cultured for 4 passages in BM supplemented with VEGF and Wnt3a (protocol 5; **Figure 3.1B**); or with VEGF, Wnt3a and RA (protocol 6; **Figure 3.1B**). In both cases, cells expressed at protein level high values (above 75%) of CD31 marker (**Figure 3.3A**) and at gene level, high values of CD31, VE-cadherin and KDR (**Figure 3.3B**). At passage 5, the non-purified monolayer of cells grown to confluence on Transwell filters for 6 days, showed discontinuous expression of ZO-1 at cell-cell contacts (**Figure 3.4C**), presented high permeability to Lucifer yellow (above 2 $x10^{-3}$ cm/min) compared to those obtained with our model consisting on $CD34^+$ derived ECs in co-culture with bovine pericytes [47] or hCMEC/D3 [82] and show relatively low TEER values (below 50 Ωxcm^2) (**Figure 3.4A and B**). When cells were purified at passage 5 (using CD31 marker) and cultured to confluence on Transwell filters for 6 days, showed improved TEER values (BM+VEGF+Wnt3a: 50±0.8 Ωxcm^2; BM+VEGF+Wnt3a+RA: 55±0.6 Ωxcm^2) (**Figure 3.5B**) and lower paracellular permeability to Lucifer yellow (BM+VEGF+Wnt3a: 1.2±0.2 $x10^{-3}$ cm/min; BM+VEGF+Wnt3a+RA: 1.2±0.1 $x10^{-3}$ cm/min) than cells cultured with BM or BM supplemented with each factor alone (**Figure 3.5A**).

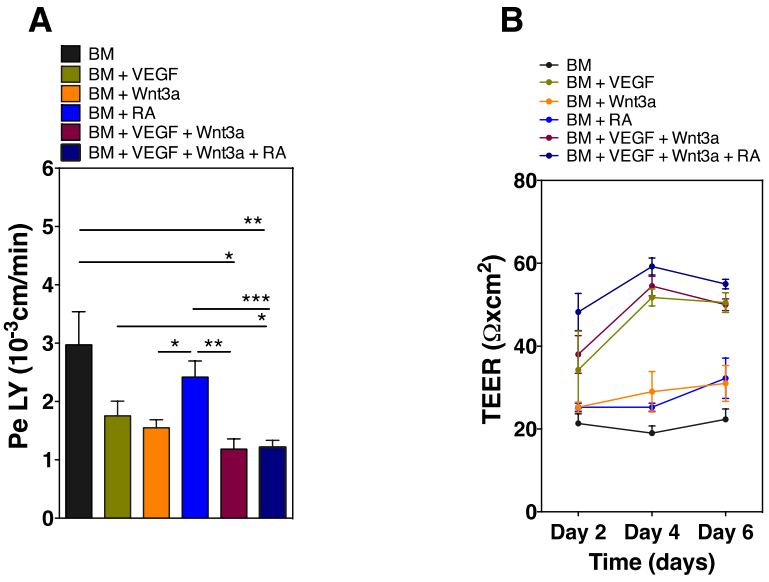

Figure 3.5 - Effect of soluble factors in the induction of BBB properties in the BLECs purified for CD31 marker. A| Paracellular permeability to Lucifer yellow (LY) of cells either exposed or not to the chemical factors with purification 6 days after being platted in the matrigel-coated filters. **B|** TEER at different time points (day 2, day 4 and day 6) for all the conditions tested in matrigel-coated filters. Values are Mean ± SEM (n=2-3 biological replicates with triplicate filters per condition). **P<0.05, **P<0.01, ***P<0.001.*

Overall, our results show that BM supplemented with both VEGF, Wnt3a and RA offered the best approach to differentiate endothelial progenitor cells into BLECs and generate a monolayer of cells with high TEER values and lower paracellular permeability to Lucifer yellow. This chemically defined media was selected for the remaining experiments. Our results further show that the purification of the cells before monolayer formation in the Transwell system is very important to achieve the most robust and functional barrier.

Screening of ECM for the induction of BBB properties in CD31⁺ cells. ECM is an important component in the maintenance of BBB integrity [42]. Brain ECs interact with the ECM by integrins (namely $\alpha1\beta1$ and $\alpha6\beta1$) and dystroglycans [210]. The integrins preferentially bind to laminin, collagen IV, and fibronectin. Dystroglycan binds to laminin, perlecan and agrin, although laminin is the primary matrix ligand. To evaluate the BBB inductive properties of ECM, we decellularized ECM from primary bovine pericytes, bovine brain capillary endothelial cells (bBCECs) and rat glial cells. We assess the efficacy of the protocol by staining the culture before and after the decellularization for phalloidin and DAPI (**Figure 3.6A**). Collagen and non-collagenous proteins were quantified by Sirius red and Fast green assay, respectively (**Figure 3.6B-D**). We found that the best condition to decellularize the ECM was between day 8 and day 12, based in a compromise of amount of deposited ECM and time (data not shown). In these conditions each type of ECM contains approximately 10% of collagen and 90% of non-collagenous content. The amount of collagen in the pericyte ECM (2 $\mu g/cm^2$) and the non-collagenous proteins in bBCEC ECM (24 $\mu g/cm^2$) were higher than in the remaining ECMs (**Figure 3.6C**). The collagen values assessed for the different ECMs are in line with the value described for mesenchymal stem cells decellularized matrix reported elsewhere [211]. To evaluate the stability of the decellularized ECM, the matrices were kept in culture media at 4ºC and 37°C, for 4 days (**Figure 3.6D**). Our results showed that approximately 50% of the collagen content was maintained after 4 days, while for non-collagenous proteins a loss of 40% was observed. Taken together, our results showed that we could prepare decellularized ECM from cells of the neurovascular unit.

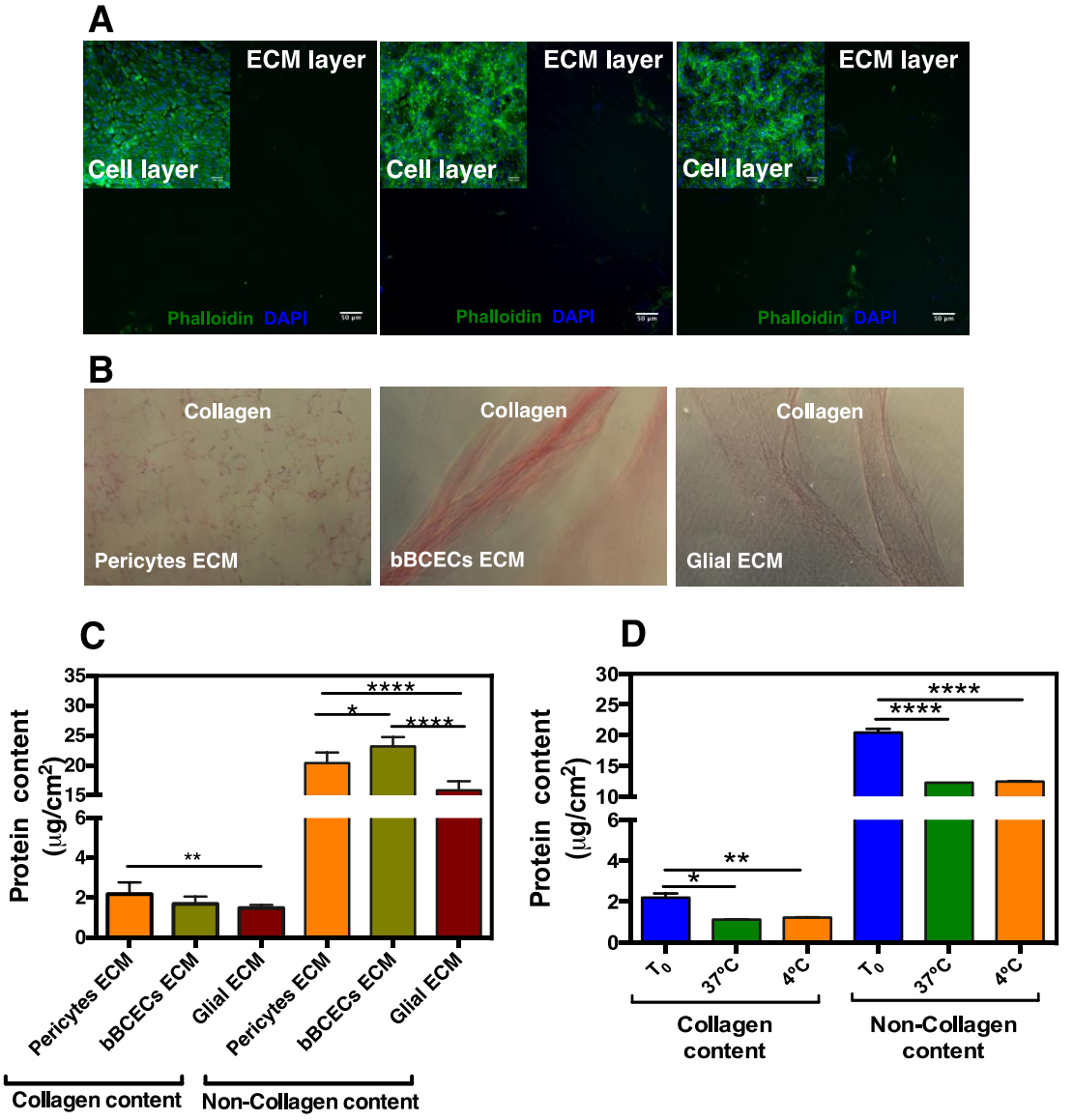

Figure 3.6 - Isolation and characterization of native decelullarized ECM from cells of the NVU. A| Evaluation of the decellularization protocol efficacy by stain against DAPI and phalloidin after 8 days of matrix production. **B|** Images of Sirius red-stained fibrillar collagen of the indicated matrices by Sirius Red/Fast Green kit. **C|** Comparison of ECM production from bovine pericytes, bBCECs and rat glial cells at day 8. **D|** Stability of the native pericytes ECM at 37°C and 4°C in terms of maintenance of the collagen and non-collagen protein content. Values are Mean ± SEM (n=3). **P<0.05, **P<0.01, ****P<0.0001.* Scale bar corresponds to 50 μm.

To evaluate the effect of decellularized ECM in the induction of BBB properties in endothelial progenitor cells, $CD31^+$ cells were cultured on top of decellularized ECMs or

fibronectin for 4 passages (ca. 16 days), in BM as control or BM supplemented with VEGF, Wnt3a and RA (**Figure 3.7**).

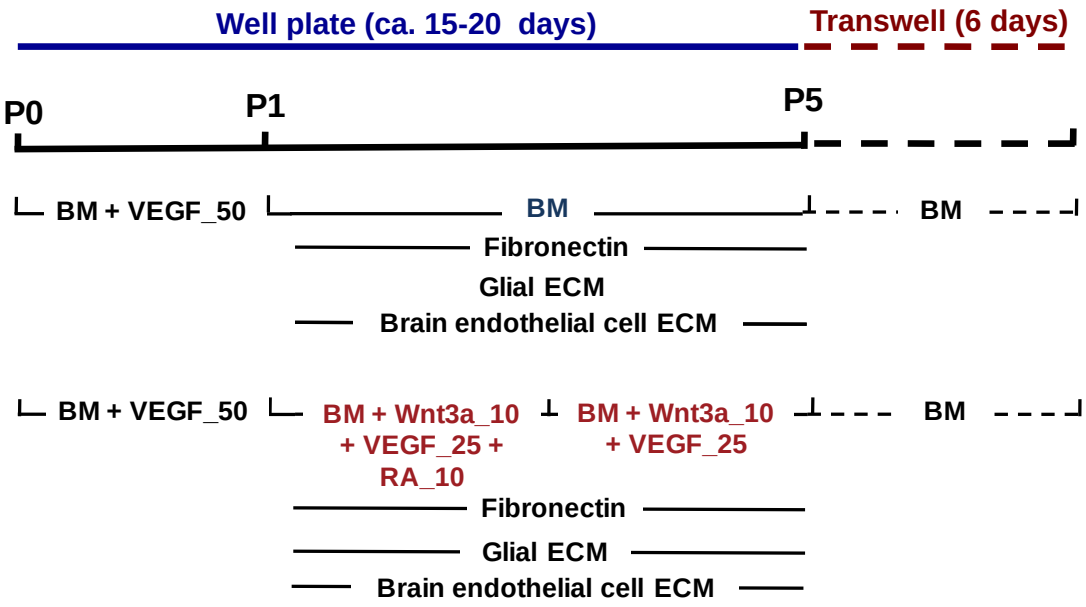

Figure 3.7 - Schematic representation of the protocols used to maturate the CD31⁺ to BELCs combinig soluble and non soluble cues. Cells were cultivated for 4 passages either in fibronectin (control) or in the decellularized ECM in BM or BM supplemented with all the inductive factors, and then purified for CD31 marker and platted in matrigel-coated filters for 6 days.

CD31⁺ cells adhered to glial and bBCEC decellularized ECM; however, they didn't adhere well to the decellularized ECM of pericytes and died after some time (**Figure 3.8**). Therefore, cells cultured in fibronectin and decellularized glial or bBCEC ECMs were characterized by flow cytometry after 4 passages.

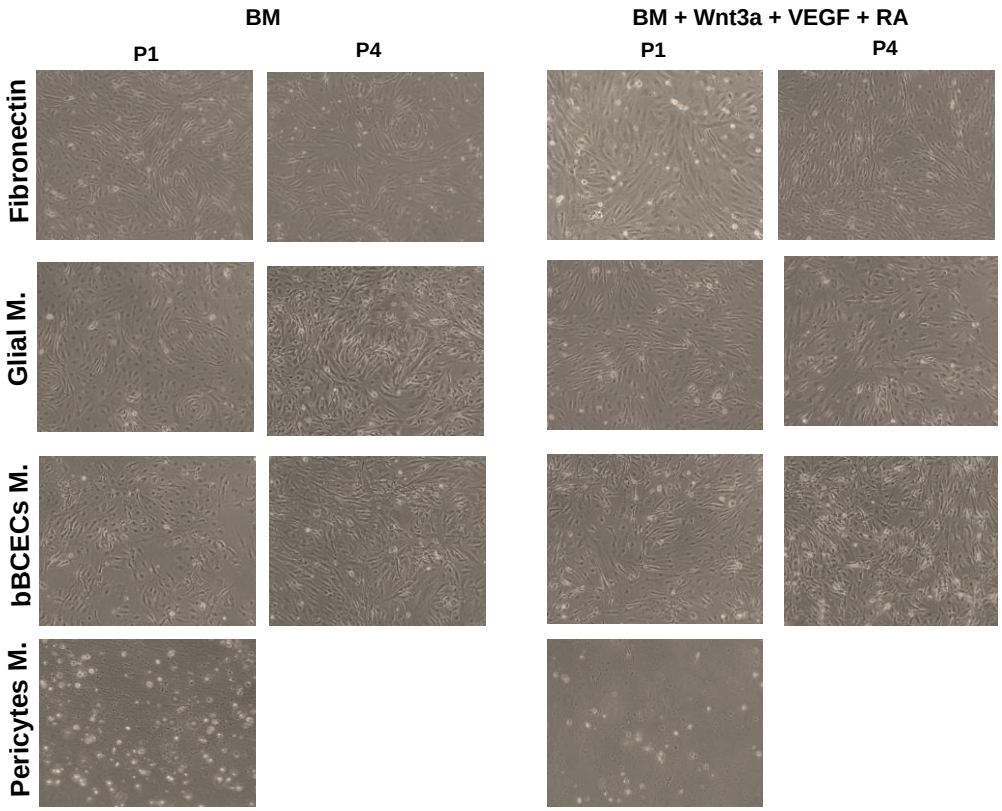

Figure 3.8 - Characterization of the adhesion and proliferation of the BLECs. The cells were platted in the different cell matrices or in fibronectin and cultivated with BM or BM+VEGF+Wnt3a+RA. At passage 1 and passage 4 their capacity to adhere and proliferate was assessed.

Cells cultured in the glial decellularized ECM presented a lower co-expression of CD31:ZO-1 and CD31:Claudin-5 than the ones cultured in fibronectin (control); however, slightly higher co-localization of CD31:Pgp (**Figure 3.9A**). Co-localization results combined with total expression of vascular and BBB markers (**Figure 3.9B**) suggest that cells cultured in glial decellularized ECM express BBB markers but they are not $CD31^+$ cells. Cells cultured in decellularized bBCEC ECM lost significantly their endothelial phenotype during the 4 passages (as evaluated by CD31 marker) and showed low co-expression of CD31:ZO-1, CD31:Claudin-5 and CD31:Pgp (**Figure 3.9A**). Gene expression analysis for BBB and endothelial markers followed by clustering analysis showed that $CD31^+$ cells cultured in fibronectin are more related to BLECs previously reported by us [204] (**Figure 3.10A**). Therefore, the decellularized glial ECM do not improve significantly the BBB phenotype of ECs as compared to fibronectin.

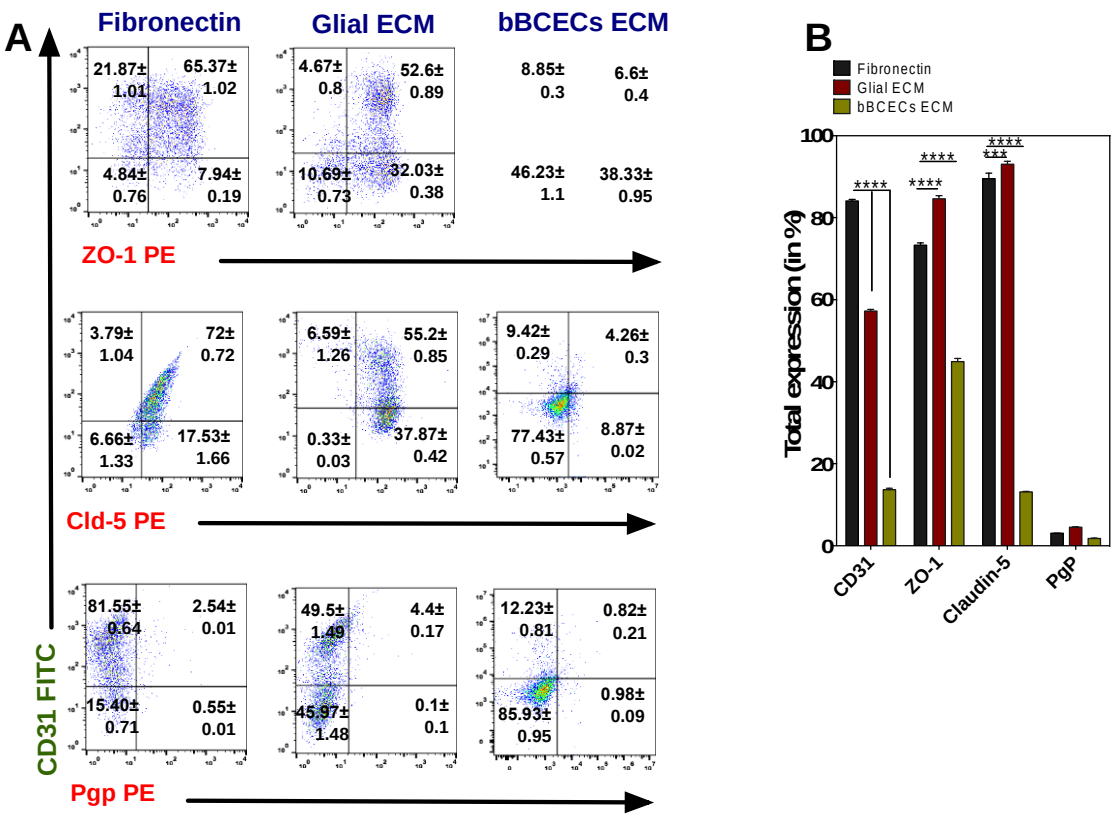

Figure 3.9 - Characterization by flow cytometry of BLECs maturated in the different decellularized matrices in the presence of soluble factors. A| Expression by flow cytometry of BBB markers (ZO-1, claudin-5 and Pgp) co-localized with CD31 marker on the cells maturated in fibronectin or decellularized matrices at passage 4. **B|** Total expression of each cell marker in the different assessed conditions. Values are Mean ± SD (n=3). ****P<0.001 and ****P<0.0001.*

Next, we evaluated the functional properties of the derived cells at passage 5, after purification for CD31 marker. Cells were cultured to confluence on Transwell filters for 6 days after which paracellular permeability to Lucifer yellow and TEER analyses were performed. Cells cultured in the decellularized glial ECM and fibronectin, but not in bBCEC ECM, showed good expression of VE-cadherin, claudin-5 and ZO-1 at cells borders, showing good intercellular communication (**Figure 3.10B**). No major differences in paracellular permeability to Lucifer yellow were observed between cells cultured in fibronectin or in decellularized ECM from glial cells; however, cells cultured in decellularized bBCEC ECM showed higher paracellular permeability than cells cultured in the other conditions (**Figure 3.10C**). On the other hand, cells cultured in fibronectin had higher TEER values than the ones cultured in the other conditions (**Figure 3.10D**).

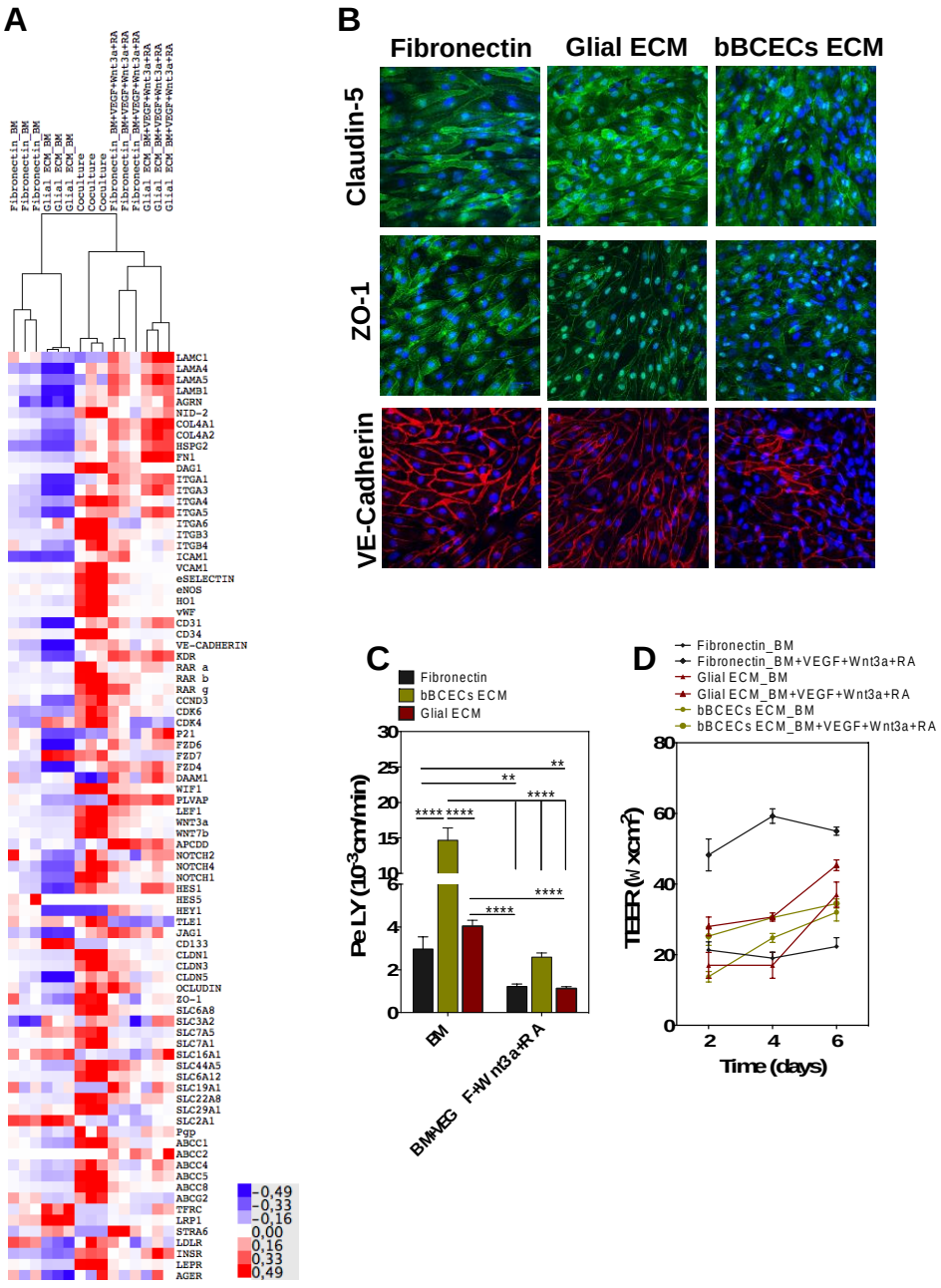

Figure 3.10 - Effect of the combination of soluble factors with decelullarized ECMs in the induction of BBB properties. A| Global gene expression levels were profiled by mRNA-Seq (replicates: 1, 2, and 3) in cells platted in matrigel-coated filters for 6 days after maturation with BM or BM+VEGF+Wnt3a+RA either in fibronectin or Glial ECM (Positive control: CD34ECs in coculture). Correlation uncentered heatmap and hierarchical clustering dendogram of the arrays are displayed. **B|** Expression of claudin-5 (green), ZO-1 (green) and VE-cadherin (red) in BLECs plated in the matrigel-coated filters for 6 days. **C|** Paracellular permeability to Lucifer yellow (LY) for purified cells, after 6 days in the matrigel-coated filters, for cells maturated in different native ECMs exposed to the different medium. **D|** TEER at different time points (day 2, day 4 and day 6) for all the conditions tested in matrigel-coated filters. Values are Mean ± SEM (n=2 biological replicates with triplicate filters per condition). ** *P<0.01, ****P<0.0001.*

Overall, our results show that from the 3 decellularized ECMs tested, only decellularized glial ECM showed promising results in terms of EC phenotype maintenance, BBB marker induction and paracellular permeability; however, the results were not significantly distant from the ones obtained with fibronectin. Therefore, subsequent tests were performed with $CD31^+$ cells cultured in fibronectin-coated plates in BM supplemented with VEGF, Wnt3a and RA.

Induction of BBB properties in $CD31^+$ cells: effect of time. The induction of BBB properties in $CD31^+$ cells cultured in fibronectin-coated plates in the presence of BM supplemented with VEGF, Wnt3a and RA was monitored by flow cytometry. Co-localization of the CD31 marker with ZO-1, claudin-5 or Pgp was quantified. Cells cultured in BM were used as control. Flow cytometry analyses were performed at passage 2 (approximately 8 days in culture) and 4 (approximately 16 days in culture). Our results show that cells cultured in BM supplemented with VEGF, Wnt3a and RA showed high co-localization of CD31 with BBB markers such as ZO-1 and claudin-5 (**Figure 3.13A**). These flow cytometry results were confirmed by confocal microscopy analyses (**Figure 3.11B**).

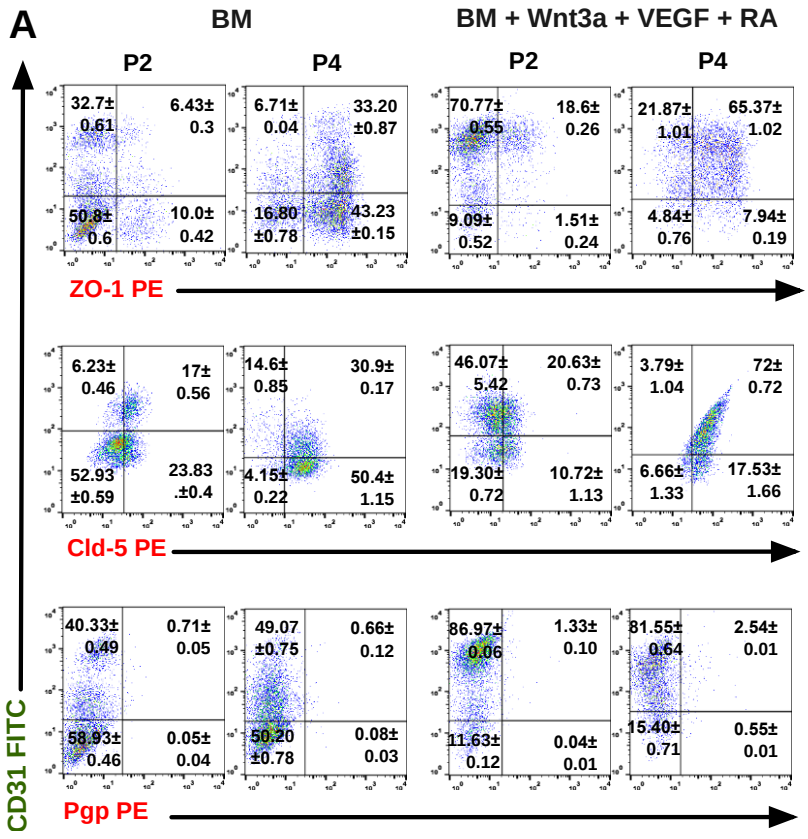

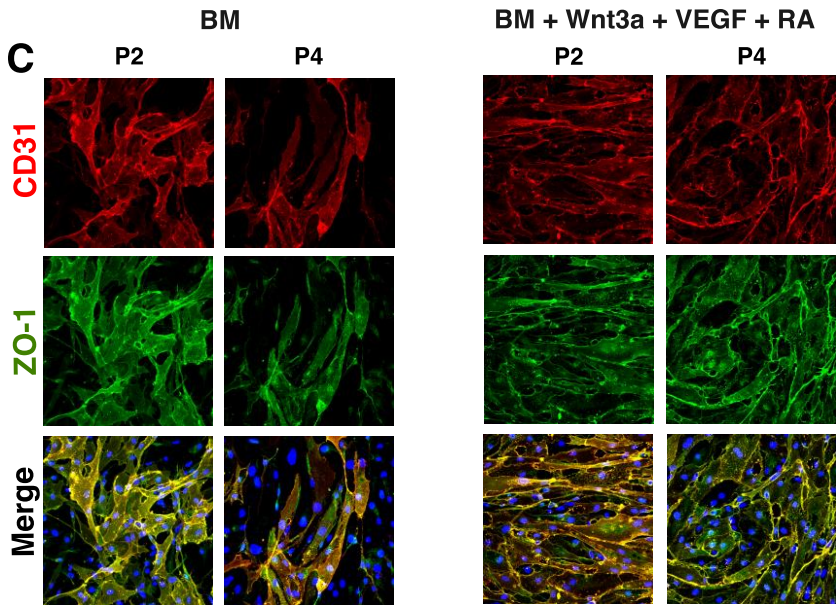

Figure 3.11 - Impact of time in the maturation of CD31⁺ to BLECs. (A) Expression by flow cytometry of BBB markers (ZO-1, claudin-5 and Pgp) co-localized with CD31 marker on the cells maturated in different inductive mediums (BM or BM+VEGF+Wnt3a+RA) at passage 2 and passage 4. **(B)** Immunofluorescence analysis for the co-localization of CD31 (red) with ZO-1 (green) proteins in the BELCs at passage 2 and 4 in fibronectin-coated plates. Scale bar corresponds to 50 μm.

As expected, the expression of BBB markers was higher than the one observed in initial endothelial progenitor cells (CD31⁺ cells) or ECs without a BBB phenotype (**Figure 3.12**).

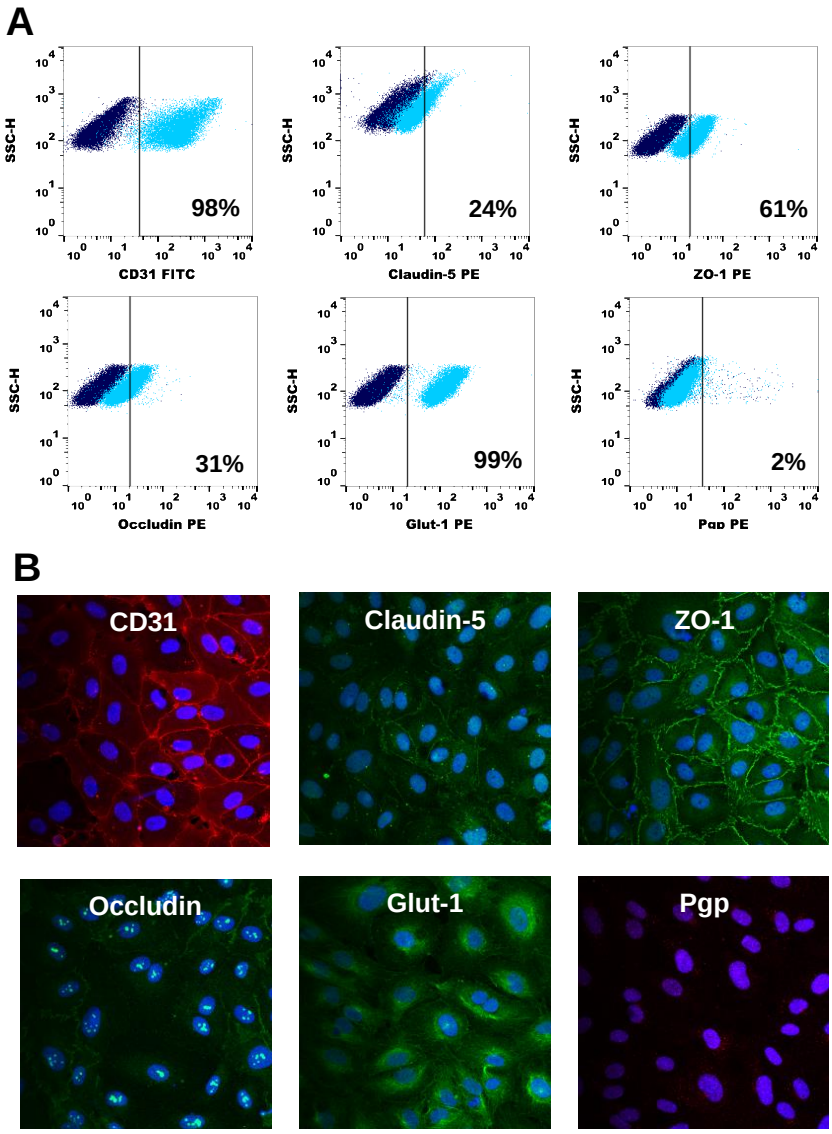

Figure 3.12 - Characterization of HUVECs for EC and BBB markers expression. A| Levels of markers expression by flow cytometry and **B|** Immunostaining of the same markers. Scale bar corresponds to 50 µm.

The co-localization between CD31 and BBB markers increased during the 4 cell passages. During this time, the differentiated cells express very low levels of Pgp. These results agree with the fact that human BBB express low levels of Pgp transporter [212]. Our results further show that cells negative for CD31 are positive for BBB markers likely indicating the presence of intermediary phenotypic stages in the cell population (**Figure 3.13 A1 and A2**).

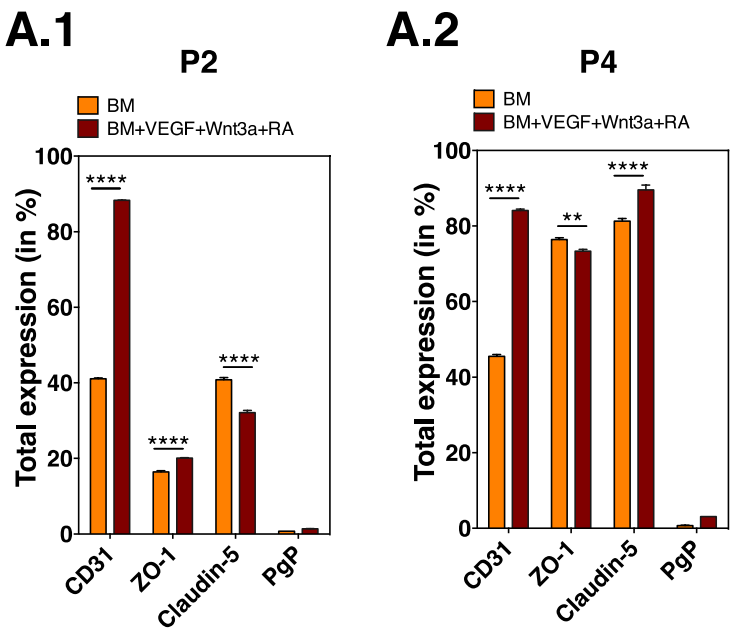

Figure 3.13 - Impact of time in the maturation of CD31⁺ to BLECs. Total expression of each cell marker in the different assessed conditions at **A.1|** passage 2 and **A.2**| passage 4. Values are Mean ± SD (n=3). ***P<0.01 and ****P<0.0001.*

Functional characterization of BLECs. CD31⁺ cells were cultured in fibronectin-coated plates in the presence of BM supplemented with VEGF, Wnt3a and RA for 4 passages. At passage 5, cells purified for CD31 marker were grown to confluence on filters for 6 days after which monolayer formation was characterized by immunocytochemistry (**Figure 3.14A**). Cells express endothelial markers at the cell membrane such as CD31 and VE-cadherin and at the cytoplasm including vWF. Moreover, cells highly express BBB markers including the TJ proteins ZO-1, claudin-5 and occludin and the Glut-1. The transporter Pgp is present at very low levels.

The differentiated cells express multiple BBB genes such as TJ (claudin-5 and occludin), influx aminoacid (SLC44A5, SLC16A1) and glucose (SLC2A1) transporters and receptors (e.g. Tf and insulin) (**Figure 3.14B**). In addition, the differentiated cells express transcripts of key efflux transporters such as BCRP and MRP family (subfamily of the ABC transporters), and they express large molecule receptors such as the receptor for advanced glycation end products (RAGE) (**Figure 3.14B and Figure 3.10A**). Based in the gene and protein expression results as well as the paracellular permeability and TEER results (**Figure 3.5**) and the clustering of the cells with our previous model, the differentiated cells are designated as BLECs.

BLECs respond to inflammatory stimuli such as TNF-α. The cells express constitutively intracellular adhesion molecule (ICAM)-1 and -2 but not vascular cell adhesion molecule (VCAM)-1 or e-selectin. With the exception of VCAM, all the molecules are up-regulated in BLECs exposed to TNF-α mediated by the activation of the pleiotropic nuclear factor–kB (NF-kB) [213] (**Figure 3.14C**).

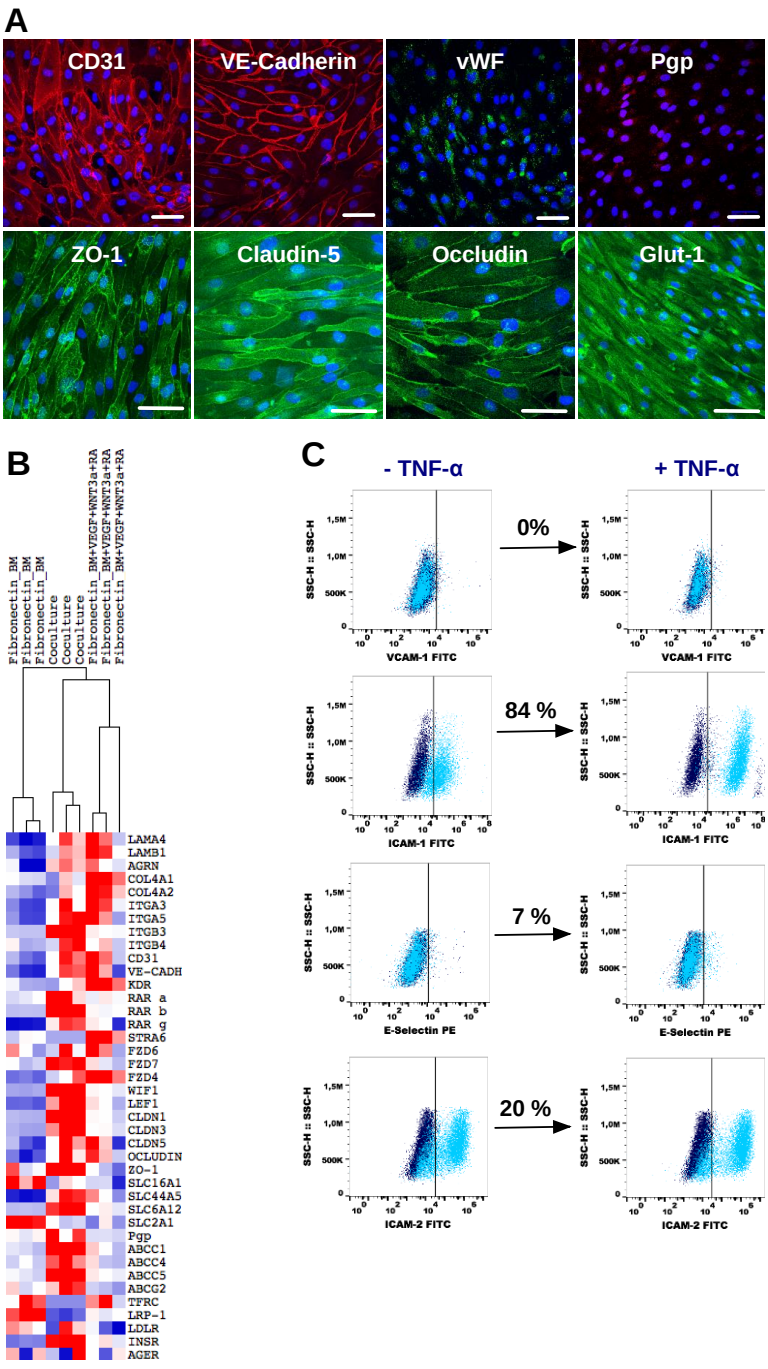

Figure 3.14 - Functional characterization of the BLECs. A| Expression of endothelial (CD31, VE-cadherin and vWF) and BBB markers (ZO-1, claudin-5, occludin, Pgp and Glut-1) in BELCs by immunofluorescence after 6 days in matrigel-coated filters. **B|** Global gene expression levels were profiled by mRNA-Seq (replicates: 1, 2, and 3) in cells platted in matrigel-coated filters for 6 days after maturation with BM or BM+VEGF+Wnt3a+RA in fibronectin (Positive control: $CD34^+$ derived ECs in coculture). Correlation uncentered heatmap and hierarchical clustering dendogram of the arrays are displayed. **C|** The expression of the adhesion molecules (VCAM-1, ICAM-1, ICAM-2 and e-selectin) was assessed by flow cytometry on passage 5 BLECs, untreated and treated by TNF-α (10 ng/mL) 24 h after exposure. Scale bar corresponds to 50 μm.

3.4. DISCUSSION

In this study we describe the derivation of BLECs from iPSCs through a two-step protocol. Initially we derived endothelial progenitor cells from human iPSCs after which they were specified into a BBB-like phenotype by exposure to BBB soluble and insoluble cues. After screening several soluble and insoluble factors, we show that endothelial progenitor cells cultured in fibronectin for 4 passages in BM supplemented with Wnt3a, VEGF and RA present the best BBB properties including a high expression of endothelial markers (CD31, VE-cadherin, vWF), an organized TJ at cell-cell junctions (ZO-1, claudin-5, occludin), the expression of nutrient transporters (Glut-1), the expression of efflux pumps (Pgp), a TEER similar to other human BBB systems (TEER of ca. 60 Ωcm^2) [204], low paracellular permeability to Lucifer yellow (ca. 1.2 $x10^{-3}$ cm/min) and the up-regulation of adhesion molecules ICAM-1, e-selectin and ICAM-2 after cell exposure to TNF-α.

Our study is the first to derive BLECs from well-defined iPSC-derived cell populations and chemically defined factors. Recent studies [61, 109, 112] have shown the derivation of BLECs from iPSCs using a three-steps differentiation protocol combining (i) differentiation of iPSCs in specific media, (ii) selective maturation of ECs in endothelial cell media and (iii) purification of the ECs by sub-culturing on collagen IV and fibronectin coated surfaces. The protocol differentiates simultaneously iPSCs into both neural (several sub-populations of neural cells) and endothelial lineages (characterized by the expression of CD31 marker). The differentiation strategy is based in a co-culture system of ECs with neural cells followed by the isolation of the ECs with BBB properties using selective adhesion to a collagen IV and fibronectin coated surface. The differentiation protocol yielded on average 11.6 BLECs per input iPSC, characterized by the co-expression of CD31 and Glut-1 markers, per input iPSC. These cells co-expressed claudin-5 (~100%), occludin (~100%), Glut-1 (~70%) and Pgp (50-70%). However, so far, it is unclear the initial and transient phenotypic stages of ECs until they reach the BLEC properties, the factors (soluble and ECM) involved in these transitions, and the functionality of the cells if they are purified for the same endothelial marker. Our differentiation protocol consists in the initial differentiation of iPSCs into endothelial progenitor cells characterized by the expression of $CD31^{+}Glut\text{-}1^{+}ZO\text{-}1^{med}Claudin\text{-}5^{med}Occludin^{med/-}$ and then in the specification of these cells into BLECs by the use of defined media and ECM for 4 passages (ca. 15-20 days). At the end of the differentiation protocol we have on average 10 BLECs per input iPSC. Recently, it has

been described a differentiation protocol of iPSCs into BLECs mediated by endothelial progenitor cells characterized by the expression of CD34 and CD144 markers [85]. However, the specification of endothelial progenitor cells into BLECs occurred by a co-culture system with C6 rat glioma cells and not by defined components in the culture media.

Our results show that the activation of Wnt3a, VEGF and RA signaling pathways is important to have a more functional BBB phenotype. Previous studies using iPSCs have shown that canonical Wnt-β-catenin [61] and RA [109, 112] signaling was necessary for the specification of BBB properties in ECs. Our results show that the activation of VEGF or RA signaling is very important to maintain the endothelial phenotype (characterized by the expression of CD31 at protein level as well as CD31, VE-cadherin and KDR at gene level) during the specification of the cells. Importantly, in both conditions, we had more than 15-25% of $CD31^-$ cells (non-endothelial phenotype), which had a significant impact in the functional properties of the barrier in these cells. A low percentage of non-ECs interfered with the endothelial barrier, making it presenting low TEER (below 50 $\Omega x cm^2$) and high paracellular permeability (above 2 $x10^{-3}$ cm/min).

From a BBB functional point of view, the activation of Wnt3a or VEGF signaling pathways is very important to have high TEER and low paracellular permeability, functional markers of a BBB phenotype. The functional properties were evaluated in cells that were purified for CD31 marker and cultured for 6 days in a Transwell system in the absence of the BBB inductive factors. Therefore, the differences in the functional properties of the barrier evaluated in a Transwell system after 6 days is due to the BBB phenotype acquired by the cells during the specification and not during the functional assay. To further demonstrate this, endothelial progenitor cells cultured in BM (without any BBB inductive factor) for 4 passages and purified for CD31 marker had significant lower TEER and higher paracellular transport than the ones cultured in BM supplemented with Wnt3a, VEGF and RA.

Our study is the first to evaluate the effect of the ECM in the specification of BLECs. ECM provides physical support and presents biomolecules (proteins, polysaccharides, small molecules, etc) that might be important for the BBB specification process [112]. It has been shown for other cells that decellularized ECM plays an important role in guiding differentiation/maturation into a specific lineage [51, 214]. Moreover, it has been demonstrated that ECM produced by cells forming the NVU (glial and pericytes) improved the barrier function in terms of resistance in the BMVECs cultured *in vitro* [215]. Our results show that endothelial progenitor cells were unable to adhere to pericyte decellularized ECM but they were able to attach to the decellularized matrix of bBCECs

and glial cells. Cells differentiated on top of decellularized glial ECM showed the highest endothelial cell phenotype and BBB marker induction after 4 passages, the highest TEER and the lowest paracellular permeability to Lucifer yellow. However, the results obtained were not significantly different from the ones obtained in fibronectin. We cannot discard the possibility that the decellularized ECM might have effect in the polarization of BLECs. This is a topic that deserves further investigation in the near future.

The BBB specification of endothelial progenitor cells is a slow process and is characterized by the co-expression of CD31 marker with ZO-1 and claudin-5. Our results indicate that the expression of ZO-1, claudin-5 and Pgp increases in $CD31^+$ cells over 4 passages. It is interesting to note that cell culture media that was less effective in maintaining endothelial phenotype contributed for the derivation of a population of cells that show high expression of BBB markers. For example, endothelial progenitor cells cultured in BM for 4 passages express high levels of ZO-1 (ca. 43%) and claudin-5 (ca. 50%) in $CD31^-$ cells. Curiously, ECs ($CD31^+$ cells) cultured in these mixed conditions show high paracellular permeability (3±0.6 $x10^{-3}$ cm/min) and low TEER (22.3±1.5 $\Omega x cm^2$). Future studies should evaluate the expression of neural (nestin and β-tubulin) [61] as well as pericyte markers (platelet-derived growth factor receptor b and NG2) [51] in these $CD31^-$ populations in order to characterized these cells for potential BBB inductors.

The BLECs derived in this work share properties identified previously by us in BLECs derived from hematopoietic stem/progenitor cells [204]. Gene clustering analysis show that iPSC-derived endothelial progenitor cells cultured in BM supplemented with Wnt3a, VEGF and RA were closer to BLECs derived from hematopoietic stem/progenitor cells than the ones differentiated in BM (without BBB inductive factors). Both BLECs have similar TEER (55±0.6 Ωxcm2 vs 56±4.04 Ωxcm2), paracellular permeability to Lucifer yellow (1.2±0.1 $x10^{-3}$ cm/min vs. 0.61±0.15 $x10^{-3}$ cm/min), expression of TJ and transporters (e.g. Glut-1). However, some differences are observed. BLECs derived from iPSCs had no up-regulation of VCAM-1 to TNF-α and show lower levels of Pgp than BLECs derived from hematopoietic stem/progenitor cells, which likely indicate differences in the development stages of the two BLEC populations.

The work presented here may contribute for a better understanding of the processes underlying the BBB development and maintenance. BBB formation is initiated at embryonic day 12 in the rat cerebral cortex by ECs that invade the neural tissue from the surrounding vascular plexus [51]. BBB-forming ECs are characterized by the expression of TJs including occludin, claudin-5 and ZO-1 and the influx transporter Glut-1. Interestingly, these cells express very low levels of Pgp that only increase during

postnatal development [51]. Our *in vitro* results recapitulate this process since low levels of Pgp and high levels of the other markers were observed in BLECs. Previous studies have derived BLECs with high expression of Pgp which may indicate a high level of BBB maturation [61, 112].

3.5. MATERIAL and METHODS

Differentiation of iPSCs into CD31⁺cells. iPSCs (passages 32-35; cord blood derived iPSCs kindly donated by Ulrich Martin [91]) were grown on mitomycin C-inactivated mouse embryonic fibroblast feeder layer in undifferentiating culture medium [(knockout Dulbecco's Modified Eagle Medium; DMEM (GIBCO)], 20% knockout serum replacer (Gibco), non-essential amino acids (1%, GIBCO), β–mercaptoethanol (0.1 mM, Sigma), L-glutamine (1 mM, Sigma) and β-FGF (5 ng/mL, PreproTech). iPSCs were passaged every 3-4 days with collagenase IV (1mg/mL, Gibco) at a typical splite ratio of 1:4 or 1:6. To initiate the differentiation, cells were treated for 45-60 min. with collagenase IV and plated on fibronectin-coated dishes (1 μg/cm^2; Calbiochem; split ratio: 1 confluent well from a MW-6 to a 100mm Petri dish) in a chemically defined medium (CDM) containing Iscove's Modified Dulbecco's Medium (IMDM; 50% (v/v), Gibco), F12 (50%, Gibco), BSA (5 mg/mL, Sigma), β-mercaptoethanol (0.1 mM, Sigma), Pen/Strep (50 U/mL:50 μg/mL, Lonza), transferrin (15 mg/mL, Sigma) and insulin (7 mg/mL, Sigma). During the 10 days of the differentiation several factors (BMP-4, bFGF, VEGF and TB4) were added to CDM medium in order to induce the formation of endothelial progenitor cells (CD31$^+$ cells). CD31$^+$ cells were isolated by MACS.

Specification of CD31⁺cells into a BBB-like phenotype. CD31$^+$ cells were platted on fibronectin-coated dishes (1 μg/cm^2; Calbiochem) and cultured in EGM-2 (Lonza) supplemented with SB 431542 (10 μM, Tocris Biosciences), bFGF (1 ng/mL, Sigma) and $VEGF_{165}$ (50 ng/mL, PeproTech) for 1 passage. Cells were then cultured in BM (EGM-2 supplemented with 10 μM SB 431542 and 1 ng/mL bFGF) or BM supplemented with VEGF (25 ng/mL), Wnt3a (10 ng/mL, R&D Systems) or RA (10 μM, Sigma) alone or in combination for 4 passages (**Figure 3.1B**).

In a separate set of experiments, CD31$^+$ cells were plated in fibronectin-coated dishes or in decellularized native ECMs from pericytes, glial cells and bBCECs in the presence of BM or BM supplemented with VEGF, Wnt3a and RA (**Figure 3.7**). During

the differentiation procedure, cells were passed systematically every 4 days, in a split ratio of 1:3. Additionally, to have a robust and consistent protocol, we tried to expose the cells to the inductive factors for 16 days.

Immunocytochemistry. Cells were fixed in cold methanol/acetone (50%/50%, v/v) for 1 min or with 4% (v/v) paraformaldehyde (PFA; electron Microscopy Science) for 10 min at RT and permeabilized with Triton X-100 (0.1%, v/v, Fluka) for 10 min, whenever required. Cells were then blocked with BSA (1%, w/v, Sigma) solution for at least 30 min followed by incubation with primary antibody (**Table 3.1**) during 1 h at RT. After washing, cells were stained with secondary antibody for 30 min in dark at RT. The nuclei of the cells were counterstained with DAPI (Sigma) and cells mounted with cell-mounting medium (DAKO). All the photos were taken with the objective of 40x oil.

Flow Cytometry. Cells were dissociated from the culture plate by exposure to Cell Dissociation Buffer (Life Technologies) for 10 min and gentle pipetting, centrifuged and ressuspended in PBS supplemented with 5% (v/v) FBS (GIBCO). The single cell suspensions were aliquoted, fixed with ice-cold methanol/acetone (50%/50% v/v) or 1% (v/v) PFA and permeabilized with 0.5% (v/v) Tween, when necessary. The cells were stained with specific primary antibodies (**Table 3.1**). Cells were further incubated with the secondary antibody when necessary (**Table 3.1**). For the co-localization experiments, ZO-1 and claudin-5 primary antibodies were conjugated with a R-Phycoerythrin (Abcam) dye to facilitate the setup of the experiment. FACS Calibur (BD Biosciences) and Accuri C6 were used for the acquisition and FlowJo was used for data analyses.

Table 3.1. Antibodies used for immunocytochemistry and flow cytometry. *Refers to antibodies only used for flow cytometry.

Antibody	Dilution	Technique	Supplier
CD31	1:50	ICC	DAKO/ Labometer
Ve-Cadherin	1:100	ICC	Life Technology
ZO-1	1:200	ICC	Life Technology
Claudin-5	1:100	ICC	Life Technology
Occludin	1:200	ICC	Life Technology
Glut-1	1:50	ICC	Millipore
Pgp	1:10	ICC	GeneTex
***FITC-Conjugated anti-CD31**	5:200	FACS	EBioscience
***PE-Conjugated anti Pgp**	5:200	FACS	Abcam
***FITC-Conjugated anti CD106**	10:100	FACS	BD Pharmingen
***PE-Conjugated anti CD62E**	5:100	FACS	BioLegend
ICAM-1	1:100	FACS	Santa Cruz Biotechnology
R-PE conjugation Kit	-	FACS	Abcam
Anti rabbit Cy3	1:100	ICC	JacksonImmunoResearch
Anti mouse Cy3	1:50	ICC	Sigma
Anti rabbit Alexa 488	1:200	ICC	Life Technology
Anti mouse Alexa 555	1:200	ICC	Life Technology

Endothelial permeability measurements. To perform the assay, 10 x10^4 cells were seeded in 0.4 µm filters (Costar) coated with matrigel and kept in culture with EGM-2 supplemented with bFGF (1 ng/mL) for 6 days. Before initiating the permeability experiment, EBM-2 was added to empty wells of a 12-well plate. Filter inserts containing the BLECs were placed in the multi-well and filled with EBM-2 containing the fluorescent integrity marker Lucifer Yellow (20 µM, Life Technologies). Plates were placed on an orbital shaker for 1 h and then withdraw from the receiver compartment. The fluorescence of the samples (inserts with cells and without cells) was quantified using the wavelengths 430/530 (excitation/emission). The permeability values were generated through the blue-norna brain exposure simulator (http://www.blue-norna.com).

Transendothelial electrical resistance. BLECs TEER (Ohmxcm²) on Transwell filters was measured using the Millicell-ERS 2 (Electrical Resistance System, Millipore). The resistance of Matrigel-coated inserts was subtracted from the resistance obtained in the presence of the endothelial cultures according to the followed equation: TEER = [(TEER, cells)-(TEER, insert)×A], where A is the area of the filter (cm^2).

Gene expression analyses. Total RNA was extracted from several conditions and isolated according RNeasy Micro Kit instructions (Quiagen) and quantified. DELTAgene assays (96.96 IFC – Fludigm) were designed for human transcripts. The pre-amplification process was performed for 18 cycles in order to obtain sensitivity down to a single cDNA molecule. The oligos were synthesized by Sigma and dissolved at a concentration of 100 µM in water. For each assay a Primer Pair Mix was prepared containing 50 µM Forward Primer and 50 µM Reverse Primer. In order to prepare 10 × Pre-amplification Primer Mix (500 nM each primer), 10 µL of each of the 96 Primer Pair Mixes (50 µM each primer) was mixed with 40 µL buffer consisting of 10 mM Tris–HCl, pH 8.0; 0.1 mM EDTA; 0.25% Tween-20. In order to prepare 10× Assay (5 µM each primer) each Primer Pair Mix was diluted by mixing 10 µL Primer Pair Mix (50 µM each primer) with 90 µL buffer consisting of 10 mM Tris–HCl, pH 8.0; 0.1 mM EDTA; 0.25% Tween-20. A pre-mix containing cDNA and primers was done and treatment with exonuclease was performed to remove non-hybridized primers. The Fluidigm® 96.96 Gene expression IFC was used with EvaGreen chemistry. After a prime of the chip, a 10x assay mix and sample mix were prepared and pipetted into the inlets. The chip was loaded and data was collected using the BioMark HDTM. Data were analyzed using Fluidigm® Real Time PCR Analysis v2.1 software. Clustering of the samples was perfomed using the Cluster 3.0 program, hierarchical clustering and complete linkage

method. The assembling of the data in terms of heat map was performed using Java TreeView v1.1 software. Genes and primer sequences are given in **Table 3.2**.

Table 3.2. Specific set of primers designed by Sigma used in Fludigm experiment.

GENE	Sense	Antisense
ABCC1	AATAGAAGTGTTGGGCTGAG	CGAGACACCTTAAAGAACAG
ABCC2	ATATAAGAAGGCATTGACCC	ATCTGTAGAACACTTGACCA
ABCC4	AATCTACAACTCGGAGTCCA	CAAGCCTCTGAATGTAAATCC
ABCC5	TCACTACATTAAGACTCTGTCC	GGATACTTTCTTTAGGACGAGAG
ABCC8	GATCATTGTGGGTGTGATTC	AGCCAGTAGAATGATGACAG
ABCG2	CAAGATGATGTTGTGATG	GATTCGTCATAGTTGTTG
ACTNβ	CGTCTTCCCCTCCATCGT	GATGGGGTACTTCAGGGTGA
AGER	GTAGATTCTGCCTCTGAACTC	CTTCACAGATACTCCCTTCTC
AGRN	GATCTTCTTTGTGAACCCTG	TATCTTCCACACAGAATCTCC
APCDD1	GGAGTCACAGTGCCATCACAT	CCTGACCTTACTTCACAGCCT
CCND3	AGACCAGCACTCCTACAG	GGCTTAGATGTGGTGTGG
CD31	AGATACTCTAGAACGGAAGG	CAGAGGTCTTGAAATACAGG
CD34	TGAAGCCTAGCCTGTCACCT	CGCACAGCTGGAGGTCTTAT
CD133	ACAACACTACCAAGGACAA	GGACTTAATCTCATCAAGAACAG
CDK4	TACCTGAGATGGAGGAGTC	GCAGAGATTCGCTTGTGT
CDK6	GAAAAGTGCAATGATTCTGGA	GAAGCGAAGTCCTCAACA
CLDN1	GAAAGACTACGTGTGACA	GGTCCTAATGTTAATGATAGTATC
CLDN3	ATCACGTCGCAGAACATC	TACACCTTGCACTGCATCTG
CLDN5	TTAACAGACGGAATGAAGTT	AAGCGAAATCCTCAGTCT
COL4A1	AAAGGGAGATCAAGGGATAG	TCACCTTTTTCTCCAGGTAG
COL4A2	AAAAGGAGATAGAGGCTCAC	GTATTCCGAAAAATCCAGCC
DAAM1	GAAGAAGAAAAGCATTCCTCAG	CAGTTTGTTCTCGGGCAG
DAG1	ATTGACTCCTACAGTTCAGG	GCATTAGAAGCCAACTGAAG
eNOS	AACGTGGAGATCACCGAG	GGGCAGAAGGAAGAGTTC
e-SELECTIN	AGCTTCCCATGGAACACAAC	CTGGGCTCCCATTAGTTCAA
FN1	CCATAGCTGAGAAGTGTTTTG	CAAGTACAATCTACCATCATCC
FZD4	TACCTCACAAAACCCCCATCC	GGCTGTATAAGCCAGCATCAT
FZD6	TCGTCAGTACCATATCCCATG	CCCATTCTGTGCATGTCTTTT
FZD7	GATGATAACGGCGATGTGA	AACAAAGCAGCCACCGCAGAC
HES1	GCCTATTATGGAGAAAAGACG	CTATCTTTCTTCAGAGCATC

HES5	AAGAGAAAAACCGACTGC	TTCTCCAGCTTGGAGTTG
HEY1	CCGGATCAATAACAGTTTGTC	CTTTTTCTAGCTTAGCAGATCC
INSR	TGTTCATCCTCTGATTCTCTG	GCTTAGATGTTCCCAAAGTC
HO1	GAAAAGCACATCCAGGCAAT	GCTGCCACATTAGGGTGTCT
HSPG2	CCACTACTTCTATTGGTCCC	GTATTGGATTGGTGGAGATTAC
ICAM1	CAAGGCCTCAGTCAGTGTGA	CCTCTGGCTTCGTCAGAATC
ITGA1	CAGGTTGGAATTGTACAGTATG	TGTCTATTCCAAGAGCTGTC
ITGA3	AGGTAATCCATGGAGAGAAG	GTAGAAGTTCTCATCCACATC
ITGA4	AAAGCTTGGATCGTACTTTG	CTCTTCCTTCCTCTCTGATG
ITGA5	AAGCTTGGATTCTTCAAACG	TCCTTTTCAGTAGAATGAGGG
ITGA6	AAATACCAAACCAACACAGG	TACTGAATCTGAGAGGGAAC
ITGB3	AATCTGCTGAAGGATAACTGT	CTCTGGGGACTGACTTGA
ITGB4	ATCTGGACAACCTCAAGAAG	GCCAAATCCAATAGTGTAGTC
JAG1	GTCTCAAAGAAGCGATCAG	ATATACTCCGCCGATTGG
KDR	GTACATAGTTGTCGTTGTAGG	TCAATCCCCACATTTAGTTC
LAMA4	GAAATTGCATTTGAAGTCCG	ACCTGTCCATTTTTCATGTG
LAMA5	ATCCTATGACTTCATCAGCC	TTGTTATAGAAGAGGGAGAGG
LAMB1	GTGTGTATAGATACTTCGCC	AAAGCACGAAATATCACCTC
LAMC1	TCTCCTCTACCTTTCAGATTG	GGTTCTGACCATAACTCAAC
LDLR	GCCATTGTCGTCTTTATGTC	AAACACATACCCATCAACGA
LEF1	AAGGAACACTGACATCAATT	TTTGGAACTTGGCTCTTG
LEPR	GGAAATCACACGAAATTCAC	GCACGATATTTACTTTGCTC
LRP1	GACTACATTGAATTTGCCAGCC	TCTTGTGGGCTCGGTTAATG
NID2	ACTGTGACCTCTACAAGTTC	CATTATACAAGGCAAAGACCC
NOTCH1	ATCTGAAATAGGAAACAAGTGAA	ATAACCAACGAACAACTACATAA
NOTCH2	AACATCTCATCCATGCTTTG	ACAGTGGTACAGGTACTTC
NOTCH4	ATTGACACCCAGCTTCTTG	GAGGACAAGGGTCTTCAA
OCLUDIN	TTCTGGATCTCTATATGGTTCA	CCACAACACAGTAGTGATAC
P21	CTCTACATCTTCTGCCTTAGT	TCTCATTCAACCGCCTAG
PGP	TGAATCTGGAGGAAGACATGAC	CCAGGCACCAAAATGAAACC
PLVAP	CAATGCAGAGATCAATTCAAGG	ACGCTTTCCTTATCCTTAGTG
RARα	CCATCCTCAGAACTCACAA	ACCAGCGAGAATTAATACCT
RARβ	CACCTAGAGGATAAGCACTT	GGACTCACTGACAGAACA
RARγ	CCACCTTCTTGCTCCTAC	CTTTCACCCTCTGTTCCT
SLC2A1	ACGCTCTGATCCCTCTCAGT	GCAGTACACACCGATGATGAAG
SLC3A2	TTGGCTCCAAGGAAGATT	GAGTAAGGTCCAGAATGACA

SLC6A8	TGAGAGAATGAGATTTCTGCTTGT	TAGGGCTCACAGGGATGG
SLC6A12	AAGGTGGTTTATTTCACAGC	TTCAAGTAGTAGATGATGCCC
SLC7A1	CCTCCTGAGACATCTTTG	CTGGAATATGACGGGAAG
SLC7A5	TTGACACCACTAAGATGAT	GTAGCAATGAGGTTCCAA
SLC16A1	ACACAAAGCCAATAAGAC	ACAGAATCCAACATAGGTA
SLC19A1	GTCAAGACCATCATCACTTTC	ACATGCAGTTCTTCATTCTG
SLC22A8	CAAGTGAATTATACCCCACAG	TGATCCCGTAGTGATATTGG
SLC29A1	GTTGGACCTCATTAGCAAAG	GCTTTGATAGAGTGGCTTTC
SLC44A5	TTTCTCCAGAGATGTTTCCC	TACAACACTTCTTGTCCCTC
STRA6	TTTGGAATCGTGCTCTCCG	AAGGTGAGTAAGCAGGACAAG
TLE1	TATTCCAGTCCAAAGAGTCC	AGATGACTTCATAGACTGTAGC
TFRC	ATGCTGACAATAACACAA	CCAAGTAGCCAATCATAA
VCAM1	ACTTGATGTTCAAGGAAGAG	TCCAGTTGAACATATCAAGC
VECADH	CGCAATAGACAAGGACATAAC	TATCGTGATTATCCGTGAGG
VWF	TGTATCTAGAAACTGAGGCTG	CCTTCTTGGGTCATAAAGTC
WIF1	AGTTGTTCAAGTTGGTTTCC	TAGCATTTTGAGGTGTTTGG
WNT3A	ATCCTCTGCCTCAAATTCT	TTCGTCTAACTCCGTTGG
WNT7B	GCTTCGTCAAGTGCAACA	GGAGTGGATGTGCAAAATG
ZO1	CCTGAACCAGTATCTGATAA	AATCTTCTCACTCCTTCTG

Expression of adhesion molecules in BLECs. The expression of the adhesion proteins was assessed by flow cytometry. After the maturation of the cells for 4 passages in the presence of all soluble factors, cells were purified for CD31 marker and platted in matrigel-coated filters. After 5 days in the filters, cells were exposed to TNF-α (10 ng/mL) for 24 h. The subsequent protocol was performed as previously described for flow cytometry experiments. The single cell suspensions were aliquoted and cells were stained with specific primary antibodies (**Table 3.1**). Cells were further incubated with the secondary antibody when necessary (**Table 3.1**). Non-treated cells were used as control.

Preparation of decellularized ECM. We have prepared decellularized ECM from three different primary cells types: bovine pericytes, bBCECs and rat glial cells. These cells were obtained according to protocols established in Romeo Cechelli's laboratory. Cells were platted in fibronectin-coated dishes (25 µg/mL) at a cell density of 30.000 cells per cm^2 during 8-12 days to allow ECM deposition. Cell layers were then

decellularized using a solution of 20 mM ammonium hydroxide (Sigma) in PBS supplemented with 0.5% Triton X-100 (Fluka). After 1 min with agitation in contact with the solution the resulting ECM layers were washed 2x with PBS and 1x with EGM-2. ECM layers were either used immediately or stored at 4°C.

Stain for actin cytoskeleton and nuclear DAPI. To visualize the actin cytoskeleton and nuclear DAPI in a confluent cell layer and in ECM layer post decellularization, we fixed the plates with 4% PFA and permeabilize with 0.1% Triton X-100. Samples were then incubated with phalloidin-fluorescein (50 µg/mL, Sigma) for 40 minutes and washed twice. The nuclei were counterstained with DAPI and kept in mounting medium. All the photos were taken with the objective of 20x in In Cell Analyzer 2200.

Stain for collagen and non-collagenous proteins. Total amounts of collagen and non-collagen proteins in the decellularized ECM were quantified using Sirius Red/Fast Green assay (Chondrex) according to the manufacturer's instructions.

Statistical Analyses. For analysis involving three or more groups, ANOVA was used, followed by a Newman-Keuls post-test. For analysis of two groups, a paired *t*-test was used. Statistical analysis was performed using GraphPad Prism software (San Diego, CA, USA). Results were considered significant when $P \leq 0.05$

.

Chapter 4

TARGETING THE NEUROGENIC NICHES OF ADULT BRAIN BY NANOPARTICLES

4.1. ABSTRACT

Stimulation of adult neurogenesis by targeting the endogenous NSCs, located in hippocampus and SVZ, has been proposed for brain repair in cases of neurodegenerative diseases. Studies have demonstrated that NPs are promising systems to deliver neurogenic molecules at the SVZ region triggering the neurogenesis process. However, these studies have administered the NPs by intracerebroventricular route, which is very invasive and requires specific medical facilities. Therefore, there is an increasing interest in identifying strategies to administer the NPs by intravenous route to facilitate their adoption. Unfortunately, it is relatively unknown the NP properties to facilitate their accumulation in the neurogenic niches. Here, we have screened different gold nanoparticles (Au NPs) formulations having variable morphology, surface chemistry and responsiveness to light for their capacity to cross the BBB and accumulate preferentially in the neurogenic niches. Results obtained in a human *in vitro* BBB model showed that Au NPs and gold nanorods (Au NRs) conjugated with Tf peptides between 169 and 230 crossed more efficiently the barrier than formulations with higher or lower peptide number per formulation. We further show that Au NRs conjugated with Tf administered intravenously in mice and activated by a near infrared light (NIR) had the highest accumulation in the neurogenic niches. Our results show the possibility of targeting more effectively the neurogenic niches by controlling the properties of NP formulations.

Keywords: Blood-brain barrier, nanoparticles, brain targeting, neurogenic niches.

4.2. INTRODUCTION

With the increasing longevity of the population, there is an increase in brain disorders, namely neurodegenerative diseases (e.g. Alzheimer's and Parkinson's disease) and stroke [28, 166, 216]. Currently, there is no commercial treatment available to restore the brain function due to the limited ability of drugs to cross the BBB [36]. Indeed, the BBB is considered as the main cause for the paucity of therapies in the most neurological disorders [36]. The transplantation of NSCs is a potential alternative to restore the brain function. However, major problems related with the cell survival and integration of new cells with the local circuitry have limited their application[217].

In last few years, another therapeutic approach has been pursued based in the modulation of the endogenous NSCs [187, 189, 191, 197] . In the adult human brain, NSCs can be found in the two germinal niches: SVZ and SGZ [170]. Upon stimulation, these cells are able to generate neurons, astrocytes and oligodendrocytes [169, 172]. Biomaterial platforms, namely NPs are very promising carriers to delivery molecules to the neurogenic niches, and therefore to modulate the activity/differentiation of the NSC [187, 189, 191, 197]. Most studies have administered the NPs by stereotaxic injection, a very invasive procedure. There is an increasing interest to achieve the same results by the intravenous administration of NPs because is safe and simpler. However, it is relatively unknown the properties of NPs to cross the BBB effectively, and accumulate in the local NSCs niche in order to release their cargo.

The current NP strategies for brain delivery are based on the receptor/carrier-mediated endocytosis and adsorptive-mediated endocytosis. The receptor/carrier-mediated endocytosis is the most common strategy for the brain delivery. Several receptors have been targeted such as Tf receptor, insulin receptor, LDL receptor-related protein receptor, among others [218, 219]. Recently, targeted Tf receptor [220-222], insulin-like growth factor receptor [147] and Glut-1 transporter [148] have been used to deliver NPs. It has been shown that modulating the affinity of anti-Tf receptor antibodies [223] and avidity of Tf conjugated NPs [222] or using peptides as alternative Tf ligand [224] and transporter [225] can improve the brain exposure and subsequently the delivery efficiency of cargo to brain parenchyma of mice.

In the current study we have screened different NP formulations having variable morphology (spherical or rod shape), surface chemistry (Au NPs-$Tf_{50/230/375}$ and Au NRs-$Tf_{17/169/307}$) and responsiveness to light for their capacity to cross the BBB and accumulate preferentially in the neurogenic niches (**Figure 4.1**).

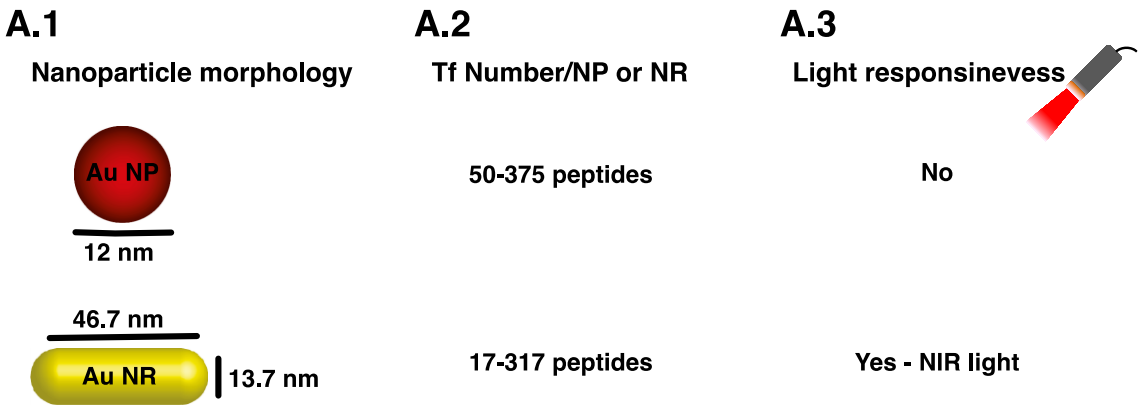

Figure 4.1 - Schematization of the different parameters that were modulated to target the BBB and the neurogenic niches. A.1| Spherical and rod shape gold NPs. **A.2|** Both nanoformulations were functionalized with different numbers of Tf peptides in order to change the avidity to the transporter. **A.3|** NIR light was used to activate the Au NRs.

Initially, we have screened the ability of the nanoformulations to cross a *in vitro* human BBB model in a Transwell system [47]. During this screening we have monitored the BBB stability after contact with the NP nanoformulations (we have measured TEER, paracellular permeability of Lucifer yellow and vascular marker expression before and after the contact with the NPs and BBB apparent permeability (Papp; we have quantified gold content in the bottom well of the Transwell system). Our *in vitro* data shows that some nanoformulations such as Au NPs-Tf_{230} and Au NRs-Tf_{169} were more efficient to cross the BBB as compared to the others. In agreement with these results, animal studies show that Au NPs-Tf_{230} and Au NRs-Tf_{169} were the most effective formulations to cross the BBB and accumulate in the mice brain. We further show that Au NRs-Tf_{230} administered intravenously in mice and activated by a near infrared (NIR) light had the highest accumulation in the neurogenic niches (**Figure 4.2**).

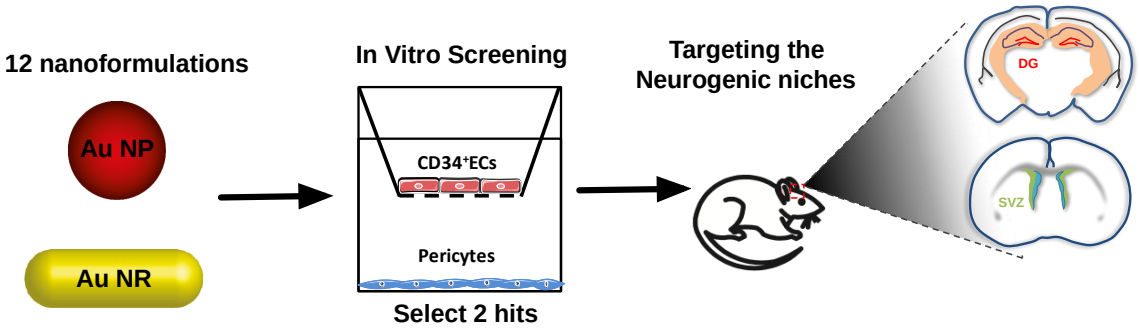

Figure 4.2 - Schematic representation of the different steps performed a long the work. We have initially screened 12 nanoformulations in our human *in vitro* BBB model, from which we selected 2 hits for the following experiments *in vivo*. These nanoformulation were administrated intravenous in a mice model and the gold content was assessed in different brain regions, namely in the neurogenic niches.

4.3. RESULTS

Preparation of the nanoparticle formulations. For the initial screening we have selected 12 nanoformulations with different morphology (**Figure 4.1A.1**), different Tf number per nanoformulation (**Figure 4.1A.2**), and light responsiveness (**Figure 4.2A.3**). Au NPs were chosen due to their biocompatibility, easy bioconjugation and morphological variety. We have selected Tf to target the brain and facilitate the transport through the BBB. Tf receptor is highly expressed in BBB ECs and recent studies [130, 220, 226, 227] have shown that Tf receptor is a good target for brain delivery. Tf peptide and not Tf protein was chosen for the conjugation to the surface of Au NPs and Au NRs because it is relatively easy to modify its surface chemistry (i.e. introduction of a thiol group at the C-terminus of peptide) and to have a high number of peptides per surface NP area. We have prepared NP formulations with variable number of Tf peptide because recent studies have shown that this parameter has an important effect in the transport of the NP formulation [130, 226] (**Figure 4.1A.2**). Au NPs having an average diameter of 12 nm and Au NRs with an aspect ratio of 46.7 x 13.7 nm were selected for the screening (**Figure 4.1A.1**). Au NRs were selected due to its morphology and absorption properties in the NIR region [228, 229]. Our hypothesis is that Au NRs could be activated in the brain, leading to a local photothermal effect and consequently help in the permeation of the BBB. We have selected Au NPs with an average diameter of 12 nm because it has been shown in previous works that small NPs are good carriers to cross the BBB [147, 220, 230].

To prepare the NP formulations with variable number of Tf, the Tf peptide (1.5 KDa) conjugated with NH_2-PEG-maleimide (5 kDa) was incubated with Au NPs or NRs for 12 h at the room temperature (**Figure 4.3**). The maleimide group reacts with the thiol group of Tf to form a stable thioether bond and the free amine group of PEG reacts with Au NPs (**Figure 4.3**). 50 (Au NPs-Tf_{50}), 230 (Au NPs-Tf_{230}) and 375 (Au NPs-Tf_{375}) Tf peptides per Au NP and 17 (Au NRs-Tf_{17}), 169 (Au NRs-Tf_{169}) and 317 (Au NRs-Tf_{317}) Tf peptides per Au NRs were prepared (**Figure 4.1A.2**). Finally, the NP formulations were coated with 2kDa thio-mPEG molecules (0.25 μmol) to increase its stability in cell culture media (**Figure 4.3**). We have performed PEG backfilling because it was recently demonstrated that this strategy improves the specific binding of NPs to a targeted cell population by overcoming the inhibitory effect of the protein corona [154, 231].

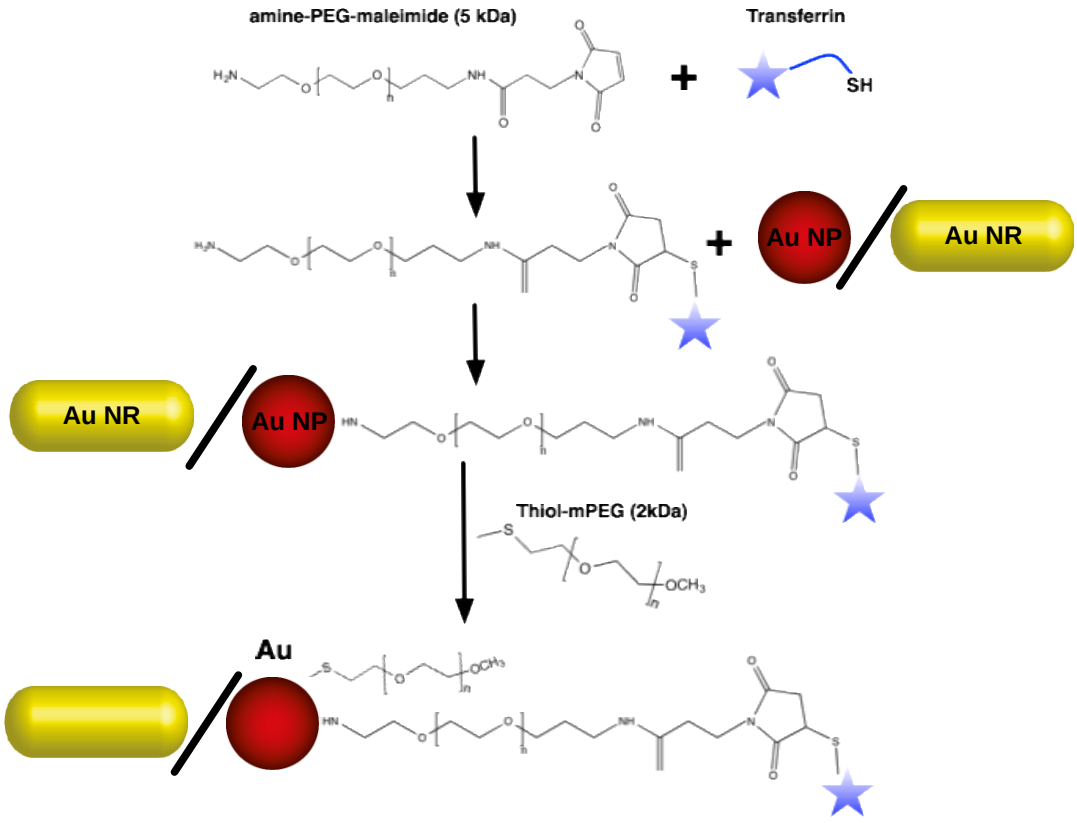

Figure 4.3 - Schematic representation of the preparation of Tf-PEG conjugate and immobilization of Tf-PEG conjugate on the surface of Au NPs and Au NRs. The thiol group of Tf peptides reacts with a maleimide group of maleimide-PEG-amine (5 kDa); the conjugate purified by dialysis and then reacted with Au NPs and Au NRs. The Tf-PEG conjugated NPs/NRs were backfilled with methoxy-terminated polyethylene glycol molecules (mPEG, 2 kDa) to prevent the unspecific adsorption of proteins on the surface of NPs/NRs.

UV-vis spectra shows a red shift in the surface plasmon resonance (SPR) band of Au NPs from 520 to 525 nm after conjugation with Tf-PEG-NH_2 due to a change in local dielectric environment or increase in the size of Au NPs (**Figure 4.4A.1**) [232]. However, there is no apparent increase in the size of Au NPs-Tf_{230} compared to bare Au NPs (**Figure 4.4A2** and **A3**). Additionally, zeta potential measurement shows that Au NPs-Tf_{230} are positively charged (+3 ± 1 mV) in comparison with the bare Au NPs (-18 ± 2 mV) (**Figure 4.4B**). We also performed stability measurement of Au NPs-Tf_{230} in EGM-2 cell culture media using UV-vis spectrophotometer. No significant increase in the size of Au NPs-Tf_{230} is observed in EGM2 media upto 24 h (**Figure 4.4C**), indicating that Pegylation of NPs surface protects Au NPs from aggregation in the cell culture media, which is a crucial parameter for the delivery of Au NPs to brain in animal model experiments.

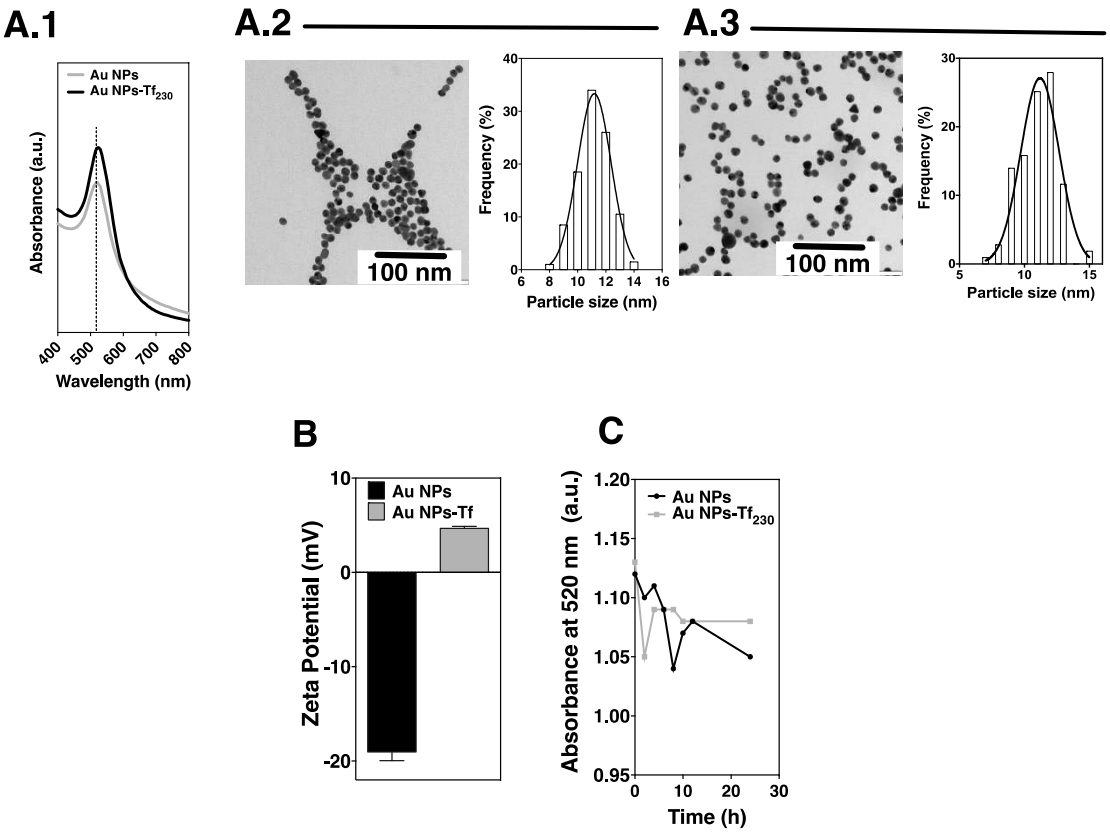

Figure 4.4 - Characterization of Au NPs. **A.1|** UV-vis spectra of bare Au NPs and Au NPs-Tf_{230}**. A.2|** Representative TEM image and particle size distribution of citrate-reduced Au NPs and **A.3|** Au NPs-Tf_{169}. **B|** Zeta potential of citrate-reduced Au NPs and Au NPs-Tf_{230}. **C|** Stability measurement of Au NPs-Tf_{230} and bare Au NPs in EGM2 media using UV-visible absorbance spectra.

Au NRs characterized by TEM reveals an aspect ratio of 46.7 x 13.7 nm (**Figure 4.5A.1**). UV-vis spectra show a red shift of 5 nm in NIR region compared to Au NRs, indicating the conjugation of Tf peptide on the surface of NRs (**Figure 4.5A.2**). Moreover, UV-visible absorbance spectra demonstrate that Au NRs and Au NRs-Tf_{169} are stable in EGM-2 media for 24 h (**Figure 4.5B**). Zeta potential characterization shows that Au NRs are positively charged (Au NRs: +5.6±0.4 mV; Au NRs-Tf_{169}: +2.4±0.3 mV) (**Figure 4.5C**).

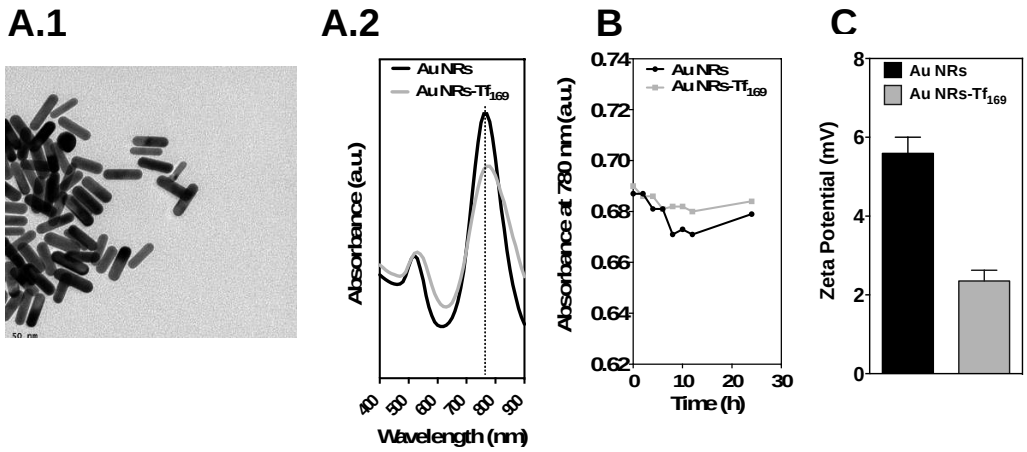

Figure 4.5 - Characterization of Au NRs. A.1| Representative TEM image of Au NRs. **A.2|** UV-vis spectra of bare Au NRs and Au NRs-Tf_{169}**. B|** Zeta potential of Au NRs and Au NRs-Tf_{169}. **C|** Stability measurement of Au NRs-Tf_{169} and Au NRs in EGM2 media using UV-vis absorbance spectra.

Effect of NP formulations in the integrity of the in vitro BBB model. Next, we evaluated the integrity and transport properties of the *in vitro* BBB model after exposure to the NP formulations for 2 h (**Figure 4.6**). We have selected a 2 h exposure of NPs to BBB model based on the previous studies performed *in vitro* and *in vivo* systems [147, 149, 220]. Upon the 2 h, the upper and bottom chamber cell culture media was removed, the cells washed, and new cell culture media was added. We measured the TEER and paracellular permeability to Lucifer yellow, before and 24 h after exposure to the NP formulations (**Figure 4.6**).

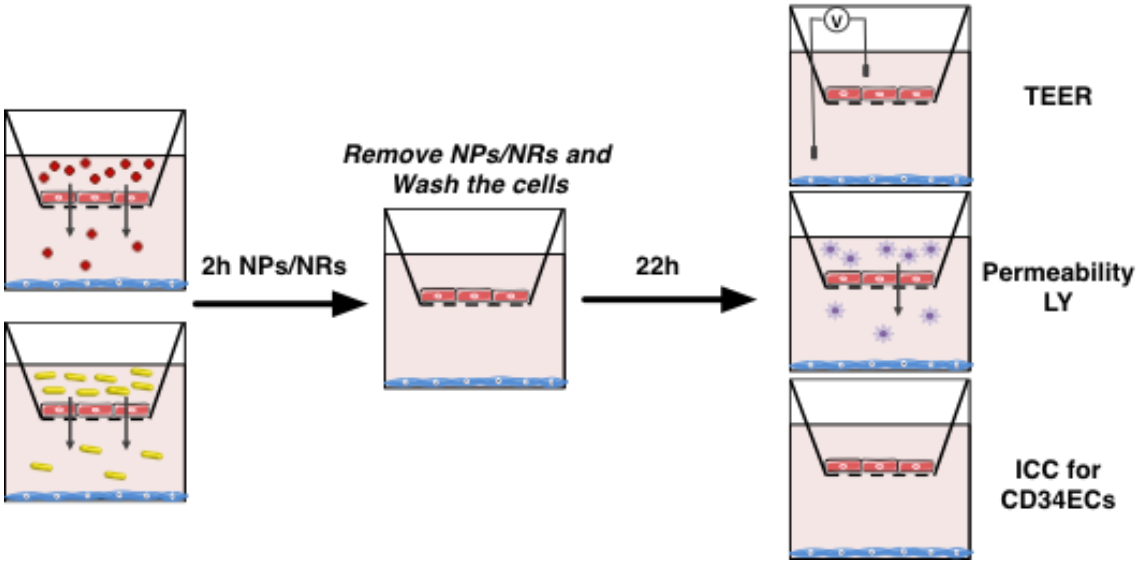

Figure 4.6 - Representative scheme of the protocol used to assess the impact of the nanoformulations in the BBB integrity. In general, the BBB *in vitro* model was incubated with Au NPs-$Tf_{50/230/375}$ or Au NPs (100 μg/mL) and Au NRs-$Tf_{17/169/317}$ or Au NRs (50 μg/mL) for 2 h in shaking conditions, after which the nanoformulations were withdrawn and the cells were washed and new media added. In case of light exposure, $CD34^+$ derived ECs were irradiated with NIR light ($2W/cm^2$ for 2 min). Then cells were kept in incubator for an additionally 22 h and functionality assessment was performed.

Our results show that Au NPs and Au NPs-$Tf_{50/230/375}$ (100 μg/mL) do not increase significantly the permeability to Lucifer yellow (**Figure 4.7A.1**) and TEER (**Figure 4.7A.2**) demonstrating no measurable damage effect in the barrier properties. Similar results have been obtained with lower concentration of Au NPs/Au NPs-$Tf_{50/230/375}$ (50 μg/mL) (**Figure 4.7B.1 and B.2**) and Au NRs/Au NR-$Tf_{17/169/317}$ (50 μg/mL; **Figure 4.7C.1 and C.2**).

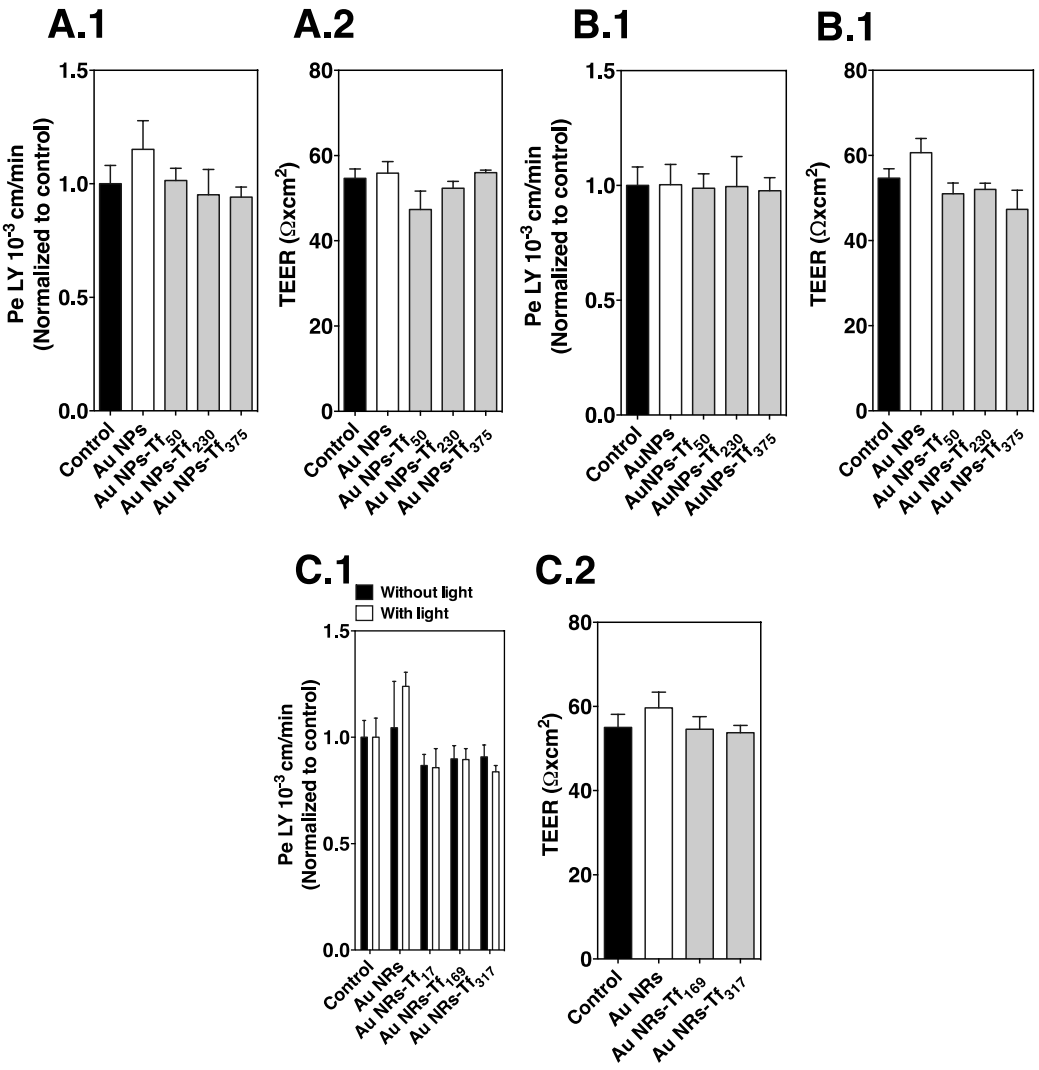

Figure 4.7 - Effect of bare and Tf functionalized NPs/NRs in the ECs monolayer integrity. A.1| Paracellular permeability to Lucifer yellow (LY) and **A.2|** TEER measurements 24 h post exposure of $CD34^+$ derived ECs to Au NPs- $Tf_{50/230/375}$ and Au NPs (100 μg/mL). Results are Mean ± SEM (n=4-12). **B.1|** Paracellular permeability to Lucifer yellow (LY) and **B.2|** TEER measurements 24 h post exposure of $CD34^+$ derived ECs to Au NPs- $Tf_{50/230/375}$ and Au NPs (50 μg/mL). Results are Mean ± SEM (n=4-12). **C.1|** Paracellular permeability to Lucifer yellow (LY) without or with light exposure and **C.2|** TEER measurements 24 h post exposure of $CD34^+$ derived ECs to Au NRs- $Tf_{17/169/317}$ and Au NRs (50 μg/mL) without light activation. Results are Mean ± SEM (n=3-13). Permeability to Lucifer yellow data are normalized against the control condition (without NPs/NRs); The value for the control is 0.804 ± 0.05 $x10^{-3}$ cm/min, which is in accordance with the values described in our previous report [47]. The TEER value for T0 (before exposure to the nanoformulations) was 55.66 ± 2.2 Ωxcm^2. Results are Mean ± SEM (more than n=10).

Immunofluorescence analyses of VE-cadherin and tight junction protein ZO-1 confirm that the contacts between ECs of BBB model are not damaged after incubation with both NPs/NRs (**Figure 4.8**).

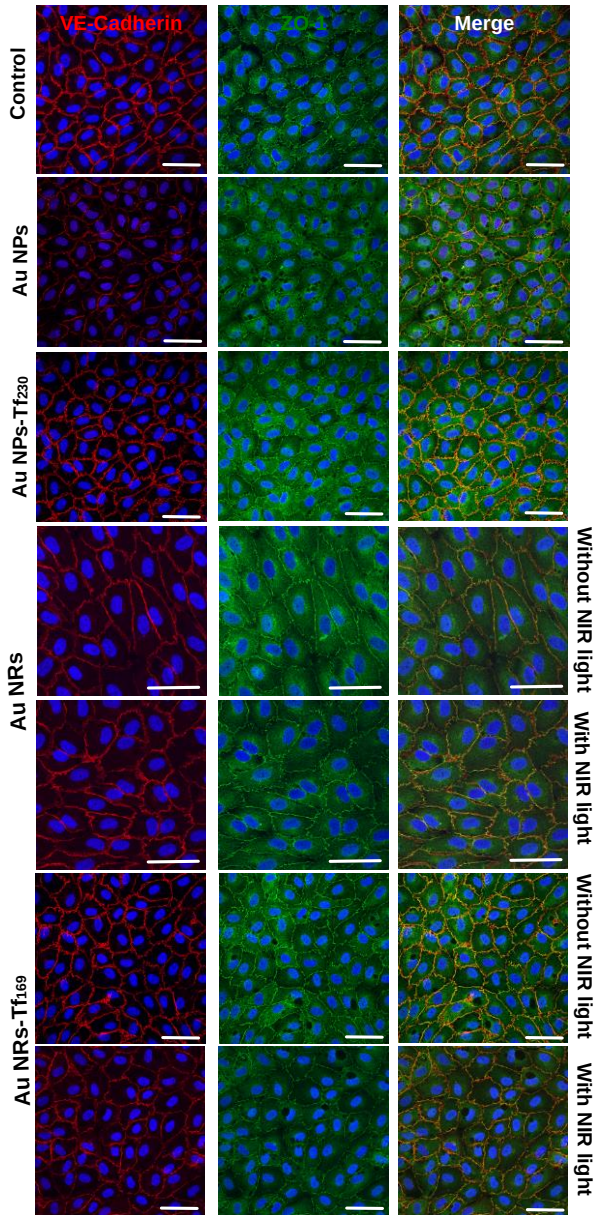

Figure 4.8 - Assessment of ECs monolayer integrity by immunocytochemistry 24 h after adding the nanoformulations. Immunoflorescence staining of $CD34^{+}$ derived ECs in matrigel-coated filters for VE-cadherin and ZO-1 proteins. Scale bar is 50 μm**.**

Local heat generated by Au NRs upon NIR light exposure might open the BBB and promote the transport of NRs across the BBB. Therefore, we have examined the integrity of *in vitro* BBB model after incubation for 2 h in the absence (i) or presence (ii) of Au NRs

under the NIR light (wavelength 780 nm, 2 w/cm^2, 2 min per pulse). The NIR laser alone had no effect in the permeability and TEER of the *in vitro* BBB model (**Figure 4.9**).

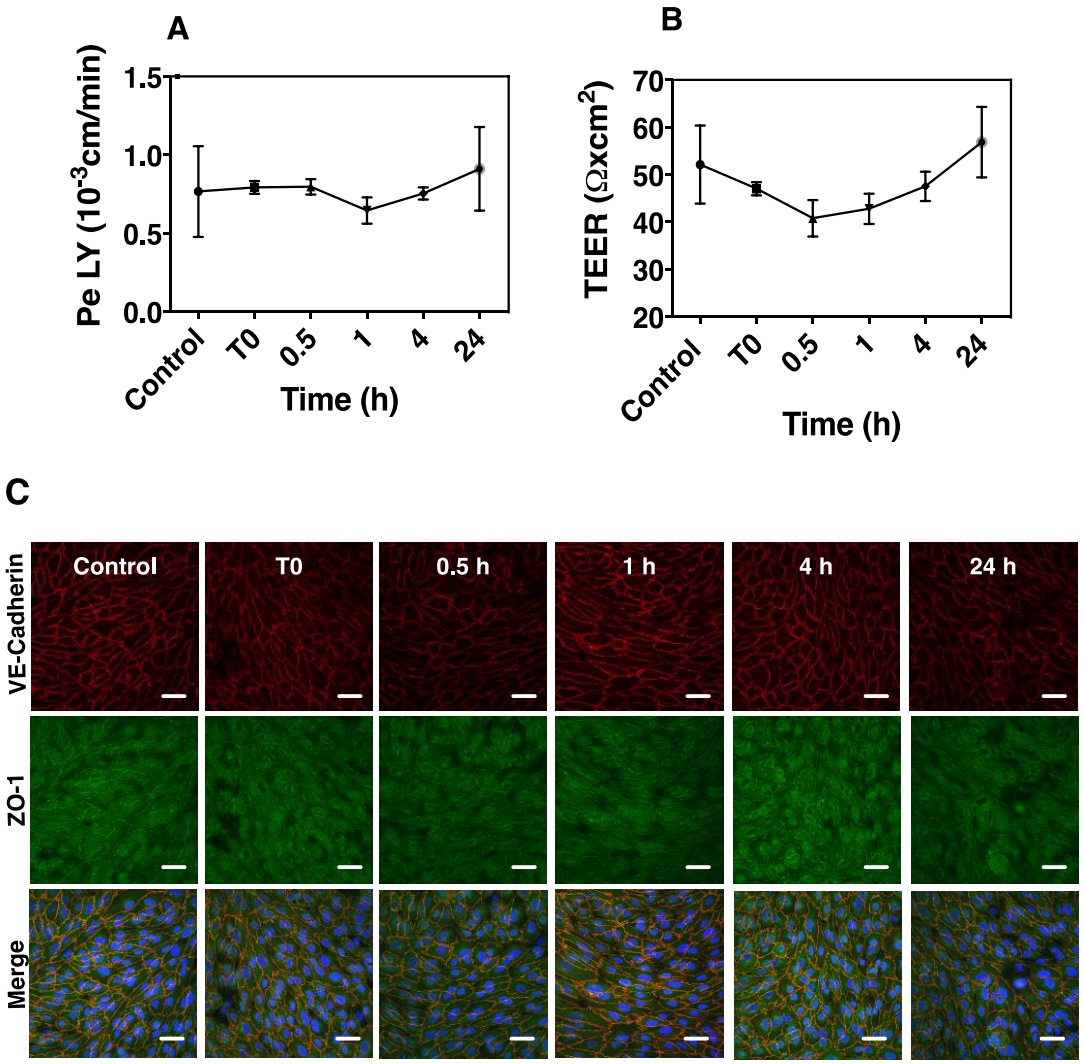

Figure 4.9 - Functionality of the *in vitro* BBB model at different time points after exposure to NIR light. CD34$^+$ derived ECs were evaluated at time zero (T0), 30 min, 1 h, 4 h and 24 h post exposure to light (2 W/cm^2; 2 min per pulse) in terms of **A|** Paracellular permeability to Lucifer yellow (LY) and **B|** TEER. The TEER value before exposure to the light was 47 ± 3.95 Ω.cm2. Results are Mean ± SEM (n=3). **C|** Immunostaining for VE-cadherin and ZO-1 proteins. Scale bar is 50 μm.

Similarly, the integrity of the BBB is not significantly affected after Au NR or Au NRs-Tf$_{17/169/317}$ (50 μg/mL) exposure and NIR light activation (**Figure 4.7C.1**). Overall, our results indicate that Au NPs and Au NRs with or without Tf peptide conjugation had no significant effect in the integrity of *in vitro* BBB model.

Effect of NP formulations in the permeation of the in vitro BBB model. Next, we evaluated the transcytosis of Au NPs-Tf and Au NRs-Tf in the BBB model. 100 μg/mL of Au NPs or Au NPs-$Tf_{50/230/375}$ and 50 μg/mL of Au NRs or Au NRs-$Tf_{17/169/317}$ were loaded in the upper compartment (apical) of BBB model system, while the lower compartment was loaded with the cell culture media. The BBB model system was incubated with these NPs/NRs for 2 h followed by withdrawn of media from upper and lower compartments and again incubated with the fresh media in both compartments for another 22 h to facilitate the transcytosis of the internalized NPs/NRs. ICP-MS was performed for samples from the lower compartment (media and bovine pericytes) to quantify the amount of NPs/NRs that passed through the BBB (**Figure 4.10**).

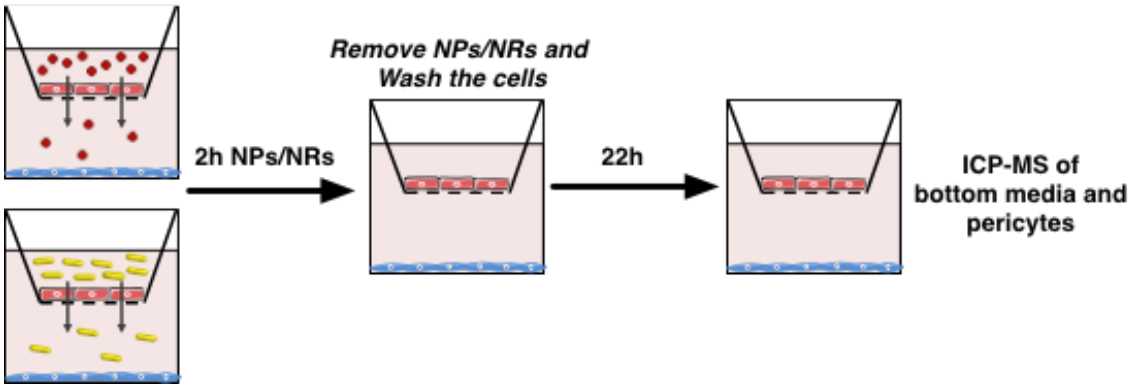

Figure 4.10 - Schematic representation of the protocol used to determine the amount of gold that crosses the *in vitro* BBB model. Briefly, the *in vitro* BBB model was exposed to the nanoformulations (50 or 100 μg/mL) for 2 h in shaking conditions, after which the NPs/NRs were removed, cells were washed and new media was added. When needed, the $CD34^+$ derived ECs were irradiated with NIR laser (2W/cm^2 for 2 min). 24 h after adding the NPs/NRs, bottom media and bovine pericytes were collected and evaluated by ICP-MS to determine gold content.

When we used 100 μg/mL of Au NPs-Tf_{230} (medium density of Tf) we observed the highest apparent permeability (Papp) across the barrier with a value of 1.3 x 10^{-7} cm/s compared to Au NPs-Tf_{50} (low density Tf), Au NPs-Tf_{375} (high density Tf) and Au NPs with Papp values of 9 x 10^{-10}, 1.4 x10^{-8} and 4.5 x 10^{-9} cm/s respectively, indicating that not only Tf peptide but also the number of Tf peptide on the surface of NPs plays an important role in controlling the transcytosis efficiency of NPs as a BBB shuttle (**Figure 4.11A.1**). Moreover, higher amount of Au NPs-Tf_{230} transcytosed through the BBB model is observed in comparison with Au NPs-$Tf_{50/375}$ and Au NPs (**Figure 4.11A.1 and A.2**). We have tested also used 50 μg/mL of Au NPs nanoformulation, but no significant

differences were observed between Au NPs-Tf_{230} and Au NPs-$Tf_{50/375}$ perhaps due to the detection sensitivity of ICP-MS (**Figure 4.11A.1 and A.2**).

When the morphology of nanoformulation was changed from spherical to rod shaped, the dependence with the number of the Tf peptide was maintained. Au NRs-Tf_{169} (medium density of Tf peptides) has the highest transcytosis capability compared to other formulations such as Au NRs-Tf_{17} (low density), Au NRs-Tf_{317} (high density) and Au NRs (**Figure 4.11B.1 and B.2**). Au NRs-Tf_{169} exhibited the highest permeability across the barrier with a Papp value of 6.4 ± 1.3 x 10^{-8} cm/s without the exposure to the NIR light, and no statistically significance increase in the Paap value (7.5 ± 1.3 x 10^{-8} cm/s) and % of transport was observed upon the NIR light exposure (**Figure 4.11B.1 and B.2**).

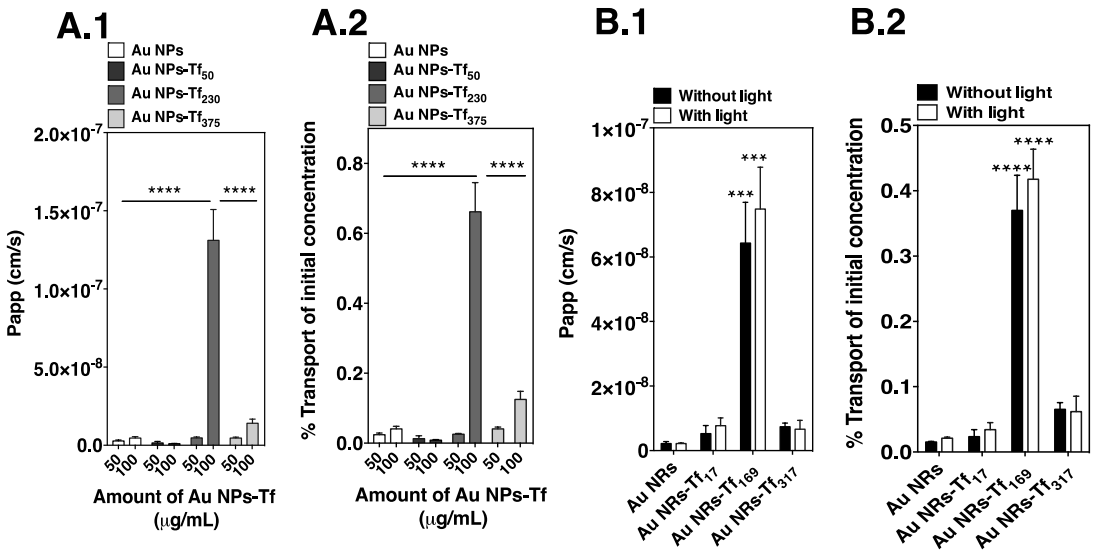

Figure 4.11 - Ability of Au NPs-Tf and Au NRs-Tf to cross the *in vitro* BBB model. **A**.1| Papp and **B.2|** % of initial concentration of Au NPs- $Tf_{50/230/375}$ and Au NPs in the bottom chamber 24 h after incubation with 50 and 100 μg/mL of NPs. **B.1|** Papp and **B.2|** and % of initial concentration of Au NRs- $Tf_{17/169/317}$ with or without light activation that crossed the BBB model 24 h after incubation with 50 μg/mL. Results are Mean ± SEM (n=3-7). ****P<0.001* and *****P<0.0001* (When compared to all other nanoformulations).

Low Papp value of Au NPs and Au NRs could be due to the ability of densely packed PEG coated Au NPs/NRs to pass through cell monolayer without damaging the monolayer integrity (**Figure 4.11**) [233]. A low number Tf per NP/NR does not significantly bind to Tf receptor due to its lower avidity to receptor, on the other hand a large number of Tf per NP/NR binds strongly with receptor due to its high avidity and

therefore is less likely available to transcytose through the barrier [222, 223]. NPs/NRs having intermediate avidity (optimum number of Tf per NP/NR) can efficiently transcytose through the barrier. Other studies have showed Papp value of 1.4±0.07 x 10^{-7} and 0.2 x 10^{-7} cm/s for Au NPs-Tf and Au NPs-miniAP4 respectively, which are in similar range to results obtained by us [220, 225]. This result implies that Tf peptide from 169 to 230 conjugated per NR or NP is an optimum number to facilitate the efficient transcytosis across the BBB model and when the number of Tf per nanoparticle are above or below this range, significant reductions in transcytosis are observed.

Interestingly, when the BBB model incubated for 10 and 90 min with Au NRs-Tf_{169} is exposed to NIR light without removing non-internalized NRs, a dramatic urge in Papp value is observed (in the 2 h time point) (**Figure 4.12A.1**). This indicates that NRs present in the vicinity of the ECs surface (non-internalized) have capability to break the integrity f BBB due to local heating by NRs after exposure to light, which is concomitant with standard Lucifer yellow permeability and immunofluorescence data (**Figure 4.12A.2 and A.3**). In another control experiment, when the integrity of BBB is compromised using mannitol, 3 folds' increase in Paap value is observed compared to untreated BBB (**Figure 4.12B.1-B.3**). Overall our results show that Tf conjugated Au NPs/NRs are compatible to BBB model without damaging the integrity of barrier.

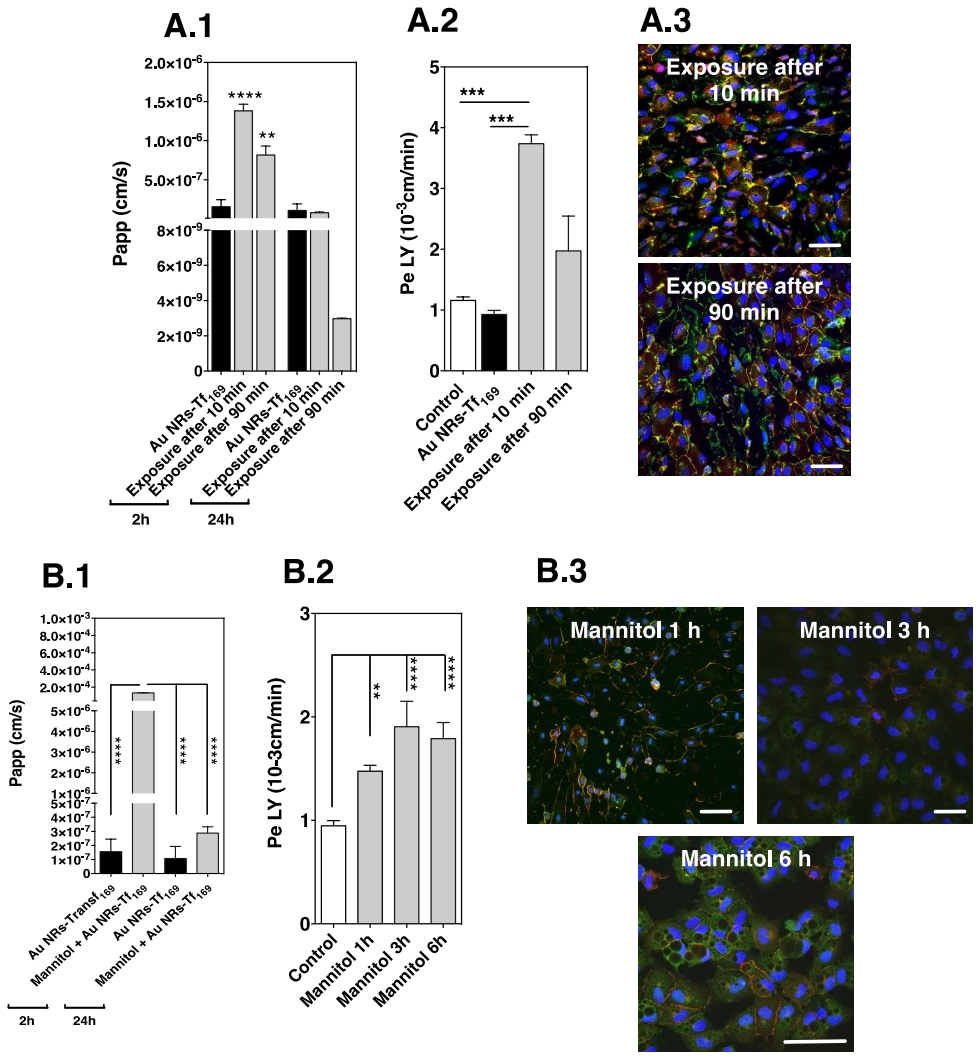

Figure 4.12 - Impairment in the integrity of the *in vitro* BBB model. In order to assess the impact of CD34$^+$ derived ECs monolayer integrity loss in the crossing of the NRs, two sets of experiments were performed: *i)* combination of NRs with light exposure; and for that CD34$^+$ derived ECs were incubated with Au NRs-Tf$_{169}$ and were exposure to the NIR light 10 min or 90 min after the incubation with the NRs; *ii)* CD34$^+$ derived ECs were exposed to Mannitol (0.9 uM) for different periods (1, 3 and 6 h) and incubated after with Au NRs-Tf$_{169}$. The integrity of the ECs monolayer was assessed 24 h after the incubation. **A.1|** Papp of Au NRs-Tf$_{169}$ that crossed the *in vitro* BBB model 2 h or 24 h after the incubation with Au NRs-Tf$_{169}$ with or without exposure to NIR laser. **A.2|** Paracellular permeability to Lucifer yellow (LY) at 24 h, when cells were irradiated at 10 min and 90 min (2W/cm^2; 2 min pulse) in the presence of the Au NRs-Tf$_{169}$. **A.3|** Staining for VE-cadherin and ZO-1 proteins in CD34+ derived ECs 24 h after incubation with Au NRs-Tf$_{169}$ with exposure to NIR light. **B.1|** Papp at 2 h or 24 h for Au NRs-Tf$_{169}$ that crossed the BBB *in vitro* model that was pre-exposed to mannitol for 3h. **B.2|** Paracellular permeability to Lucifer yellow (LY) after incubation with mannitol for different periods. **B.3|** Immunostaining for VE-cadherin and ZO-1 proteins after incubation with Mannitol. Results are Mean ± SEM (n=3) ***P*<0.01 and *****P*<0.0001.

In vivo study of Au NPs-Tf and Au NRs-Tf capacity to cross the BBB and accumulate in the neurogenic regions. After determining the 2 hits (Au NPs-Tf_{230} and Au NRs-Tf_{169}) from the *in vitro* BBB studies, *in vivo* studies were performed to determine whether these nanoformulations can improve the delivery of NPs/NRs to brain and particularly the accumulation in the neurogenic niches compared to non-neurogenic regions. 1 mg of Au NPs-Tf, Au NRs-Tf, Au NPs and Au NRs (200 μL of 5 mg/mL) were injected intravenously in mice. In case of Au NRs, the NIR light was exposed onto animal head for 2 min 1 h after the administration of Au NRs-Tf_{169}. The mice were sacrificed 2 h after the administration of the nanoformulations by NaCl perfusion, and neurogenic niches (SVZ and hippocampus) and non-neurogenic regions (remaining brain) were excised, washed with PBS and lyophilized to quantify the gold contents using ICP-MS (**Figure 4.13**).

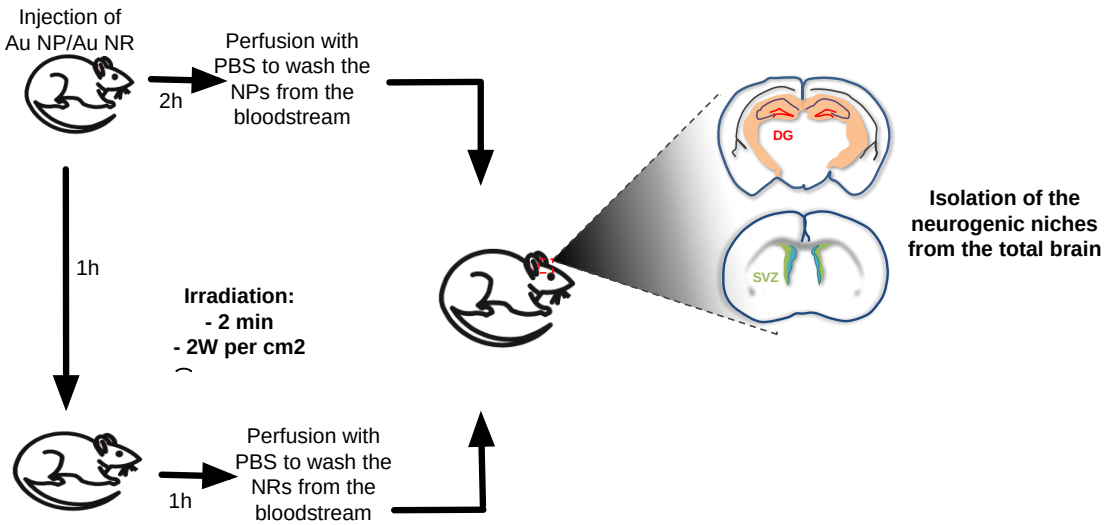

Figure 4.13 - Schematic representation of the protocol used *in vivo* to determine the amount of gold that accumulates in the mice brain, specifically in the neurogenic niches. 200 uL (5mg/mL) of colloidal suspensions of NPs/NRs were administered to animals through an intravenous route. In case of NIR light exposure, the animals were anesthetized again 1 h post administration of NRs and irradiated (2W/cm^2 for 2 min). 2 h post the injection, the animals were sacrificed and the different brain regions were collected for ICP-MS analysis.

A large percentage of Au NPs-Tf_{230} is accumulated in total brain compared to bare Au NPs in a similar manner observed in *in vitro* BBB model due to a moderate avidity of Au NPs-Tf_{230} with Tf receptor at the BBB of brain (**Figure 4.14A.1**). However, no statistically difference of Au NP accumulation is found between the neurogenic and the

non-neurogenic regions (**Figure 4.14A.2**). Additionally, we observed less accumulation of Au NPs-Tf_{375} in the mice brain (**Figure 4.14A.1**), and therefore the same condition for NRs was not selected. Our results show that NPs avidity plays an important role in the transcytosis behavior and a large amount of Au NPs-Tf_{230} accumulates in the mice brain.

In case of animals administrated with 1 mg of Au NRs-Tf_{169} and exposed with the NIR light, a large amount of NRs was accumulated in the total brain compared to conditions without light exposure and control Au NRs (**Figure 4.14B.1**). In detailed analysis, Au NRs-Tf_{169} preferentially accumulates in the neurogenic niche without the NIR light exposure, however 2 folds increase in the accumulation of NRs in neurogenic niche is observed under the NIR light exposure (**Figure 4.14B.2**). Although the total amount of NPs or NRs combined with the NIR light exposure is similar in total brain, NRs are mostly accumulated in SVZ while NPs are accumulated in hippocampus niche (**Figure 4.14C.1 and C.2**). Au NPs-Tf_{230} have higher tendency to transcytose in the non-neurogenic niche of the brain (**Figure 4.14C.2**).

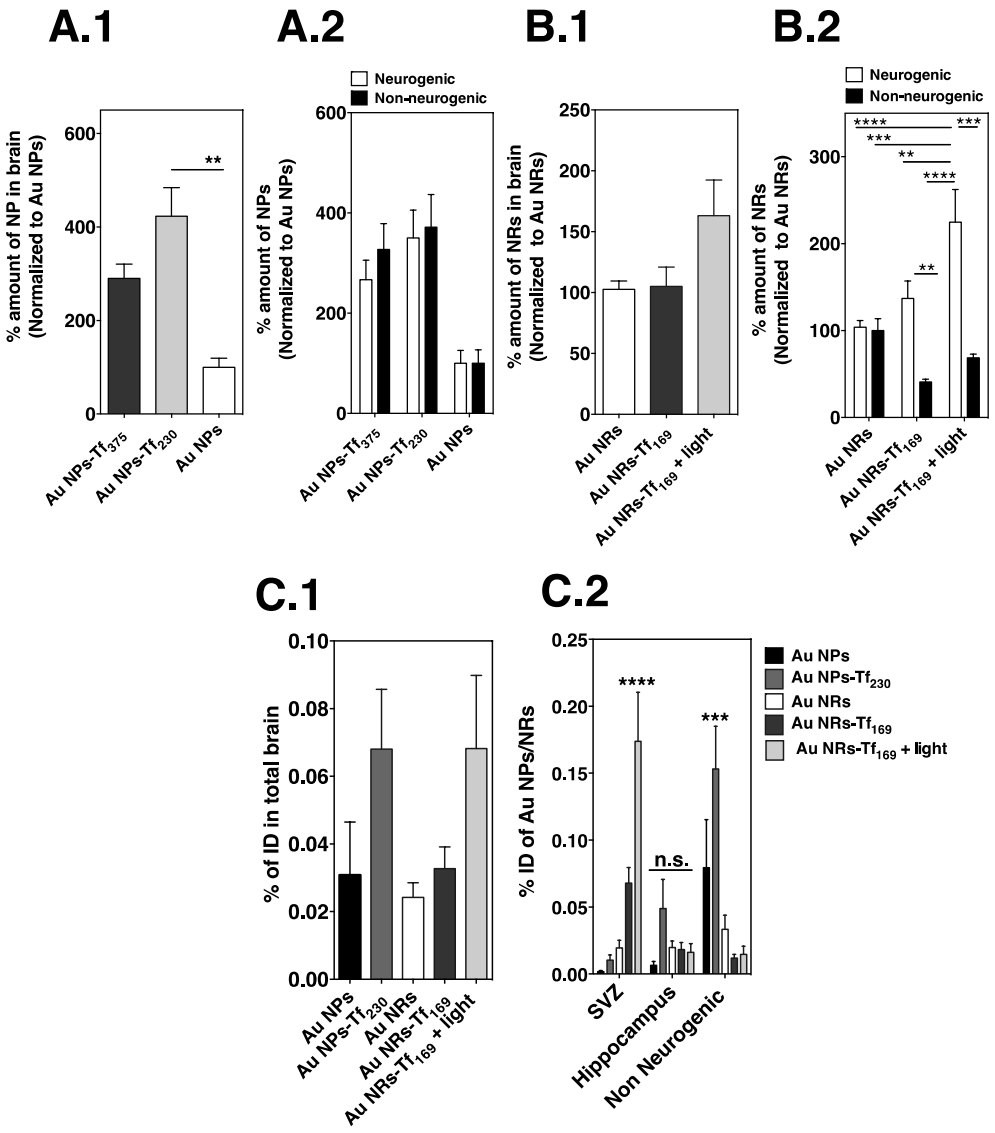

Figure 4.14 - Determination of the gold content in different brain regions in a mice model by ICP-MS analysis. Quantification of NPs **A.1|** in total mice brain and **A.2**| in the neurogenic (DG and SVZ) and non-neurogenic niches of the mice. Quantification of NRs **B.2|** in total mice brain and **B.2**| in the neurogenic (DG and SVZ) and non-neurogenic niches of the mice. Amount of gold **C.1**| in the total mice brain and **C.2**| in the different brain regions normalized to the initial administrated dose (1 mg/mice). Results are average ± SEM (n=6-9 animals). ***P<0.01*, ****P<0.001* and *****P<0.0001*.

4.4. DISCUSSION

In this study we describe the development of nanoformulations to target the neurogenic niches. We have screened three parameters: i) NPs morphology (spherical and rod shape), ii) number of Tf peptides per NP/NR surface and iii) responsiveness to light, to modulate the BBB permeation and their capability to target the neurogenic niches. We have selected gold nanoformulations since they are biocompatibility, easy to synthesize, and can be tuned in terms of size and shape. We have used Tf to functionalize these NPs/NRs, since several works have reported the targeting to Tf receptor as an efficient pathway to cross the BBB [130, 220, 226, 227]. Moreover, recent studies [130, 226] have shown that the avidity of the nanoformulations to the Tf receptor modulates the accumulation of NPs in the brain endothelium and in our work we have decided to use also different amounts of Tf peptide in the surface of the NPs/NRs (17-375 peptides). The last parameter evaluated was the light responsiveness of NRs to the NIR light [228, 229] with expectations to increase the BBB crossing. After an initial screening of 12 nanoformulations in the human *in vitro* BBB model described previously by us [47], we selected two hits (Au NPs-Tf_{230} and Au NRs-Tf_{169}) that were evaluated in a animal model. Our results show data both nanoformulations are able to cross the BBB and target the brain, and the combination of Au NRs-Tf_{169} with NIR light induces a preferential accumulation in the neurogenic niches.

Our results show that the 12 nanoformulations do not have a significant impact in the integrity of the *in vitro* BBB model that was assessed by paracellular permeability to Lucifer yellow, TEER measurement and immunocytochemistry for ZO-1 and VE-Cadherin proteins. Importantly, the NIR light exposure was not detrimental to the BBB monolayer integrity, in the absence of Au NRs or when applied after removing the NRs from the top of BBB model. However, when the cells were irradiated in the presence of Au NRs-Tf_{169} we observed an increase in the permeability, probably due to the local heating, phenomenon that is known to promote an increase in the permeability of the brain ECs by opening the barrier temporarily [234] and that has been also reported by other types of nanoformulations [235]. The Au NPs-Tf_{230} and Au NRs-Tf_{169} (without exposure of the NIR light) show Papp values of 1.3 $x10^{-7}$ cm/s and 6.4 ± 1.3 $x10^{-8}$ cm/s, respectively; Au NRs-Tf_{169} combined with light exposure increases the Papp value to 7.5 ± 1.3 $x10^{-8}$ cm/s, although no statistically significance is observed. Previous studies have shown a Papp values in the similar range (1.4±0.07 $x10^{-7}$ and 0.2 $x10^{-7}$ cm/s for Au NPs-Tf [220] and Au NPs-miniAP4 [230], respectively). Overall, we demonstrate that a

medium number of Tf peptides between 169 and 230 in the surface of NRs and NPs, respectively, are the best conditions to achieve a higher permeation across the BBB.

Although a lot of researches have been explored towards the delivery of NPs to brain, targeting and efficient delivery of biomolecule conjugated NPs to different regions of the brain is still elusive. One of the major goals of this work is to use these nanoformulations to target the brain neurogenic niche. Previously, it was reported that NPs are able to activate endogenous NSCs [187, 189, 191, 197], however only few studies have shown [166, 195] that there is accumulation of NPs (PLGA) in the neurogenic niches specially in hippocampus of the brain, after a systemic administration. Au NPs-Tf and Au NRs-Tf are stable in complete EC medium (with 2% FBS) for 24 h, indicating that these nanoformulations would be stable inside the animal body after the administration. The surface modification of nanoformulation with PEG molecules prevent the adsorption of blood proteins onto the surface of NPs/NRs thereby decreasing their clearance by the reticuloendothelial system and consequently enhances the NPs capacity to cross the BBB and accumulate in the brain [154, 159, 231]. Based on *in vitro* BBB validation, we have selected Au NPs-Tf_{230} and Au NRs-Tf_{169} as best candidates for *in vivo* experiments. The nanoformulations were injected in the mice tail vein and 2 h after the administration, the animals were sacrificed and the brains were collected to perform the ICP-MS to determine the gold content. Our results showed that both nanoformulations were able to accumulate in the mice brain, however Au NRs-Tf_{169} were preferentially accumulated in the SVZ region compared to Au NPs-Tf_{230}. Additionally, a significant improvement in the accumulation of NRs in SVZ niche was found when animals were exposed to NIR light after administration of Au NRs-Tf_{169}. SVZ niche is the largest germinal area of the adult human brain, working as a reservoir of adult NSCs that can be activated for brain repair [199] and this area, is characterized by a more permissive vasculature [184, 199]. We hypothesize that more leakiness of these neurogenic niche along with efficient targeting of Au NRs-Tf_{169} to Tf receptor in neurogenic niche facilitate the large accumulation. The exposure of NIR light may induce the local heating effect due to the vicinity of NRs to brain ECs that can enhance the BBB crossing into the brain [235]. Higher amount of Au NPs-Tf_{230} was found in hippocampus region than other nanoformulations, which was also observed by others [166, 195]. The total amount of Au NPs-Tf_{230} and Au NRs-Tf_{169} accumulated in the brain was similar, probably due to the presence of higher amount of Au NPs-Tf_{230} in non-neurogenic regions of the brain. Wiley *et al.* have shown higher accumulation of Au NPs (size 45 and 80 nm) conjugated with Tf protein (Tf between 20-30 per NP) in brain parenchyma [130]. In our study Tf peptide having cysteine terminal at C terminus was chosen to

provide orientation to Tf peptide on the surface of NPs/NRs. The key difference between our work and the work of Wiley *et al.* rely on the targeting ligand and, while we use a small peptide they use human holo-Tf protein which we expected to have a different dissociation constant. Indeed, at a similar ligand density (Au NPs-Tf_{230} vs 200 Tf proteins Au NPs of Wiley *et al.*, our nanoformulations have a large accumulation of NPs in animal brain. Nevertheless, other parameters that may affect the binding of the ligand to the receptor, such as surface charge and size of the NP, can not be discard.

In summary, we show that a specific number of Tf peptide (between 169 to 230) per NR/NP can improve the BBB crossing both *in vitro* and *in vivo*. These Au NRs-Tf_{169} preferentially accumulate in neurogenic niche and NIR light exposure additionally promotes this accumulation. The specific targeting and accumulation of these nanoformulations opens new possibilities for the treatment of brain diseases by modulating the endogenous NSCs niches to promote the neurogenesis and ultimately the brain repair.

4.5. MATERIAL and METHODS

Synthesis of Au NPs. Citrate-reduced AuNPs were synthetized using Turkevich method. In general 90 mL of 1 mM $HAuCl_4$ solution was boiled at 100°C followed by addition of 120 mg of sodium citrate dossilved in 10 mL of Milli-Q water. The solution was boiled until the solution color turned from light yellow to ruby-red.

Synthesis of Au NRs. Au NRs were synthesized as published before [236]. In general, Au seed solution was prepared by adding 12.5 μL of 0.1 M $HAuCl_4$ in cetyltrimethylammonium bromide (CTAB) (5 mL, 0.1 M) solution. This solution was vigorously stirred using a magnetic stirrer. After 5 min of stirring, an ice cold sodium borohydride solution (0.6 mL, 10 mM) was added in the solution and kept stirring for another 2 min. Then the solution was left at 25°C for 8 min. To prepare Au NRs, $AgNO_3$ solution (3.2 mL, 50 mM) was added in CTAB solution (200 mL, 0.1 M) and mixed gently. 1 mL of 0.1 M $HAuCl_4$ was added in this solution, changing the color of solution from transparent to yellow-orange. Then, ascorbic acid solution (1.5 mL, 100 mM) was added in Au-CTAB solution and mixed gently, followed by addition of 1.5 mL of seed solution. The resulting solution was left at 28°C for 2 h. Au NRs were purified from spherical Au NPs using centrifugation at 9000 g for 30 min.

Transmission electron microscopy characterization. The morphology and size of Au NPs and Au NRs were analyzed by TEM. The sample was prepared by drop-casting the Au NPs/NRs on Formvar carbon-coated grids and allowed to dry before performing TEM measurement. TEM analyses were carried out on a Jeol JEM-1011 microscope operated at an accelerating voltage of 100 kV. A minimum of 100 NPs was measured using Image J software for the particle size analysis.

Conjugation of Tf peptide to Au NPs and Au NRs. The ratio of amine-PEG-maleimide to Tf was 0.02: 0.04 μmol (for Au NPs-Tf_{50}), 0.3: 0.6 μmol (for Au NPs-Tf_{230}) and 1: 1.5 μmol (for Au NPs-Tf_{375}) and these ratios were reacted in 100 mM PBS (1ml, pH 7.0) for 1 h followed by purification of conjugate using an Amicon centrifugal unit (cut-off 3 kDa) at 9000 g for 5 min. The purification was done twice to remove free Tf peptides. The collected conjugates for both ratios was reacted with 12 mg of Au NPs for 12 h followed by addition of 0.5 mmol of thiol-PEG (2 kDa) for 30 min. Tf conjugated Au NPs were pelleted by centrifugation at 14000 rpm for 20 min, and unbound conjugates and thiol-PEG were removed with supernatant. The Au NP pellets were resuspended in sterile 10 mM PBS (pH 7.2). To prepare Tf conjugated Au NRs, the ratio of amine-PEG-maleimide to Tf was 0.02: 0.04 μmol (for Au NRs- Tf_{17}), 0.2: 0.4 μmol (for Au NRs-Tf_{169}) and 1: 1.5 μmol (for Au NRs-Tf_{317}) was used and these ratios were reacted in 1 mL of 100 mM PBS (pH 7.0) for 1h followed by purification as described above. Prior to functionalization of PEG-Tf conjugate, 1 mg/mL of Au NRs were reacted with 0.1 mg of thiol-PEG (2 kDa) at RT for 2 days to remove CTAB from the surface of Au NRs. PEG modified Au NRs were centrifuged at 9000 g for 30 min to remove the unreacted PEG. PEG-modified Au NRs were used to further functionalized with different PEG-Tf conjugate as described above. To backfill the Tf functionalized Au NPs or NRs, 0.5 mg of thiol-mPEG (2kDa) was incubated with 1 mg/mL of Au NPs-$Tf_{50/230/375}$ and Au NRs-$Tf_{17,169,317}$ under dark condition for 1h followed by centrifugation to remove unbound PEG.

Quantification of the number of Tf peptide per Au NP/Au NR. The amount of immobilized peptide was determined indirectly by estimating the peptide that remained in solution after the conjugation. The peptides in the stock solution (PEG-Tf conjugate) and supernatants of Au NPs-Tf and Au NRs-Tf were quantified by spectrophotometry at 280 nm using the Beer-Lambert law and an extinction coefficient of 5600 $M^{-1}cm^{-1}$. The amount of immobilized peptide was estimated by subtracting the amount of peptide in supernatants from the initial added amount. The number of peptide per Au NP was

obtained by dividing the number of peptide per mL of solution by the number of Au NPs per mL of solution.

Zeta potential measurements. Zeta (ζ) potential of the Au NPs, Au NRs, Au NPs-Tf and Au NRs-Tf (suspended in 1 mM KCl) was measured by light scattering via a Zeta PALS Zeta Potential Analyzer (Brookhaven Instruments Corporation). All data were recorded with at least 6 runs with a relative residual value (measure of data fit quality) of 0.03.

Particle size analysis. Particle size was also determined using dynamic light scattering (DLS) *via* Zeta PALS Zeta Potential Analyzer and Zeta Plus Particle Sizing Software, v. 2.27 (Brookhaven Instruments Corporation). NPs suspended in PBS or cell culture medium (EGM-2 containing 2% FBS) and sonicated for short times (< 10 min) were used. Typically, all sizing measurements were performed at 25 °C, and all data were recorded at 90°, with an equilibration time of 5 min and individual run times of 60 s (5 runs per measurement). The average diameters described in this work are number-weighted average diameters.

***In vitro* BBB model.** The *in vitro* BBB model was established according with our previous work [47]. Briefly, $CD34^+$ were isolated from human umbilical cord blood and differentiated into ECs by cultivation with endothelial cell medium (EGM-2; Lonza) supplemented with 20% fetal bovine serum (FBS; Life technologies) and 50 ng/mL of $VEGF_{165}$ (PeproTech Inc) in 1% (w/v) gelatin-coated 24-well plates ($2x10^5$ cells/well). ECs were observed in culture dishes after 15-20 days. Cells were expanded in 1% (w/v) gelatin-coated 100 mm Petri dishes (BD Falcon) in EGM-2 medium (with all supplements except FBS and gentamycin/amphotericin), supplemented with 2% (v/v) FBS, 50 μg/mL gentamycin (Biochrom AG) and 1 ng/mL bFGF (Sigma).

The BBB model was established by using a coculture system of bovine pericytes and $CD34^+$ derived ECs. The bovine pericytes were seeded at a cell density of 45×10^3 on the bottom of 12 well plate (Costar) coated with 1% gelatin and one day after $CD34^+$ derived ECs were seeded at a density of 80×10^3 in matrigel-coated (BD Biosciences) 0.4 μm Transwell inserts (Costar). Co-culture model was kept in EGM-2 supplemented 2% (v/v) FBS, 50 μg/mL gentamycin (Biochrom AG) and 1 ng/mL bFGF for 6 days before performing the experiments.

Permeability measurements. We have placed the Transwell insert having $CD34^+$ derived ECs in a new 12 well plate containing EBM-2 media. Filter inserts were filled with EBM-2 media containing the fluorescent integrity marker Lucifer yellow (20 μM, Life Technologies). The plates were placed on an orbital shaker for 1h followed by withdraw of media from the receiver compartment. For each experiment, at least three inserts with cells and without cells were tested. The fluorescence of the samples (inserts with cells and without cells) was quantified using the wavelengths 430/530 (excitation/emission). The Pe values were generated through the blue-norna brain exposure simulator (http://www.blue-norna.com). The monolayer integrity was accepted for values between 0.6-1.2 x 10^{-3} cm/min.

Transendothelial electrical resistance measurements. TEER (Ohmxcm²) of $CD34^+$ derived ECs on Transwell filters was measured using the Millicell-ERS 2 (Electrical Resistance System, Millipore). The resistance of Matrigel-coated inserts was subtracted from the resistance obtained in the presence of the endothelial cultures according to the followed equation:

TEER=[(TEER, cells)-(TEER, insert)×A], where A is the area of the filter (cm^2). For each experiment, at least three inserts with cells and without cells were tested. The TEER representing the monolayer integrity was accepted for values higher than 50 $\Omega x cm^2$.

Immunocytochemistry analysis. Cells were fixed in cold 4% (v/v) PFA (Alfa Aesar) for 10 min at room temperature and permeabilized with 0.1% (v/v) Triton X-100 (Fluka) for 10 min. Cells were then blocked with 1% (w/v) BSA (Sigma) solution for at least 30 min followed by incubation with primary antibody (ZO-1: 1:200 dilution, Invitrogen; VE-Cadherin: 1:100 dilution, Santa Cruz) during 1 h at room temperature. After washing, cells were stained with secondary antibody (Alexa 488 Anti-rabbit: 1:200 dilution; Alexa 555 Anti-mouse: 1:200 dilution) for 30 min in dark at room temperature. The nuclei of the cells were counterstained with DAPI and cells were mounted with cell-mounting medium from DAKO. All images were taken using confocal microscopy (Zeiss) with 40x objective in oil.

Transcytosis experiments of Au NPs-Tf and Au NRs-Tf with the BBB models. To evaluate the transcytosis of Au NPs-$Tf_{50/230/375}$, Au NRs-$Tf_{17/169/317}$, bare Au NP and bare Au NRs across the BBB, the experiments were done as follow. The acceptor compartments of the 12-wells of BBB models were filled with 1.5 mL EGM-2 media (with

all supplements except FBS and gentamycin/amphotericin) supplemented with 2 % (V/V) FBS, 50 µg/mL gentamycin and 1 ng/mL bFGF). Different amount (0-100 µg/mL) of Au NPs-Tf, Au NRs-Tf, Au NPs and Au NRs were added to the donor compartment having EGM-2 media for 2 h in shaking conditions at 37ºC and 5% CO_2. After 2 h, the media from the different compartments were withdrawn and stored at 4°C; cells were washed and fresh media was added in the compartments and kept in incubator for 24 h followed by permeability measurement and the assessment of monolayer integrity. Simultaneously, media and pericytes from bottom part was collected for ICP-MS analysis to quantify the transcytosis of Au NPs and Au NRs. In case of light exposure experiments, the cells incubated with Au NRs for 2 h were washed with media to remove the non-internalized Au NRs followed by irradiation with the NIR laser of wavelength 780 nm for 2 min at 2W/cm^2. Permeability measurement, TEER, evaluation of the monolayer integrity and transcytosis of Au NRs were assessed as described above.

Estimation of apparent permeability. Au NPs or Au NRs present in acceptor compartments after different experiments were analyzed by ICP-MS. For each experiment, at least three samples were analyzed by ICP-MS. Apparent permeability (Papp) for each sample was determined by the following equation 1:

$$Papp = \left(\frac{dQ}{dt}\right) * \left(\frac{1}{A}\right) * \left(\frac{1}{C_0}\right) \ (cm/s)$$

dQ/dt refers to the amount of gold present in the acceptor compartment at the function of time (µg/s), A to the area of the insert (cm^2) and C_0 to the initial concentration of the NPs/NRs added to the donor compartment (µg/mL).

The percentage of transport was calculated using the following equation 2:

$$T\% = \left(\frac{C_A(t)}{C_D(t_0)}\right) * 100$$

Where $C_A(t)$ is the amount of NPs/NRs present in the acceptor donor after 2 or 24h and $C_D(t_0)$ is the initial amount added into the donor compartment at time 0h.

For ICP-MS measurement, samples were digested with 1% HCl before performing the measurements. Per each sample, 3 readings were performed and data were obtained in average ± SD.

In vivo experiments

Animals: C57BL/6 inbred strain was used for the *in vivo* experiments. The animals were housed in cages placed in a ventilated, temperature-controlled room. The animals were kept at 22º C room temperature, 45-65 % humidity, and under a 12 h light/dark cycle. A commercial diet (pellets) and filtered water were available *ad libitum*. The animals had also, structural enrichment to favor normal animal behavior.

Animal treatment for determination of the gold content in brain: For this study, 6 or 9 mice were used per condition. Mice were anesthetized with 4% isoflurane and then kept with 1.5% isoflurane by mask. 200 µL (5 mg/mL) of Au NPs-$Tf_{230/375}$, Au NPs, Au NRs-Tf_{169} and Au NRs were injected in the tails of anesthetized mice. In case of light exposure experiments, the heads of mice were clean shaved and irradiated with the NIR laser of wavelength 780 nm for 2 min at 2W/cm^2 post 1 h administration of Au NRs-Tf_{169}. 2h post-administration of NPs/NRs, the animals were fully anesthetized with sodium pentobarbital and perfused with a solution of NaCl. Different organs and brain regions (SVZ, hippocampus and whole brain) were then excised and washed with PBS. Different brain regions were lyophilized and analyzed by ICP-MS.

Statistical Analyses. For analysis involving three or more groups, ANOVA was used, followed by a Newman-Keuls post-test. Statistical analysis was performed using GraphPad Prism software (San Diego, CA, USA). Results were considered significant when $P \leq 0.05$

Chapter 5

DISCUSSION

DISCUSSION

The current thesis is divided in 2 experimental chapters. The first experimental chapter presents a chemically defined differentiation protocol to obtain BLECs from iPSCs. The methodology combines the derivation of vascular progenitor cells followed by their differentiation into BLECs. Soluble factors such as VEGF, Wnt3a and RA are crucial for the induction of the BBB phenotype as confirmed by a better endothelial maintenance and BBB functionality. The second experimental chapter presents nanoformulations that are efficient to cross the BBB and accumulate in the neurogenic niches. We show that a particular combination of NP morphology, density of Tf peptide in the surface of the NP as well as its light responsiveness leads to a nanoformulation able to accumulate preferentially in the neurogenic regions. Moreover, our *in vitro* human BBB model derived from hematopoietic stem cells predicted efficiently the *in vivo* transport of the NPs. The current work is a further step for our understanding of the crucial factors involved in the derivation of brain ECs and the mechanisms underlying the BBB transport, particularly at the neurogenic regions.

Impact of soluble factors in the derivation of BLECs

Angiogenesis, differentiation and maturation are the crucial steps that lead to a proper BBB [66, 67, 78]. During these phases, several soluble factors have been proposed to be important. VEGF has been shown to be the major factor for the induction of the neural angiogenesis, promoting the recruitment of the ECs to the neuroectoderm, while the Wnt-β-catenin signaling pathway has been reported to be crucial for the BBB differentiation and specification [72-74]. Additionally, other factors such as RA were proposed in several studies [58, 109] as having an important role in the BBB differentiation and maturation, since it was shown its secretion by the glial cells [58]. In the current work VEGF seems to be the major factor responsible for the maintenance of the endothelial phenotype and this was demonstrated by the high levels of CD31 obtained in FACS, even when cells were only cultivated with this factor. Moreover, VEGF leads to an increase in the expression of other ECs markers, such us VE-cadherin and KDR genes when compared to BM. On the other hand, Wnt3a seems to be important in the induction of BBB properties in the vascular progenitor cells derived from iPSCs, as demonstrated by the decrease of permeability to Lucifer yellow ($1.2\pm0.2 \times 10^{-3}$ cm/min) and by the increase of TEER ($50\pm0.8\ \Omega x cm^2$). Finally, RA appears as a factor that is able to tune both events; either it helps the maintenance of the endothelial phenotype as

observed by the expression CD31, VE-cadherin and KDR, and when combined with VEGF and Wnt3a is able to maintain a low paracellular permeability (1.2±0.1 $x10^{-3}$ cm/min) and to improve TEER (55±0.6 Ωxcm^2).

The importance of the soluble factors is well patented by our experimental results showing that purified cells cultured under different conditions have significant differences in terms of permeability to Lucifer yellow and TEER. This might be related to the fact that these factors may promote the stabilization and proper localization of the TJ proteins [237]. Indeed, in the literature exposure to RA [109] and Wnt3a [47] has shown to induce a continuous expression of TJ proteins, such us occludin, claudin-5 and -1 in BLECs.

Our work focused in 3 soluble factors; however, it is likely that other factors are involved in the differentiation of the vascular progenitor cells into BLECs. BBB inductive factors, such us Wnt7a or 7b [61, 72, 73], Ang-1 [69, 70, 238, 239] and Shh [57, 240] have been shown to be involved in the specification of endothelial progenitor cells into BLECs. For instances, Alvarez and co-authors have shown that Shh can promote an increase in TEER in human BBB ECs [57] and in a different context, Shh was shown to induce an increase in Pgp expression. So, is plausible to assume that the addition of some of these factors could potentiate the BLECs phenotype in our cells. We have used the 3 factors at specific time points of the differentiation protocol: first the exposure of the cells to VEGF (50 ng/mL), followed by the incubation of the cells to all the three factors (25 ng/mL VEGF, 10 ng/mL Wnt3a and 10 μM RA) for 1 passage and finally by the exposure of the cells to VEGF (25 ng/mL) and Wnt3a (10 ng/mL) during 3 passages. Other studies performed, but not shown in this thesis, allowed us to conclude that this time points were important for the development of the BBB phenotype in the cells. For instances, keeping the RA along all the passages or incubating the cells for just 1 passage with Wnt3a resulted in a higher paracellular permeability. Indeed, in other works in literature, the authors have shown that with only 2 days exposure to RA (5-10 μM) it was possible to improve some of the BBB features in the brain ECs [58, 109]. This suggests, that the exposure to RA for small periods is enough to promote an improvement in the BBB phenotype. Nevertheless, with our model we are able to test other time points (e.g. add RA only in the end of the differentiation) and validate their importance by permeability to Lucifer yellow and TEER.

One of the main advantages of our differentiation protocol is the use of a well-defined population of vascular progenitor cells and soluble factors to generate BLECs. Previous studies [61, 85] have used co-culture protocols to generate BLECs; however, in these conditions, it is more difficult to determine the signaling pathways and molecular players involved during the endothelial specification. Another main advantage of our

differentiation protocol is that we are able to obtain a large number of BLECs from a single undifferentiated iPSCs (10 BLECs per input iPSC). With our platform, since we are using soluble factors to maturate the $CD31^+$ cells, we are able to expand our pool of cells along the passages, increasing the scalability of our system. Indeed, after 5 passages we were able to increase the initial number of ECs in 70-80%, something that was never described in the previous works.

Impact of non-soluble factors in the derivation of BLECs

The ECM is one of major component of the BBB. Due to its localization near the brain ECs is believed that the ECM is important during BBB development [42]. Indeed, some *in vivo* works have shown that some of the proteins present in the ECM are important for BBB maturation and function [241-243], and also ECM produced by other cells from the NVU, namely astrocytes and pericytes, show an improvement in the electrical resistance of the brain ECs [64, 65]. In a different context, it has been shown that decellularized ECM is able to guide the differentiation/maturation of cells into specific lineages [211, 244]. In our work, we intended to understand if native decellularized ECM could have an impact in the differentiation/maturation of the vascular progenitor cells into BLECs. During our differentiation protocol, we used ECM from glial cells and bBECs and we observed, after 4 passages, a better preservation of endothelial and BBB markers when cells were cultured in glial ECM, when compared to bBCECs ECM. Moreover, when we performed functional tests in purified cells cultivated in the decellularized ECM, we observed a decrease in paracellular permeability to Lucifer yellow and increase in TEER in cells cultivated in glial ECM when compared to the other matrix. Contrarily to our expectations, none of the native ECM was able to perform better than our control condition (cells cultivated in fibronectin). In the literature, it is suggested that brain ECs in early phases of development respond to fibronectin signaling [76]. It is possible that our cells are still presenting an earlier stage phenotype of BBB development, and because of that are more responsive to fibronectin rather than a more complex ECM.

Purified versus non-purified ECs

In our work we have observed, that depending on the protocol used to differentiate/maturate the vascular progenitor ECs into BLECs, we have different degrees of maintenance of the endothelial phenotype (50-88 % of $CD31^+$ cells). When we assess the BBB function in the mix culture of $CD31^+$ and $CD31^-$ cells, we observed high values of paracellular permeability to Lucifer yellow and low values of TEER, even in the conditions (BM+VEGF and BM+VEGF+Wnt3a+RA) where we only have

approximately 15 % of contaminant cells. When a second purification step, before platting the cells in matrigel-coated Transwell filters, was performed, we decrease the permeability and increase TEER for all the conditions used in our work, implying that even a low percentage of contaminant cells can interfere in the formation of a good and functional endothelial monolayer.

Nanoparticles as platforms to target neurogenic niches and trigger brain repair

In the current work, we aimed at developing a set of nanoformulations to target the brain, cross the BBB and, ultimately, accumulate in the neurogenic niches. We screened several NP formulations having different features (morphology, peptide density and light responsiveness) initially in a *in vitro* BBB model followed by their *in vivo* evaluation. We have used gold NPs because they present unique optical, electronic and magnetic properties which make it possible to detect by microscopy and analytic techniques [245]. In addition, these NPs can be synthesized with variable size and shape. To facilitate the targeting and transport of the NPs trough the BBB, we selected Tf peptide [220]. Several reports in the literature [130, 220, 226, 246, 247] have shown that targeting the Tf transporter is a good strategy to cross the BBB, which is correlated with the high expression of this transmembrane protein in the brain ECs [248, 249]. Moreover, the mode of binding to the Tf receptor affects the transcytosis pathway. Indeed, Niewoehner and co-authors [226] have shown, using a Brain Shuttle module, that monovalent and bivalent bind of a monoclonal antibody fragment affects the BBB transcytosis and consequently intracellular localization. This work proposes that the monovalent bind, which is more similar to the natural Tf binding, facilitates the transcytosis, whereas the bivalent bind promotes the accumulation in the lysosomes. In the same line of evidence, Wiley *et al.* [130] have shown that by playing with the density of Tf protein in the surface of Au NPs is possible to modulate the accumulation in brain parenchyma. In our work we have decided to use a Tf peptide, which has been described previously to promote BBB transcytosis [220], instead of Tf protein since the thiol group introduced at C terminus can support a specific orientation of the peptide. Moreover, the density of Tf peptide on top of the NPs/NRs was between 17 and 375 peptides per NP/NR, that goes in line with previous work developed by Wiley and collaborators [220]. We have used citrate AuNPs (mean size of 10-12 nm) and AuNRs (46.7 nm x 13.7 nm) [250]. In the literature, several works have shown that Au NPs with small sizes are good carriers to cross the BBB [147, 220, 230], and the size choose for Au NRs was a compromise

between the maintenance of their plasmonic properties, their capacity to respond to NIR light and the number of Tf peptides that we can functionalize in the cell surface.

We have observed *in vitro* that the medium density (Au NPs-Tf_{230} and Au NRs-Tf_{169}) was the optimal density to have the best Papp values (Au NPs-Tf_{230}: 1.3 x 10^{-7} cm/s and Au NRs-Tf_{169}: 6.4 ± 1.3 x10^{-8} cm/s), revealing the highest transcytosis when compared to the other densities or bare NPs and NRs. Our observations are in accordance with the literature in terms of Papp values [220, 230], and also the avidity effect seems to be present in our system, as suggested previously by others [130, 226]. Importantly, we observed by permeability to Lucifer yellow, TEER and immunocytochemistry, that the nanoformulations do not affect the brain ECs monolayer integrity.

Nanoparticles that heat once activated by a NIR laser have enhanced transport properties through the BBB. Au NRs respond to this light by increasing the local temperature [228, 229], and by using this property we hypothesized that this temperature increase in the vicinity of the Au NRs would lead to a locally more leaky barrier improving the BBB transcytosis. To assess the impact of the activation of the Au NRs-Tf by the NIR light, we used the 3 nanoformulations, Au NRs-$Tf_{17/169/317}$, and once more we observed that the best peptide density in combination with the light was the 169 peptides per NR (Papp: 7.5 ± 1.3 x 10^{-8} cm/s). Contrarily to the expected we didn't observe an improvement in the Au NRs-Tf transcytosis when compared to the absence of light. One possible justification for this result, is the fact that we are removing Au NRs-Tf and washing the cells before irradiation and, in reality, only a significantly small number of Au NRs-Tf (the ones that are interacting with the membrane barrier) are responsible for the thermal effect. Nevertheless, we uncovered that this washing step was crucial to maintain the monolayer integrity.

Our final goal during this work, was to develop a nanoformulation that besides crossing the BBB, could accumulate preferentially in the neurogenic niches. In the literature, only a few works have shown a higher accumulation in these regions when compared to other brain areas [166, 195]. To evaluate this accumulation, we performed *in vivo* studies with C57BL/6 mice. Our results showed that Au NPs-Tf_{230} accumulate more in the mice brain when compared to the other nanoformulations tested, but this accumulation is present in all of the brain. On the other hand, when we combined the Au NRs-Tf_{169} with the NIR we improved the BBB crossing and we enhanced the preferential accumulation in the neurogenic niches, namely in SVZ region. The differences between the *in vitro* and *in vivo* data for the AuNRs-Tf_{169} light activated, might result from the fact that *in vivo* we have the Au NRs in the vicinity of the brain ECs and they may induce a

temperature effect that can enhance the BBB crossing. Nevertheless, future works should be performed in a way to understand if this can affect the normal permeability of the BBB. In the literature a study with magnetic NPs [235], has shown that after magnetic heating with radiofrequency field was possible to observe by MRI an increase in the animal brain of the NPs, and also an increase in BBB permeability by Evans blue dye. Nevertheless, if the animals were allowed to recover after administration and irradiation (wait 2 h before injecting Evans blue and sacrifice) the authors observed that the NPs were present in the brain tissue but the BBB was no longer permeable to Evans blue. This suggests that the increase in the BBB permeability was transient. It is possible that in our study, since we are allowing the animals to recover for 1 h after administration and irradiation, the same events may occur.

Chapter 6

FUTURE WORK

FUTURE WORK

Although some questions have been answer during the development of this thesis, there is still some future work that can be done in order to clarify some of the open questions.

Future studies should be done in a way to identify if the BLECs derived from iPSCs can be used for the generation of a robust and and stable human *in vitro* BBB model. Our data already demonstrate that the monoculture of our iPSCs-derived ECs, present lower permeability when compared to the ECs derived from the hematopoietic stem cells (1.2 Vs 2 $x10^{-3}$ cm/min) [47]. In the literature, several works [47, 61, 85, 109] report co-culture systems as crucial for the developing of a BBB *in vitro* model. We hypothesize that the co-culture of iPSCs-derived brain ECs co-cultured with other cells from the NVU, namely astrocytes and pericytes can allow the creation of a new *in vitro* BBB model. Some efforts, using bovine pericytes and rat glial cells, are already being made in order to assess this possibility. Nevertheless, since we are using iPSCs-derived brain ECs it is a good opportunity to create a fully human *in vitro* BBB model, and some works have shown that indeed it is possible to generate NPCs [251, 252] and pericytes [94] from iPSCs.

Another aspect that was evaluated during the development of this thesis, was the use of ECM along the differentiation/maturation of the BLECs. In the literature, proteins from the ECM have been shown to be important at several stages, either by promoting cell proliferation, survival [76] and stability [242, 243] or by regulating the maturation and function of the BBB [241]. In our work, contrarily to our expectations, we didn't observe any beneficial impact in using native ECM from bBCECs or glial cells in opposite to fibronectin (1 $\mu g/cm^2$) in terms of BBB markers expression, endothelial phenotype stability and BBB function. Future studies can be performed in away to identify the importance of the ECM at different moments of the protocol. For instance, instead of maturating the cells in the native ECMs, we could use it in the Transwell systems, going in line with some studies reported previously [65, 215, 253]. It is expected that with this strategy we can improve the BBB function in the iPSCs-derived brain ECs and also to induce cell polarization in terms of transporters. Moreover, this strategy can be use simultaneously with the co-culture system [65, 253]. It would be also interesting to characterized these matrices by proteomics [254] in order to identify the major

components of each native ECMs, and to correlate it with the results with the fibronectin-coating.

An important outcome of this work, due to the use of iPSCs to generate the brain-like ECs, is the possibility to generate a disease BBB model. Impairment of the BBB in several brain disorders, leads to inflammation perpetuations and neurodegeneration [67]. In some cases, it is clear that BBB breakdown is a consequence of a specific event such as traumatic brain injury or ischemic stroke [255]. In other cases, especially in chronic neurodegenerative conditions like Multiple Sclerosis, Alzheimer'sand Parkinson's disease, it remains unclear if it is a downstream process or if it plays a role in disease onset and development [256, 257]. Taking advantages of already patient-derived iPSCs from some of these diseases with a genetic background [104-107], it can by hypothesis the possibility to differentiate the iPSCs into BLECs, creating a patient-specific BBB model.

Future works, regarding the BBB crossing of the NPs, should be performed in away to understand the mechanisms behind these events. In order to confirm that the NPs are only crossing by receptor-mediated transcytosis, an inhibitor of the Tf receptor should be use (Dansylcadaverine [258]) to block the receptor. To perform these experiments, a pre-blocking of the ECs with the inhibitor should be preformed, followed by the incubation of the cells with the nanoformulations that demonstrated the highest Papp values (AuNPs-Tf_{230} and AuNRs-Tf_{169}) to have sensibility in the ICP-MS analysis. Since we are incubating the BLECs with the NPs for 2 h, it is plausible to assume that it would be needed to keep the inhibitor during the NPs incubation.

In the literature, studies have shown differences in terms of NPs localization in the cells [130] and in terms of internalization pathways [226] according with the ligand density in the NPs surface. Future efforts should be done in a way to evaluate the co-localization of the NPs with vesicles markers, such as EEA1 and Rab7 for early and late endosomes respectively, and LAMP2 for lysosomes. These assessments must be performed immediately after the cells exposer to the NPs (at 2 h) and after 24 h, to evaluate the differences at both stages of internalization. On the other hand, *in vivo* future studies should be performed in a way to confirm the presence of NPs in the brain parenchyma and not only inside the brain ECs.

In our work we observed that the combination of AuNRs-Tf_{169} with NIR light leads to a preferential accumulation of this nanoformulation in the neurogenic niches after intravenous administration. In a way to prove that this fact can indeed improve the local neurogenesis and ultimately induce brain repair, studies should evaluate markers of the

neurogenic process (e.g. number of NeuN-positive cells). Nevertheless, the nanoformulations should be modify in a way to transport small molecules [187, 189, 191] that can improve neurogenesis. An another interesting aspect to assess in future, is the use of this nanoformulations in a disease animal model.

REFERENCES

REFERENCES

1. Cardoso, F.L., D. Brites, and M.A. Brito, *Looking at the blood-brain barrier: molecular anatomy and possible investigation approaches.* Brain Res Rev, 2010. **64**(2): p. 328-63.
2. Abbott, N.J., L. Ronnback, and E. Hansson, *Astrocyte-endothelial interactions at the blood-brain barrier.* Nat Rev Neurosci, 2006. **7**(1): p. 41-53.
3. Abbott, N.J., et al., *Structure and function of the blood-brain barrier.* Neurobiol Dis, 2010. **37**(1): p. 13-25.
4. Liddelow, S.A., *Fluids and barriers of the CNS: a historical viewpoint.* Fluids Barriers CNS, 2011. **8**(1): p. 2.
5. Ballabh, P., A. Braun, and M. Nedergaard, *The blood-brain barrier: an overview: structure, regulation, and clinical implications.* Neurobiol Dis, 2004. **16**(1): p. 1-13.
6. Ehrlich, P., *Das Sauerstoff-Bedürfniss des Organismus : eine farbenanalytische Studie.* Hirschwald, Berlin., 1885.
7. Ehrlich, P., *Ueber die beziehungen von chemischer constitution, verteilung und pharmakologischer wirkung. Gesammelte Arbeiten zur Immunitaetsforschung.* Hirschwald, Berlin., 1904.
8. Goldmann, E., *Vitalfarbung am zentralnervensystem. .* bhandl Konigl preuss Akad Wiss, 1913. **1**: p. 1-60.
9. Wilhelm, I., C. Fazakas, and I.A. Krizbai, *In vitro models of the blood-brain barrier.* Acta Neurobiol Exp (Wars), 2011. **71**(1): p. 113-28.
10. Persidsky, Y., et al., *Blood-brain barrier: structural components and function under physiologic and pathologic conditions.* J Neuroimmune Pharmacol, 2006. **1**(3): p. 223-36.
11. Zlokovic, B.V., *The blood-brain barrier in health and chronic neurodegenerative disorders.* Neuron, 2008. **57**(2): p. 178-201.
12. Naik, P. and L. Cucullo, *In vitro blood-brain barrier models: current and perspective technologies.* J Pharm Sci, 2012. **101**(4): p. 1337-54.
13. Tsaioun, K., M. Bottlaender, and A. Mabondzo, *ADDME--Avoiding Drug Development Mistakes Early: central nervous system drug discovery perspective.* BMC Neurol, 2009. **9 Suppl 1**: p. S1.
14. Cecchelli, R., et al., *Modelling of the blood-brain barrier in drug discovery and development.* Nat Rev Drug Discov, 2007. **6**(8): p. 650-61.
15. Hallier-Vanuxeem, D., et al., *New strategy for alerting central nervous system toxicity: Integration of blood-brain barrier toxicity and permeability in neurotoxicity assessment.* Toxicol In Vitro, 2009. **23**(3): p. 447-53.
16. Jeffrey, P. and S. Summerfield, *Assessment of the blood-brain barrier in CNS drug discovery.* Neurobiol Dis, 2010. **37**(1): p. 33-7.
17. Bernacki, J., et al., *Physiology and pharmacological role of the blood-brain barrier.* Pharmacol Rep, 2008. **60**(5): p. 600-22.
18. Johansson, B.B., *Blood-Brain Barrier: Role of Brain Endothelial Surface Charge and Glycocalyx*, in *Ischemic Blood Flow in the Brain*, Y.F. M.D., M.T. M.D., and A.K. M.D., Editors. 2001, Springer Japan. p. 33-38.
19. Abbott, N.J., *Astrocyte-endothelial interactions and blood-brain barrier permeability.* J Anat, 2002. **200**(6): p. 629-38.
20. Hellinger, E., et al., *Comparison of brain capillary endothelial cell-based and epithelial (MDCK-MDR1, Caco-2, and VB-Caco-2) cell-based surrogate blood-brain barrier penetration models.* Eur J Pharm Biopharm, 2012. **82**(2): p. 340-51.

21. Wolburg, H. and A. Lippoldt, *Tight junctions of the blood-brain barrier: development, composition and regulation.* Vascul Pharmacol, 2002. **38**(6): p. 323-37.
22. Hawkins, B.T. and T.P. Davis, *The blood-brain barrier/neurovascular unit in health and disease.* Pharmacol Rev, 2005. **57**(2): p. 173-85.
23. Nag, S., *Morphology and Properties of Brain Endothelial Cells*, in *The Blood-Brain and Other Neural Barriers: Reviews and Protocols*, S. Nag, Editor. 2011, Springer: Methods in Molecular Biology.
24. Wolburg, H., et al., *Localization of claudin-3 in tight junctions of the blood-brain barrier is selectively lost during experimental autoimmune encephalomyelitis and human glioblastoma multiforme.* Acta Neuropathol, 2003. **105**(6): p. 586-92.
25. Nitta, T., et al., *Size-selective loosening of the blood-brain barrier in claudin-5-deficient mice.* J Cell Biol, 2003. **161**(3): p. 653-60.
26. Furuse, M., et al., *A single gene product, claudin-1 or -2, reconstitutes tight junction strands and recruits occludin in fibroblasts.* J Cell Biol, 1998. **143**(2): p. 391-401.
27. Hirase, T., et al., *Occludin as a possible determinant of tight junction permeability in endothelial cells.* J Cell Sci, 1997. **110 (Pt 14)**: p. 1603-13.
28. Bolton, S.J., D.C. Anthony, and V.H. Perry, *Loss of the tight junction proteins occludin and zonula occludens-1 from cerebral vascular endothelium during neutrophil-induced blood-brain barrier breakdown in vivo.* Neuroscience, 1998. **86**(4): p. 1245-57.
29. Persidsky, Y., et al., *Rho-mediated regulation of tight junctions during monocyte migration across the blood-brain barrier in HIV-1 encephalitis (HIVE).* Blood, 2006. **107**(12): p. 4770-80.
30. Brown, R.C. and T.P. Davis, *Hypoxia/aglycemia alters expression of occludin and actin in brain endothelial cells.* Biochem Biophys Res Commun, 2005. **327**(4): p. 1114-23.
31. Huber, J.D., R.D. Egleton, and T.P. Davis, *Molecular physiology and pathophysiology of tight junctions in the blood-brain barrier.* Trends Neurosci, 2001. **24**(12): p. 719-25.
32. Mark, K.S. and T.P. Davis, *Cerebral microvascular changes in permeability and tight junctions induced by hypoxia-reoxygenation.* Am J Physiol Heart Circ Physiol, 2002. **282**(4): p. H1485-94.
33. Matter, K. and M.S. Balda, *Signalling to and from tight junctions.* Nat Rev Mol Cell Biol, 2003. **4**(3): p. 225-36.
34. Abbruscato, T.J. and T.P. Davis, *Protein expression of brain endothelial cell E-cadherin after hypoxia/aglycemia: influence of astrocyte contact.* Brain Res, 1999. **842**(2): p. 277-86.
35. Gabathuler, R., *Approaches to transport therapeutic drugs across the blood-brain barrier to treat brain diseases.* Neurobiol Dis, 2010. **37**(1): p. 48-57.
36. Pardridge, W.M., *Blood-brain barrier delivery.* Drug Discov Today, 2007. **12**(1-2): p. 54-61.
37. Gu, Y., et al., *Caveolin-1 regulates nitric oxide-mediated matrix metalloproteinases activity and blood-brain barrier permeability in focal cerebral ischemia and reperfusion injury.* J Neurochem, 2012. **120**(1): p. 147-56.
38. Song, L., S. Ge, and J.S. Pachter, *Caveolin-1 regulates expression of junction-associated proteins in brain microvascular endothelial cells.* Blood, 2007. **109**(4): p. 1515-23.
39. Choi, Y.K. and K.W. Kim, *Blood-neural barrier: its diversity and coordinated cell-to-cell communication.* BMB Rep, 2008. **41**(5): p. 345-52.
40. Dore-Duffy, P. and K. Cleary, *Morphology and Properties of Pericytes*, in *The Blood Brain and Other Neural Barriers: Reviews and Protocols*, S. Nag, Editor. 2011, Springer: Methods in Molecular Biology.

41. Sa-Pereira, I., D. Brites, and M.A. Brito, *Neurovascular unit: a focus on pericytes.* Mol Neurobiol, 2012. **45**(2): p. 327-47.
42. Baeten, K.M. and K. Akassoglou, *Extracellular matrix and matrix receptors in blood-brain barrier formation and stroke.* Dev Neurobiol, 2011. **71**(11): p. 1018-39.
43. Dore-Duffy, P., et al., *CNS microvascular pericytes exhibit multipotential stem cell activity.* J Cereb Blood Flow Metab, 2006. **26**(5): p. 613-24.
44. Armulik, A., A. Abramsson, and C. Betsholtz, *Endothelial/pericyte interactions.* Circ Res, 2005. **97**(6): p. 512-23.
45. Hori, S., et al., *A pericyte-derived angiopoietin-1 multimeric complex induces occludin gene expression in brain capillary endothelial cells through Tie-2 activation in vitro.* J Neurochem, 2004. **89**(2): p. 503-13.
46. Dohgu, S., et al., *Brain pericytes contribute to the induction and up-regulation of blood-brain barrier functions through transforming growth factor-beta production.* Brain Res, 2005. **1038**(2): p. 208-15.
47. Cecchelli, R., et al., *A Stable and Reproducible Human Blood-Brain Barrier Model Derived from Hematopoietic Stem Cells.* Plos One, 2014. **9**(6).
48. Hayashi, K., et al., *Effects of hypoxia on endothelial/pericytic co-culture model of the blood-brain barrier.* Regul Pept, 2004. **123**(1-3): p. 77-83.
49. Berezowski, V., et al., *Contribution of glial cells and pericytes to the mRNA profiles of P-glycoprotein and multidrug resistance-associated proteins in an in vitro model of the blood-brain barrier.* Brain Res, 2004. **1018**(1): p. 1-9.
50. Vandenhaute, E., et al., *Modelling the neurovascular unit and the blood-brain barrier with the unique function of pericytes.* Curr Neurovasc Res, 2011. **8**(4): p. 258-69.
51. Daneman, R., et al., *Pericytes are required for blood-brain barrier integrity during embryogenesis.* Nature, 2010. **468**(7323): p. 562-6.
52. Armulik, A., et al., *Pericytes regulate the blood-brain barrier.* Nature, 2010. **468**(7323): p. 557-61.
53. Nag, S., *Morphology and Properties of Astrocytes*, in *The Blood-Brain Barrier and Other Neural Barriers: Reviews and Protocols*, S. Nag, Editor. 2011, Spinger: Methods in Molecular Biology.
54. Haseloff, R.F., et al., *In search of the astrocytic factor(s) modulating blood-brain barrier functions in brain capillary endothelial cells in vitro.* Cell Mol Neurobiol, 2005. **25**(1): p. 25-39.
55. Colgan, O.C., et al., *Influence of basolateral condition on the regulation of brain microvascular endothelial tight junction properties and barrier function.* Brain Res, 2008. **1193**: p. 84-92.
56. Siddharthan, V., et al., *Human astrocytes/astrocyte-conditioned medium and shear stress enhance the barrier properties of human brain microvascular endothelial cells.* Brain Res, 2007. **1147**: p. 39-50.
57. Alvarez, J.I., et al., *The Hedgehog pathway promotes blood-brain barrier integrity and CNS immune quiescence.* Science, 2011. **334**(6063): p. 1727-31.
58. Mizee, M.R., et al., *Retinoic acid induces blood-brain barrier development.* J Neurosci, 2013. **33**(4): p. 1660-71.
59. Weidenfeller, C., C.N. Svendsen, and E.V. Shusta, *Differentiating embryonic neural progenitor cells induce blood-brain barrier properties.* J Neurochem, 2007. **101**(2): p. 555-65.
60. Lippmann, E.S., et al., *Blood-brain barrier modeling with co-cultured neural progenitor cell-derived astrocytes and neurons.* J Neurochem, 2011. **119**(3): p. 507-20.
61. Lippmann, E.S., et al., *Derivation of blood-brain barrier endothelial cells from human pluripotent stem cells.* Nat Biotechnol, 2012. **30**(8): p. 783-91.

62. Savettieri, G., et al., *Neurons and ECM regulate occludin localization in brain endothelial cells.* Neuroreport, 2000. **11**(5): p. 1081-4.
63. Tilling, T., et al., *Expression and adhesive properties of basement membrane proteins in cerebral capillary endothelial cell cultures.* Cell Tissue Res, 2002. **310**(1): p. 19-29.
64. Hartmann, C., et al., *The impact of glia-derived extracellular matrices on the barrier function of cerebral endothelial cells: an in vitro study.* Exp Cell Res, 2007. **313**(7): p. 1318-25.
65. Zobel, K., U. Hansen, and H.J. Galla, *Blood-brain barrier properties in vitro depend on composition and assembly of endogenous extracellular matrices.* Cell Tissue Res, 2016. **365**(2): p. 233-45.
66. Liebner, S., C.J. Czupalla, and H. Wolburg, *Current concepts of blood-brain barrier development.* Int J Dev Biol, 2011. **55**(4-5): p. 467-76.
67. Obermeier, B., R. Daneman, and R.M. Ransohoff, *Development, maintenance and disruption of the blood-brain barrier.* Nat Med, 2013. **19**(12): p. 1584-96.
68. Koh, G.Y., *Orchestral actions of angiopoietin-1 in vascular regeneration.* Trends Mol Med, 2013. **19**(1): p. 31-9.
69. Lee, S.W., et al., *SSeCKS regulates angiogenesis and tight junction formation in blood-brain barrier.* Nat Med, 2003. **9**(7): p. 900-6.
70. Valable, S., et al., *VEGF-induced BBB permeability is associated with an MMP-9 activity increase in cerebral ischemia: both effects decreased by Ang-1.* J Cereb Blood Flow Metab, 2005. **25**(11): p. 1491-504.
71. Liebner, S. and K.H. Plate, *Differentiation of the brain vasculature: the answer came blowing by the Wnt.* J Angiogenes Res, 2010. **2**: p. 1.
72. Stenman, J.M., et al., *Canonical Wnt signaling regulates organ-specific assembly and differentiation of CNS vasculature.* Science, 2008. **322**(5905): p. 1247-50.
73. Daneman, R., et al., *Wnt/beta-catenin signaling is required for CNS, but not non-CNS, angiogenesis.* Proc Natl Acad Sci U S A, 2009. **106**(2): p. 641-6.
74. Liebner, S., et al., *Wnt/beta-catenin signaling controls development of the blood-brain barrier.* J Cell Biol, 2008. **183**(3): p. 409-17.
75. James, J.M. and Y.S. Mukouyama, *Neuronal action on the developing blood vessel pattern.* Semin Cell Dev Biol, 2011. **22**(9): p. 1019-27.
76. Wang, J. and R. Milner, *Fibronectin promotes brain capillary endothelial cell survival and proliferation through alpha5beta1 and alphavbeta3 integrins via MAP kinase signalling.* J Neurochem, 2006. **96**(1): p. 148-59.
77. Osada, T., et al., *Interendothelial claudin-5 expression depends on cerebral endothelial cell-matrix adhesion by beta(1)-integrins.* J Cereb Blood Flow Metab, 2011. **31**(10): p. 1972-85.
78. Blanchette, M. and R. Daneman, *Formation and maintenance of the BBB.* Mech Dev, 2015. **138 Pt 1**: p. 8-16.
79. Helms, H.C., et al., *In vitro models of the blood-brain barrier: An overview of commonly used brain endothelial cell culture models and guidelines for their use.* J Cereb Blood Flow Metab, 2016. **36**(5): p. 862-90.
80. Aday, S., et al., *Stem Cell-Based Human Blood-Brain Barrier Models for Drug Discovery and Delivery.* Trends Biotechnol, 2016. **34**(5): p. 382-93.
81. Bernas, M.J., et al., *Establishment of primary cultures of human brain microvascular endothelial cells to provide an in vitro cellular model of the blood-brain barrier.* Nat Protoc, 2010. **5**(7): p. 1265-72.
82. Weksler, B.B., et al., *Blood-brain barrier-specific properties of a human adult brain endothelial cell line.* FASEB J, 2005. **19**(13): p. 1872-4.
83. Sano, Y., et al., *Establishment of a new conditionally immortalized human brain microvascular endothelial cell line retaining an in vivo blood-brain barrier function.* J Cell Physiol, 2010. **225**(2): p. 519-28.

84. Weksler, B., I.A. Romero, and P.O. Couraud, *The hCMEC/D3 cell line as a model of the human blood brain barrier.* Fluids Barriers CNS, 2013. **10**(1): p. 16.
85. Minami, H., et al., *Generation of Brain Microvascular Endothelial-Like Cells from Human Induced Pluripotent Stem Cells by Co-Culture with C6 Glioma Cells.* PLoS One, 2015. **10**(6): p. e0128890.
86. Boyer-Di Ponio, J., et al., *Instruction of circulating endothelial progenitors in vitro towards specialized blood-brain barrier and arterial phenotypes.* PLoS One, 2014. **9**(1): p. e84179.
87. Takahashi, K. and S. Yamanaka, *Induction of Pluripotent Stem Cells from Mouse Embryonic and Adult Fibroblast Cultures by Defined Factors.* Cell, 2006. **126**(4): p. 663-676.
88. Takahashi, K., et al., *Induction of Pluripotent Stem Cells from Adult Human Fibroblasts by Defined Factors.* Cell, 2007. **131**(5): p. 861-872.
89. Loh, Y.-H., et al., *Reprogramming of T Cells from Human Peripheral Blood.* Cell Stem Cell, 2010. **7**(1): p. 15-19.
90. Loh, Y.-H., et al., *Generation of induced pluripotent stem cells from human blood.* Blood, 2009. **113**(22): p. 5476-5479.
91. Haase, A., et al., *Generation of Induced Pluripotent Stem Cells from Human Cord Blood.* Cell Stem Cell, 2009. **5**(4): p. 434-441.
92. Ferreira, L.S., et al., *Vascular progenitor cells isolated from human embryonic stem cells give rise to endothelial and smooth muscle like cells and form vascular networks in vivo.* Circ Res, 2007. **101**(3): p. 286-94.
93. Kane, N.M., et al., *Pluripotent stem cell differentiation into vascular cells: A novel technology with promises for vascular re(generation).* Pharmacology & Therapeutics, 2011. **129**(1): p. 29-49.
94. Orlova, V.V., et al., *Functionality of endothelial cells and pericytes from human pluripotent stem cells demonstrated in cultured vascular plexus and zebrafish xenografts.* Arterioscler Thromb Vasc Biol, 2014. **34**(1): p. 177-86.
95. Costa, M., et al., *Derivation of endothelial cells from human embryonic stem cells in fully defined medium enables identification of lysophosphatidic acid and platelet activating factor as regulators of eNOS localization.* Stem Cell Research, 2013. **10**(1): p. 103-117.
96. Zhang, P., et al., *Short-term BMP-4 treatment initiates mesoderm induction in human embryonic stem cells.* Blood, 2008. **111**(4): p. 1933-1941.
97. James, D., et al., *Expansion and maintenance of human embryonic stem cell-derived endothelial cells by TGFbeta inhibition is Id1 dependent.* Nat Biotechnol, 2010. **28**(2): p. 161-6.
98. Pitrez, P.R., et al., *Vascular disease modeling using induced pluripotent stem cells: Focus in Hutchinson-Gilford Progeria Syndrome.* Biochem Biophys Res Commun, 2016. **473**(3): p. 710-8.
99. Lippmann, E.S., et al., *Modeling the blood-brain barrier using stem cell sources.* Fluids Barriers CNS, 2013. **10**(1): p. 2.
100. Grskovic, M., et al., *Induced pluripotent stem cells--opportunities for disease modelling and drug discovery.* Nat Rev Drug Discov, 2011. **10**(12): p. 915-29.
101. Sterneckert, J.L., P. Reinhardt, and H.R. Scholer, *Investigating human disease using stem cell models.* Nat Rev Genet, 2014. **15**(9): p. 625-39.
102. Weiss, N., et al., *The blood-brain barrier in brain homeostasis and neurological diseases.* Biochim Biophys Acta, 2009. **1788**(4): p. 842-57.
103. Yagi, T., et al., *Establishment of Induced Pluripotent Stem Cells from Centenarians for Neurodegenerative Disease Research.* PLoS One, 2012. **7**(7).
104. Kondo, T., et al., *Modeling Alzheimer's disease with iPSCs reveals stress phenotypes associated with intracellular Abeta and differential drug responsiveness.* Cell Stem Cell, 2013. **12**(4): p. 487-96.

105. Israel, M.A., et al., *Probing sporadic and familial Alzheimer's disease using induced pluripotent stem cells.* Nature, 2012. **482**(7384): p. 216-20.
106. Byers, B., H.L. Lee, and R. Reijo Pera, *Modeling Parkinson's disease using induced pluripotent stem cells.* Curr Neurol Neurosci Rep, 2012. **12**(3): p. 237-42.
107. Song, B., et al., *Neural differentiation of patient specific iPS cells as a novel approach to study the pathophysiology of multiple sclerosis.* Stem Cell Res, 2012. **8**(2): p. 259-73.
108. Robinton, D.A. and G.Q. Daley, *The promise of induced pluripotent stem cells in research and therapy.* Nature, 2012. **481**: p. 295-305.
109. Lippmann, E.S., et al., *A retinoic acid-enhanced, multicellular human blood-brain barrier model derived from stem cell sources.* Sci Rep, 2014. **4**: p. 4160.
110. Wilson, H.K., et al., *Exploring the effects of cell seeding density on the differentiation of human pluripotent stem cells to brain microvascular endothelial cells.* Fluids Barriers CNS, 2015. **12**: p. 13.
111. Patel, R. and A.J. Alahmad, *Growth-factor reduced Matrigel source influences stem cell derived brain microvascular endothelial cell barrier properties.* Fluids Barriers CNS, 2016. **13**.
112. Katt, M.E., et al., *Human Brain Microvascular Endothelial Cells Derived from the BC1 iPS Cell Line Exhibit a Blood-Brain Barrier Phenotype.* PLoS One, 2016. **11**(4): p. e0152105.
113. Wolburg, H., et al., *Brain endothelial cells and the glio-vascular complex.* Cell Tissue Res, 2009. **335**(1): p. 75-96.
114. Deli, M.A., et al., *Permeability studies on in vitro blood-brain barrier models: physiology, pathology, and pharmacology.* Cell Mol Neurobiol, 2005. **25**(1): p. 59-127.
115. Dehouck, M.P., et al., *An easier, reproducible, and mass-production method to study the blood-brain barrier in vitro.* J Neurochem, 1990. **54**(5): p. 1798-801.
116. Boveri, M., et al., *Induction of blood-brain barrier properties in cultured brain capillary endothelial cells: comparison between primary glial cells and C6 cell line.* Glia, 2005. **51**(3): p. 187-98.
117. Gumbleton, M. and K.L. Audus, *Progress and limitations in the use of in vitro cell cultures to serve as a permeability screen for the blood-brain barrier.* J Pharm Sci, 2001. **90**(11): p. 1681-98.
118. Pardridge, W.M., *Drug targeting to the brain.* Pharm Res, 2007. **24**(9): p. 1733-44.
119. Goldsmith, M., L. Abramovitz, and D. Peer, *Precision nanomedicine in neurodegenerative diseases.* ACS Nano, 2014. **8**(3): p. 1958-65.
120. Patel, T., et al., *Polymeric nanoparticles for drug delivery to the central nervous system.* Adv Drug Deliv Rev, 2012. **64**(7): p. 701-5.
121. Kreuter, J., *Drug delivery to the central nervous system by polymeric nanoparticles: what do we know?* Adv Drug Deliv Rev, 2014. **71**: p. 2-14.
122. Kreuter, J., *Drug targeting with nanoparticles.* Eur J Drug Metab Pharmacokinet, 1994. **19**(3): p. 253-6.
123. Barbu, E., et al., *The potential for nanoparticle-based drug delivery to the brain: overcoming the blood-brain barrier.* Expert Opin Drug Deliv, 2009. **6**(6): p. 553-65.
124. Lockman, P.R., et al., *Nanoparticle technology for drug delivery across the blood-brain barrier.* Drug Dev Ind Pharm, 2002. **28**(1): p. 1-13.
125. Cupaioli, F.A., et al., *Engineered nanoparticles. How brain friendly is this new guest?* Prog Neurobiol, 2014. **119-120**: p. 20-38.
126. Karatas, H., et al., *A nanomedicine transports a peptide caspase-3 inhibitor across the blood-brain barrier and provides neuroprotection.* J Neurosci, 2009. **29**(44): p. 13761-9.

127. Aktas, Y., et al., *Development and brain delivery of chitosan-PEG nanoparticles functionalized with the monoclonal antibody OX26.* Bioconjug Chem, 2005. **16**(6): p. 1503-11.
128. Gao, X., et al., *Overcoming the blood-brain barrier for delivering drugs into the brain by using adenosine receptor nanoagonist.* ACS Nano, 2014. **8**(4): p. 3678-89.
129. Choi, C.H., et al., *Mechanism of active targeting in solid tumors with transferrin-containing gold nanoparticles.* Proc Natl Acad Sci U S A, 2010. **107**(3): p. 1235-40.
130. Wiley, D.T., et al., *Transcytosis and brain uptake of transferrin-containing nanoparticles by tuning avidity to transferrin receptor.* Proc Natl Acad Sci U S A, 2013. **110**(21): p. 8662-7.
131. Kong, S.D., et al., *Magnetic targeting of nanoparticles across the intact blood-brain barrier.* J Control Release, 2012. **164**(1): p. 49-57.
132. Yemisci, M., et al., *Systemically administered brain-targeted nanoparticles transport peptides across the blood-brain barrier and provide neuroprotection.* J Cereb Blood Flow Metab, 2015. **35**(3): p. 469-75.
133. Song, Q., et al., *Lipoprotein-based nanoparticles rescue the memory loss of mice with Alzheimer's disease by accelerating the clearance of amyloid-beta.* ACS Nano, 2014. **8**(3): p. 2345-59.
134. Koffie, R.M., et al., *Nanoparticles enhance brain delivery of blood-brain barrier-impermeable probes for in vivo optical and magnetic resonance imaging.* Proc Natl Acad Sci U S A, 2011. **108**(46): p. 18837-42.
135. Zhang, C., et al., *Dual-functional nanoparticles targeting amyloid plaques in the brains of Alzheimer's disease mice.* Biomaterials, 2014. **35**(1): p. 456-65.
136. Hanada, S., et al., *Cell-based in vitro blood-brain barrier model can rapidly evaluate nanoparticles' brain permeability in association with particle size and surface modification.* Int J Mol Sci, 2014. **15**(2): p. 1812-25.
137. Sonavane, G., K. Tomoda, and K. Makino, *Biodistribution of colloidal gold nanoparticles after intravenous administration: effect of particle size.* Colloids Surf B Biointerfaces, 2008. **66**(2): p. 274-80.
138. Etame, A.B., et al., *Design and potential application of PEGylated gold nanoparticles with size-dependent permeation through brain microvasculature.* Nanomedicine, 2011. **7**(6): p. 992-1000.
139. Decuzzi, P., et al., *Size and shape effects in the biodistribution of intravascularly injected particles.* J Control Release, 2010. **141**(3): p. 320-7.
140. Kolhar, P., et al., *Using shape effects to target antibody-coated nanoparticles to lung and brain endothelium.* Proc Natl Acad Sci U S A, 2013. **110**(26): p. 10753-8.
141. Lockman, P.R., et al., *Nanoparticle surface charges alter blood-brain barrier integrity and permeability.* J Drug Target, 2004. **12**(9-10): p. 635-41.
142. Bramini, M., et al., *Imaging approach to mechanistic study of nanoparticle interactions with the blood-brain barrier.* ACS Nano, 2014. **8**(5): p. 4304-12.
143. Huang, X., et al., *The shape effect of mesoporous silica nanoparticles on biodistribution, clearance, and biocompatibility in vivo.* ACS Nano, 2011. **5**(7): p. 5390-9.
144. Kreuter, J., et al., *Covalent attachment of apolipoprotein A-I and apolipoprotein B-100 to albumin nanoparticles enables drug transport into the brain.* J Control Release, 2007. **118**(1): p. 54-8.
145. Jallouli, Y., et al., *Influence of surface charge and inner composition of porous nanoparticles to cross blood-brain barrier in vitro.* Int J Pharm, 2007. **344**(1-2): p. 103-9.

146. Petri, B., et al., *Chemotherapy of brain tumour using doxorubicin bound to surfactant-coated poly(butyl cyanoacrylate) nanoparticles: revisiting the role of surfactants.* J Control Release, 2007. **117**(1): p. 51-8.
147. Shilo, M., et al., *Transport of nanoparticles through the blood-brain barrier for imaging and therapeutic applications.* Nanoscale, 2014. **6**(4): p. 2146-52.
148. Gromnicova, R., et al., *Glucose-coated gold nanoparticles transfer across human brain endothelium and enter astrocytes in vitro.* PLoS One, 2013. **8**(12): p. e81043.
149. Guerrero, S., et al., *Improving the brain delivery of gold nanoparticles by conjugation with an amphipathic peptide.* Nanomedicine (Lond), 2010. **5**(6): p. 897-913.
150. Ulbrich, K., et al., *Transferrin- and transferrin-receptor-antibody-modified nanoparticles enable drug delivery across the blood-brain barrier (BBB).* Eur J Pharm Biopharm, 2009. **71**(2): p. 251-6.
151. Jiang, W., et al., *Conjugation of functionalized SPIONs with transferrin for targeting and imaging brain glial tumors in rat model.* PLoS One, 2012. **7**(5): p. e37376.
152. Ulbrich, K., T. Knobloch, and J. Kreuter, *Targeting the insulin receptor: nanoparticles for drug delivery across the blood-brain barrier (BBB).* J Drug Target, 2011. **19**(2): p. 125-32.
153. Martinez-Veracoechea, F.J. and D. Frenkel, *Designing super selectivity in multivalent nano-particle binding.* Proc Natl Acad Sci U S A, 2011. **108**(27): p. 10963-8.
154. Walkey, C.D., et al., *Nanoparticle size and surface chemistry determine serum protein adsorption and macrophage uptake.* J Am Chem Soc, 2012. **134**(4): p. 2139-47.
155. Doshi, N., et al., *Flow and adhesion of drug carriers in blood vessels depend on their shape: a study using model synthetic microvascular networks.* J Control Release, 2010. **146**(2): p. 196-200.
156. Masserini, M., *Nanoparticles for brain drug delivery.* ISRN Biochem, 2013. **2013**: p. 238428.
157. Li, S.D. and L. Huang, *Nanoparticles evading the reticuloendothelial system: role of the supported bilayer.* Biochim Biophys Acta, 2009. **1788**(10): p. 2259-66.
158. Lee, S.Y., M. Ferrari, and P. Decuzzi, *Shaping nano-/micro-particles for enhanced vascular interaction in laminar flows.* Nanotechnology, 2009. **20**(49): p. 495101.
159. Nance, E.A., et al., *A dense poly(ethylene glycol) coating improves penetration of large polymeric nanoparticles within brain tissue.* Sci Transl Med, 2012. **4**(149): p. 149ra119.
160. Arvizo, R.R., et al., *Modulating pharmacokinetics, tumor uptake and biodistribution by engineered nanoparticles.* PLoS One, 2011. **6**(9): p. e24374.
161. Zensi, A., et al., *Albumin nanoparticles targeted with Apo E enter the CNS by transcytosis and are delivered to neurones.* J Control Release, 2009. **137**(1): p. 78-86.
162. Reimold, I., et al., *Delivery of nanoparticles to the brain detected by fluorescence microscopy.* Eur J Pharm Biopharm, 2008. **70**(2): p. 627-32.
163. Wohlfart, S., et al., *Kinetics of transport of doxorubicin bound to nanoparticles across the blood-brain barrier.* J Control Release, 2011. **154**(1): p. 103-7.
164. Georgieva, J.V., et al., *Surface characteristics of nanoparticles determine their intracellular fate in and processing by human blood-brain barrier endothelial cells in vitro.* Mol Ther, 2011. **19**(2): p. 318-25.
165. Yildirimer, L., et al., *Toxicology and clinical potential of nanoparticles.* Nano Today, 2011. **6**(6): p. 585-607.

166. Tsai, Y.M., et al., *Curcumin and its nano-formulation: the kinetics of tissue distribution and blood-brain barrier penetration.* Int J Pharm, 2011. **416**(1): p. 331-8.
167. Zhang, X.D., et al., *Toxicologic effects of gold nanoparticles in vivo by different administration routes.* Int J Nanomedicine, 2010. **5**: p. 771-81.
168. Syvanen, S., et al., *Species differences in blood-brain barrier transport of three positron emission tomography radioligands with emphasis on P-glycoprotein transport.* Drug Metab Dispos, 2009. **37**(3): p. 635-43.
169. Santos, T., et al., *Nanomedicine Approaches to Modulate Neural Stem Cells in Brain Repair.* Trends Biotechnol, 2016. **34**(6): p. 437-9.
170. Ming, G. and H. Song, *Adult Neurogenesis in the Mammalian Brain: Significant Answers and Significant Questions.* Neuron, 2011. **70**(4): p. 687-702.
171. Kempermann, G., H. Song, and F.H. Gage, *Neurogenesis in the Adult Hippocampus.* Cold Spring Harb Perspect Biol, 2015. **7**(9): p. a018812.
172. Santos, T., et al., *Nanomedicine boosts neurogenesis: new strategies for brain repair.* Integr Biol (Camb), 2012. **4**(9): p. 973-81.
173. Kernie, S.G. and J.M. Parent, *Forebrain Neurogenesis after Focal Ischemic and Traumatic Brain Injury.* Neurobiol Dis, 2010. **37**(2): p. 267-74.
174. Estrada, C. and M. Murillo-Carretero, *Nitric oxide and adult neurogenesis in health and disease.* Neuroscientist, 2005. **11**(4): p. 294-307.
175. Carreira, B.P., et al., *Nitric oxide stimulates the proliferation of neural stem cells bypassing the epidermal growth factor receptor.* Stem Cells, 2010. **28**(7): p. 1219-30.
176. Ekdahl, C.T., Z. Kokaia, and O. Lindvall, *Brain inflammation and adult neurogenesis: the dual role of microglia.* Neuroscience, 2009. **158**(3): p. 1021-9.
177. Liu, J., et al., *Increased neurogenesis in the dentate gyrus after transient global ischemia in gerbils.* J Neurosci, 1998. **18**(19): p. 7768-78.
178. Jiang, W., et al., *Cortical neurogenesis in adult rats after transient middle cerebral artery occlusion.* Stroke, 2001. **32**(5): p. 1201-7.
179. Dempsey, R.J., et al., *Stroke-induced progenitor cell proliferation in adult spontaneously hypertensive rat brain: effect of exogenous IGF-1 and GDNF.* J Neurochem, 2003. **87**(3): p. 586-97.
180. Arvidsson, A., et al., *Neuronal replacement from endogenous precursors in the adult brain after stroke.* Nat Med, 2002. **8**(9): p. 963-70.
181. Darsalia, V., et al., *Stroke-induced neurogenesis in aged brain.* Stroke, 2005. **36**(8): p. 1790-5.
182. Lin, R., et al., *Neurogenesis is enhanced by stroke in multiple new stem cell niches along the ventricular system at sites of high BBB permeability.* Neurobiol Dis, 2015. **74**: p. 229-39.
183. Palmer, T.D., A.R. Willhoite, and F.H. Gage, *Vascular niche for adult hippocampal neurogenesis.* J Comp Neurol, 2000. **425**(4): p. 479-94.
184. Tavazoie, M., et al., *A specialized vascular niche for adult neural stem cells.* Cell Stem Cell, 2008. **3**(3): p. 279-88.
185. Jin, K., et al., *Evidence for stroke-induced neurogenesis in the human brain.* Proc Natl Acad Sci U S A, 2006. **103**(35): p. 13198-202.
186. Lledo, P.M., M. Alonso, and M.S. Grubb, *Adult neurogenesis and functional plasticity in neuronal circuits.* Nat Rev Neurosci, 2006. **7**(3): p. 179-93.
187. Maia, J., et al., *Controlling the neuronal differentiation of stem cells by the intracellular delivery of retinoic acid-loaded nanoparticles.* ACS Nano, 2011. **5**(1): p. 97-106.
188. Saraiva, C., et al., *Nanoparticle-mediated brain drug delivery: Overcoming blood-brain barrier to treat neurodegenerative diseases.* J Control Release, 2016. **235**: p. 34-47.

189. Santos, T., et al., *Polymeric nanoparticles to control the differentiation of neural stem cells in the subventricular zone of the brain.* ACS Nano, 2012. **6**(12): p. 10463-74.
190. Schmidt, A., et al., *Selective targeting of adenoviral vectors to neural precursor cells in the hippocampus of adult mice: new prospects for in situ gene therapy.* Stem Cells, 2007. **25**(11): p. 2910-8.
191. Esteves, M., et al., *Retinoic acid-loaded polymeric nanoparticles induce neuroprotection in a mouse model for Parkinson's disease.* Front Aging Neurosci, 2015. **7**: p. 20.
192. Wang, Y., et al., *Bioengineered sequential growth factor delivery stimulates brain tissue regeneration after stroke.* J Control Release, 2013. **172**(1): p. 1-11.
193. Li, X., et al., *Manipulating neural-stem-cell mobilization and migration in vitro.* Acta Biomater, 2012. **8**(6): p. 2087-95.
194. Lim, T.C., et al., *Chemotactic recruitment of adult neural progenitor cells into multifunctional hydrogels providing sustained SDF-1alpha release and compatible structural support.* Faseb j, 2013. **27**(3): p. 1023-33.
195. Tiwari, S.K., et al., *Curcumin-loaded nanoparticles potently induce adult neurogenesis and reverse cognitive deficits in Alzheimer's disease model via canonical Wnt/beta-catenin pathway.* ACS Nano, 2014. **8**(1): p. 76-103.
196. Conway, A. and D.V. Schaffer, *Biomaterial microenvironments to support the generation of new neurons in the adult brain.* Stem Cells, 2014. **32**(5): p. 1220-9.
197. Saraiva, C., et al., *MicroRNA-124 loaded nanoparticles enhance brain repair in Parkinson's disease.* J Control Release, 2016. **235**: p. 291-305.
198. Gaudin, A., et al., *Squalenoyl adenosine nanoparticles provide neuroprotection after stroke and spinal cord injury.* Nat Nanotechnol, 2014. **9**(12): p. 1054-1062.
199. Alvarez-Buylla, A. and J.M. Garcia-Verdugo, *Neurogenesis in adult subventricular zone.* J Neurosci, 2002. **22**(3): p. 629-34.
200. Bennett, L., et al., *Circumventricular organs: a novel site of neural stem cells in the adult brain.* Mol Cell Neurosci, 2009. **41**(3): p. 337-47.
201. Hourai, A. and S. Miyata, *Neurogenesis in the circumventricular organs of adult mouse brains.* J Neurosci Res, 2013. **91**(6): p. 757-70.
202. Xin, H., et al., *The brain targeting mechanism of Angiopep-conjugated poly(ethylene glycol)-co-poly(epsilon-caprolactone) nanoparticles.* Biomaterials, 2012. **33**(5): p. 1673-81.
203. Palmer, A.M., *The role of the blood–CNS barrier in CNS disorders and their treatment.* Neurobiology of Disease, 2010. **37**: p. 3-12.
204. Cecchelli, R., et al., *A stable and reproducible human blood-brain barrier model derived from hematopoietic stem cells.* PLoS One, 2014. **9**(6): p. e99733.
205. Ferreira, L.S., et al., *Vascular progenitor cells isolated from human embryonic stem cells give rise to endothelial and smooth muscle like cells and form vascular networks in vivo.* Circulation Research, 2007. **101**(3): p. 286-94.
206. Engelhardt, B. and S. Liebner, *Novel insights into the development and maintenance of the blood-brain barrier.* Cell Tissue Res, 2014. **355**(3): p. 687-99.
207. Daneman, R., et al., *Wnt/beta-catenin signaling is required for CNS, but not non-CNS, angiogenesis.* PNAS, 2009. **106**: p. 641-646.
208. Paolinelli, R., et al., *Wnt Activation of Immortalized Brain Endothelial Cells as a Tool for Generating a Standardized Model of the Blood Brain Barrier In Vitro.* Plos One, 2013. **8**(8).
209. Liebner, S., et al., *Wnt/beta-catenin signaling controls development of the blood-brain barrier.* Journal of Cell Biology, 2008. **183**(3): p. 409-417.
210. del Zoppo, G.J. and R. Milner, *Integrin-matrix interactions in the cerebral microvasculature.* Arterioscler Thromb Vasc Biol, 2006. **26**(9): p. 1966-75.

211. Prewitz, M.C., et al., *Tightly anchored tissue-mimetic matrices as instructive stem cell microenvironments.* Nature Methods, 2013. **10**(8): p. 788-+.
212. Uchida, Y., et al., *Quantitative targeted absolute proteomics of human blood-brain barrier transporters and receptors.* J Neurochem, 2011. **117**(2): p. 333-45.
213. Collins, T., et al., *Transcriptional regulation of endothelial cell adhesion molecules: NF-kappa B and cytokine-inducible enhancers.* FASEB J, 1995. **9**(10): p. 899-909.
214. Prewitz, M.C., et al., *Tightly anchored tissue-mimetic matrices as instructive stem cell microenvironments.* Nat Methods, 2013. **10**(8): p. 788-94.
215. Hartmann, C., et al., *The impact of glia-derived extracellular matrices on the barrier function of cerebral endothelial cells: An in vitro study.* Experimental Cell Research, 2007. **313**(7): p. 1318-1325.
216. Mozaffarian, D., et al., *Heart disease and stroke statistics--2015 update: a report from the American Heart Association.* Circulation, 2015. **131**(4): p. e29-322.
217. Lindvall, O. and Z. Kokaia, *Stem cells in human neurodegenerative disorders--time for clinical translation?* J Clin Invest, 2010. **120**(1): p. 29-40.
218. Krol, S., et al., *Therapeutic benefits from nanoparticles: the potential significance of nanoscience in diseases with compromise to the blood brain barrier.* Chem Rev, 2013. **113**(3): p. 1877-903.
219. Neuwelt, E., et al., *Strategies to advance translational research into brain barriers.* Lancet Neurol, 2008. **7**(1): p. 84-96.
220. Prades, R., et al., *Delivery of gold nanoparticles to the brain by conjugation with a peptide that recognizes the transferrin receptor.* Biomaterials, 2012. **33**(29): p. 7194-205.
221. Cui, Y., et al., *Transferrin-conjugated magnetic silica PLGA nanoparticles loaded with doxorubicin and paclitaxel for brain glioma treatment.* Biomaterials, 2013. **34**(33): p. 8511-20.
222. Wiley, D.T., et al., *Transcytosis and brain uptake of transferrin-containing nanoparticles by tuning avidity to transferrin receptor.* Proceedings of the National Academy of Sciences of the United States of America, 2013. **110**(21): p. 8662-8667.
223. Yu, Y.J., et al., *Boosting Brain Uptake of a Therapeutic Antibody by Reducing Its Affinity for a Transcytosis Target.* Science Translational Medicine, 2011. **3**(84).
224. Staquicini, F.I., et al., *Systemic combinatorial peptide selection yields a non-canonical iron-mimicry mechanism for targeting tumors in a mouse model of human glioblastoma.* J Clin Invest, 2011. **121**(1): p. 161-73.
225. Oller-Salvia, B., et al., *MiniAp-4: A Venom-Inspired Peptidomimetic for Brain Delivery.* Angewandte Chemie, 2016. **55**(2): p. 572-5.
226. Niewoehner, J., et al., *Increased brain penetration and potency of a therapeutic antibody using a monovalent molecular shuttle.* Neuron, 2014. **81**(1): p. 49-60.
227. Ponka, P. and C.N. Lok, *The transferrin receptor: role in health and disease.* International Journal of Biochemistry & Cell Biology, 1999. **31**(10): p. 1111-1137.
228. Chen, H., et al., *Gold nanorods and their plasmonic properties.* Chem Soc Rev, 2013. **42**(7): p. 2679-724.
229. Alkilany, A.M., et al., *Gold nanorods: their potential for photothermal therapeutics and drug delivery, tempered by the complexity of their biological interactions.* Adv Drug Deliv Rev, 2012. **64**(2): p. 190-9.
230. Oller-Salvia, B., et al., *MiniAp-4: A Venom-Inspired Peptidomimetic for Brain Delivery.* Angew Chem Int Ed Engl, 2016. **55**(2): p. 572-5.
231. Dai, Q., C. Walkey, and W.C. Chan, *Polyethylene glycol backfilling mitigates the negative impact of the protein corona on nanoparticle cell targeting.* Angew Chem Int Ed Engl, 2014. **53**(20): p. 5093-6.

232. Bozanic, D.K., et al., *Glycogen and gold nanoparticle bioconjugates: controlled plasmon resonance via glycogen-induced nanoparticle aggregation.* Rsc Advances, 2013. **3**(23): p. 8705-8713.
233. Nance, E.A., et al., *A dense poly(ethylene glycol) coating improves penetration of large polymeric nanoparticles within brain tissue.* Science Translational Medicine, 2012. **4**(149): p. 149ra119.
234. Kiyatkin, E.A. and H.S. Sharma, *Permeability of the blood-brain barrier depends on brain temperature.* Neuroscience, 2009. **161**(3): p. 926-39.
235. Tabatabaei, S.N., et al., *Remote control of the permeability of the blood-brain barrier by magnetic heating of nanoparticles: A proof of concept for brain drug delivery.* J Control Release, 2015. **206**: p. 49-57.
236. Nikoobakht, B. and M.A. El-Sayed, *Preparation and growth mechanism of gold nanorods (NRs) using seed-mediated growth method.* Chemistry of Materials, 2003. **15**(10): p. 1957-1962.
237. Sims-Mourtada, J., et al., *Sonic Hedgehog promotes multiple drug resistance by regulation of drug transport.* Oncogene, 2007. **26**(38): p. 5674-9.
238. Gavard, J., V. Patel, and J.S. Gutkind, *Angiopoietin-1 prevents VEGF-induced endothelial permeability by sequestering Src through mDia.* Dev Cell, 2008. **14**(1): p. 25-36.
239. Shen, F., et al., *Coexpression of angiopoietin-1 with VEGF increases the structural integrity of the blood-brain barrier and reduces atrophy volume.* J Cereb Blood Flow Metab, 2011. **31**(12): p. 2343-51.
240. Wang, Y., et al., *Interleukin-1beta induces blood-brain barrier disruption by downregulating Sonic hedgehog in astrocytes.* PLoS One, 2014. **9**(10): p. e110024.
241. Menezes, M.J., et al., *The extracellular matrix protein laminin alpha2 regulates the maturation and function of the blood-brain barrier.* J Neurosci, 2014. **34**(46): p. 15260-80.
242. Poschl, E., et al., *Collagen IV is essential for basement membrane stability but dispensable for initiation of its assembly during early development.* Development, 2004. **131**(7): p. 1619-28.
243. Yao, Y., et al., *Astrocytic laminin regulates pericyte differentiation and maintains blood brain barrier integrity.* Nat Commun, 2014. **5**: p. 3413.
244. Lin, H., et al., *Influence of decellularized matrix derived from human mesenchymal stem cells on their proliferation, migration and multi-lineage differentiation potential.* Biomaterials, 2012. **33**(18): p. 4480-9.
245. Rai, A., et al., *Biocompatibility Issues of Organic and Inorganic Nanomaterials*, in *Frontiers in Biomaterials*, S.C.H. Zhu, Editor. 2014, Bentham Science Publishers. p. 274-303.
246. Clark, A.J. and M.E. Davis, *Increased brain uptake of targeted nanoparticles by adding an acid-cleavable linkage between transferrin and the nanoparticle core.* Proc Natl Acad Sci U S A, 2015. **112**(40): p. 12486-91.
247. Ye, D., et al., *Nanoparticle accumulation and transcytosis in brain endothelial cell layers.* Nanoscale, 2013. **5**(22): p. 11153-65.
248. Jefferies, W.A., et al., *Transferrin receptor on endothelium of brain capillaries.* Nature, 1984. **312**(5990): p. 162-3.
249. Moos, T. and E.H. Morgan, *Transferrin and transferrin receptor function in brain barrier systems.* Cell Mol Neurobiol, 2000. **20**(1): p. 77-95.
250. Velasco-Aguirre, C., et al., *Peptides and proteins used to enhance gold nanoparticle delivery to the brain: preclinical approaches.* Int J Nanomedicine, 2015. **10**: p. 4919-36.
251. Ebert, A.D., et al., *EZ spheres: a stable and expandable culture system for the generation of pre-rosette multipotent stem cells from human ESCs and iPSCs.* Stem Cell Res, 2013. **10**(3): p. 417-27.

252. Sareen, D., et al., *Human induced pluripotent stem cells are a novel source of neural progenitor cells (iNPCs) that migrate and integrate in the rodent spinal cord.* J Comp Neurol, 2014. **522**(12): p. 2707-28.
253. Han, S., et al., *Constructive remodeling of a synthetic endothelial extracellular matrix.* Scientific Reports, 2015. **5**(18290): p. 1-10.
254. Byron, A., J.D. Humphries, and M.J. Humphries, *Defining the extracellular matrix using proteomics.* Int J Exp Pathol, 2013. **94**(2): p. 75-92.
255. Khatri, R., et al., *Blood-brain barrier, reperfusion injury, and hemorrhagic transformation in acute ischemic stroke.* Neurology, 2012. **79**(13 Suppl 1): p. S52-7.
256. Lee, H. and I.S. Pienaar, *Disruption of the blood-brain barrier in Parkinson's disease: curse or route to a cure?* Front Biosci (Landmark Ed), 2014. **19**: p. 272-80.
257. Zlokovic, B.V., *Neurovascular pathways to neurodegeneration in Alzheimer's disease and other disorders.* Nat Rev Neurosci, 2011. **12**(12): p. 723-38.
258. Paulo, C.S., et al., *Differential internalization of amphotericin B--conjugated nanoparticles in human cells and the expression of heat shock protein 70.* Biomaterials, 2013. **34**(21): p. 5281-93.